AQUITARD CONTAMINANT STORAGE AND FLUX

By

GORDON HITCHINGS BROWN

A DISSERTATION PRESENTED TO THE GRADUATE SCHOOL
OF THE UNIVERSITY OF FLORIDA IN PARTIAL FULFILLMENT
OF THE REQUIREMENTS FOR THE DEGREE OF
DOCTOR OF PHILOSOPHY

UNIVERSITY OF FLORIDA

2014

To my parents,
and my family

ACKNOWLEDGMENTS

I would like to thank my family, including my wife, my daughter, and my parents for their encouragement in this endeavor. At the University of Florida, within the Engineering School of Sustainable Infrastructure and Environment (ESSIE), the Department of Environmental Engineering Sciences provided financial and technical support, in particular, my advisor Dr. Michael D. Annable and former ESSIE post-doc Dr. Harold Klammer.

Much of the work upon which this dissertation is based was supported by the U.S. Environmental Protection Agency through its Office of Research and Development with funding provided by the Strategic Environmental Research and Development Program (SERDP), a collaborative effort involving the U.S. Environmental Protection Agency (EPA), the U.S. Department of Energy (DOE), and the U.S. Department of Defense (DoD). It has not been subjected to Agency review and, therefore, does not necessarily reflect the views of the Agency and no official endorsement should be inferred. EPA researchers Dr. Michael C. Brooks, Dr. A. Lynn Wood, and Dr. Junqi Huang were instrumental in guiding the model development and results analysis.

TABLE OF CONTENTS

Page

LIST OF TABLES

LIST OF FIGURES

LIST OF SYMBOLIC NOTATION

DNAPL	Dense non-aqueous phase liquid
TCE	Trichloroethylene
PCE	Tetrachloroethylene
SDM	Source depletion model
1D	One-dimensional
2D	Two-dimensional
C_0	Source zone initial flux-averaged concentration [ML^{-3}]
$C(t)$	Source zone flux-averaged concentration at time t [ML^{-3}]
$\chi(\tau)$	Source zone dimensionless concentration at dimensionless time τ
χ_R	Source dimensionless flux-averaged concentration at time of remediation
$\bar{\chi}(p)$	Source zone dimensionless flux-averaged concentration in the Laplace domain
C'	Aquitard concentration [ML^{-3}]
C_T'	Aquitard total concentration [ML^{-3}]
C_s'	Aquitard solid phase concentration [MM^{-1}]
C_w'	Aquitard aqueous phase concentration [ML^{-3}]
C'_{peak}	Peak concentration in aquitard [ML^{-3}]
$\chi'(\tau)$	Dimensionless aquitard concentration at dimensionless time τ
$\bar{\chi}'(\zeta, p)$	Aquitard dimensionless concentration in the Laplace Domain
χ'_{peak}	Peak dimensionless concentration in aquitard
X	Fraction of source mass removed
A_{SZ}	Source zone cross sectional area [L^2]

M_0	Source zone initial mass [M]
M_{OA}	Source mass per unit area [ML^{-2}]
$M(t)$	Source mass at time t [M]
$\mu(\tau)$	Source zone dimensionless mass at dimensionless time τ
μ_R	Source dimensionless mass remaining at time of remediation
$M'(t)$	Stored mass per unit area in the aquitard at time t [ML^{-2}]
$\mu'(\tau)$	Dimensionless aquitard mass per unit area at dimensionless time τ
μ'_{BD}	Aquitard dimensionless mass per unit area at time back diffusion starts
$M'_{\max}$	Maximum aquitard mass per unit
J_0	Source zone initial flux [$ML^{-2}T^{-1}$]
$J'(t)$	Aquitard back diffusion flux at time t [$ML^{-2}T^{-1}$]
J'_{peak}	Peak back diffusion flux [$ML^{-2}T^{-1}$]
J_T'	Total aquitard flux [$ML^{-2}T^{-1}$]
$\varphi'(\tau)$	Dimensionless aquitard flux at dimensionless time τ
τ	Dimensionless time
τ_{BD}	Dimensionless time back diffusion starts
τ^*	Dimensionless time the source is exhausted or completely removed
T_R	Post remedial dimensionless time
T_R^*	Post remedial dimensionless time the source is exhausted or completely removed
q	Groundwater flux through source zone [LT^{-1}]
q_z'	Vertical groundwater flux through aquitard [LT^{-1}]

v_z'	Vertical seepage velocity [LT^{-1}]
z	Depth in aquitard below boundary [L]
ζ	Dimensionless depth in the aquitard below boundary
R'	Aquitard retardation factor [-]
η	Aquitard porosity [-]
ρ_b	Aquitard bulk density [ML^{-3}]
θ_w	Volumetric water content [-]
K_d'	Distribution coefficient [LM^{-3}]
S_w	Aquitard water content [-]
ϕ	Aquitard tortuosity [-]
a_L	Aquitard dispersivity [L]
D_w	Aqueous diffusion constant [L^2T^{-1}]
D_s'	Effective diffusion constant [L^2T^{-1}]
D_z'	Aquitard hydrodynamic dispersion coefficient [L^2T^{-1}]
Γ	Empirical parameter that accounts for flow field heterogeneity, DNAPL distribution, and the correlation between the two [-]
β	Source to aquitard mass transfer coefficient [-]
β_R	Post remedial source to aquitard mass transfer coefficient [-]
ψ	Source decay function [T^{-1}]
ψ_R	Post remedial source decay function [T^{-1}]
σ	Aquitard diffusion timescale [T]
σ_R	Post remedial aquitard diffusion timescale [T]
r	Reaction term in aquitard [$ML^{-3}T^{-1}$]

λ'	First-order aquitard degradation constant [T^{-1}]
Λ	Dimensionless decay coefficient
P_e	Peclet number in aquitard [-]
MR	Fractional mass reduction
FR	Fractional flux reduction

Abstract of Dissertation Presented to the Graduate School
of the University of Florida in Partial Fulfillment of the
Requirements for the Degree of Doctor of Philosophy

AQUITARD CONTAMINANT STORAGE AND FLUX

By

GORDON HITCHINGS BROWN

May 2014

Chair: Michael D. Annable
Major: Environmental Engineering Sciences

A one-dimensional diffusion model with a semi-infinite domain was used to investigate the effects of dense non-aqueous phase liquid (DNAPL) source zone dissolution and remediation on the storage and release of contaminants from aquitards. Source zone dissolution was represented by a power-law source depletion model, which served as a time variable boundary condition to the diffusion equation used to describe mass transport in the aquitard. Two key variables were used to assess source zone dissolution behavior on aquitard mass storage and release: the power-law exponential term Γ, which reflects the influence of the source zone architecture, and a new variable defined herein as the source to aquitard mass transfer coefficient β, which reflects the influences of both the source characteristics and the aquitard media properties. As Γ increased or as β increased due to more rapid source dissolution, the dimensioned aquitard concentrations, depth of penetration, and long term back diffusion flux decreased. However, when β increased due to increased sorption, the dimensioned concentrations and back diffusion increased but the depth of penetration decreased. The duration of aquitard mass loading was found to be significantly less than the duration of mass release. Moreover, the mass per unit area stored in the

aquitard was three or more orders of magnitude less than the initial DNAPL source zone mass per unit area, and the back diffusion flux from the aquitard was typically four or more orders of magnitude less than the initial source zone mass flux. Contaminant decay in the aquitard λ' was modeled at 1-3 orders of magnitude lower than aquifer ranges for λ and as λ' increased both the mass stored and the back diffusion flux decreased. At the upper range of λ', decay was high enough such that no back diffusion occurred. Vertical leakage in the aquitard q_z' was modeled at 4 orders of magnitude less than the groundwater velocity in the aquifer. Downward q_z' increased dimensioned aquitard mass storage, both the loading and back diffusion mass flux, and the depth of penetration while upward q_z' decreased dimensioned storage, flux, and penetration. At high vertical upward leakage rates back diffusion from the aquitard was not observed. Additionally, the effects of partial source zone remediation were investigated, and the results suggest that source remediation can have a favorable effect on long term back diffusion risk. In the short term following remediation, back diffusion from the aquitard was elevated due to the increased concentration gradient and in the long term, back diffusion was reduced by remediation.

CHAPTER 1
REVIEW OF LITERATURE

Overview

The presence of aqueous contaminants in low conductivity media downgradient of suspected or known dense non-aqueous phase liquid (DNAPL) source zones has been attributed to diffusional transport [*Ball et al.,* 1997; *Liu and Ball*, 2002; *Chapman and Parker,* 2005; *Parker et al.,* 2008]. A groundwater plume will provide the concentration gradient required to move contaminants into an initially uncontaminated low conductivity layer. Over time the source mass will be depleted, the resulting plume concentrations will decrease, and the concentration gradient will reverse. Mass then diffuses out of the low conductivity layers (a phenomenon known as back diffusion) potentially leading to plume persistence [*Chapman and Parker,* 2005*; Parker et al.,* 2008]. Because of this, it has been suggested that remedial efforts may be ineffective at reducing risk, based on maximum contaminant limits (MCLs), since contaminant mass in low conductivity layers can serve as a secondary source to the plume long after the original DNAPL source mass has been removed or isolated [*Parker et al.,* 2008*; Sale et al.,* 2008].

Contemporary Related Work

Ball et al. [1997] used high-resolution sampling of a soil core to investigate the distribution of contaminants in an aquitard downgradient of contaminant sources at Dover Air Force Base, Delaware. Aqueous concentrations of tetrachloroethene (PCE) were higher in the aquifer compared to those in the underlying aquitard, suggesting forward diffusion of PCE into the aquitard. In contrast, trichloroethene (TCE) was detected at relatively lower aqueous concentrations in the aquifer compared to those in

the underlying aquitard, suggesting that TCE loading had terminated and that back diffusion had begun. Sheet piling was used to hydraulically isolate the test area, and three additional soil cores were collected over approximately three years [*Liu and Ball*, 2002]. Conditions to induce back diffusion within the sheet piling through water circulation were maintained over the final two years of the study, and results were consistent with those expected with back diffusion as the dominant transport process. Field data were evaluated using a multilayer one-dimensional (1D) analytical model of diffusional transport in the aquitard based on the convolution method. Inverse methods were utilized to fit the model to the field data by estimating the historic concentration-time series in the aquifer (i.e., upper boundary condition) using several different approaches [*Ball et al.*, 1997; *Liu and Ball*, 1998]. The solutions provided reasonable fits to the aquitard data but were non-unique in that very different boundary conditions generated very similar aquitard concentration profiles.

Similar approaches were used to investigate aquitard profiles at a TCE-contaminated site in Connecticut [*Parker et al.,* 2004; *Chapman and Parker*, 2005]. The loading of the TCE into the aquitard was likely due to both diffusion and pumping in the lower aquifer, which created a strong downward gradient across the aquitard and thus downward advective flow [*Parker et al.,* 2004]. The source was isolated with sheet piling and six years later, coring in the plume showed low concentrations near the aquifer/aquitard interface and higher concentrations with depth in the aquitard [*Chapman and Parker*, 2005]. These profiles, along with persistent concentrations in the surficial aquifer just above the aquitard interface suggested plume persistence due to back diffusion. A 1D diffusion model was used to predict the measured concentration

profiles in the aquitard, and the agreement with field data improved by using a stepped, declining source compared to a constant-concentration boundary condition [*Parker et al.,* 2004; *Chapman and Parker*, 2005].

In addition to aquitards, *Parker et al.* [2008] investigated back diffusion from discrete, thin clay layers downgradient of a DNAPL source zone. Groundwater concentrations were observed to decrease by several orders of magnitude in the first five years after hydraulic isolation of the source, yet they remained above MCLs in the downgradient sampling transects. Cores into the clay layers showed lower concentration in regions near the aquifer interface, and higher concentrations deeper into the clay, indicating back diffusion releases. Two-dimensional (2D) modeling by *Parker et al.* [2008] employed a constant concentration boundary condition in the aquifer with discrete low conductivity layers present. After 30 years, the source was terminated and TCE diffusion out of the low conductivity layers was observed for up to 200 years.

Finally, several laboratory and modeling methods were used to elucidate the effect of reduced contaminant loading on downgradient water quality [*Sale et al.,* 2008; *Chapman et al.,* 2012; *Seyedabbasi et al.,* 2012]. In the *Sale et al*, [2008] laboratory and modeling work, a two-layer laboratory aquifer model, with an upper layer of sand and a lower layer of silt, was used to demonstrate back diffusion from the lower layer once the source was turned off. The results were fit with a two dimensional model with constant concentration boundary conditions. The investigators reported that 15 to 44% of contaminant mass was stored in the aquitard and the modeling projected that the stored mass would release for many years after the source was terminated. In another

study, a sand tank was packed with several clay lenses and subjected to a constant concentration of bromide and fluorescein for 25 days, followed by clean water flow. Approximately 60 days after the influent concentration was terminated and replaced by clean water flow, the contributions to the effluent due to back diffusion were 4 orders of magnitude lower than the initial influent concentrations [*Chapman et al.,* 2012]. Another modeling study set up many small low conductivity lenses with pooled DNAPL and then looked at the contribution of both the dissolved DNAPL and matrix diffusion from the lenses as components in the plume [*Seyedabbasi et al.,* 2012]. Results showed that in the mass discharge rate, the contribution of matrix diffusion increased for the more soluble species whereas NAPL and mixed contributions were more dominant in the less soluble contaminants.

In summary, these studies have used field and laboratory data to identify and demonstrate the importance of back diffusion, and have used diffusion models to help interpret the data. These experiments and models however, have often used constant-concentration boundary conditions, or step-changes in concentration as the boundary condition, which are idealized approximations of source-zone dissolution. An exception is the work of *Liu and Ball* [1998, 1999, 2002], which considered complex functions for boundary conditions; however, their work focused on estimating the boundary condition from the measured concentration profile in the aquitard. Nevertheless, the field site characteristics that contribute to the significance of diffusive storage and release have not been clearly established.

During the decades or centuries required for groundwater to completely dissolve a DNAPL spill, the source architecture may change due to local depletion in the higher

hydraulic conductivity zones, potentially weakening the overall source strength (i.e., the mass discharge from the source zone) and plume concentration [*NRC*, 2004; *Falta et al.,* 2005a]. Both laboratory and field studies have documented reductions in mass discharge as a result of active source depletion [*Fure et al.,* 2006; *Page et al.,* 2007; *Kaye et al.,* 2008; *McGuire et al.,* 2006; *Brooks et al.,* 2008*; DiFilippo and Brusseau,* 2008]. In addition, both laboratory [*Fure et al.,* 2006; *Suchomel and Pennell*, 2006; *Brusseau et al.,* 2008; *Kaye et al.,* 2008; *DiFilippo and Brusseau*, 2011] and field studies [*McGuire et al.,* 2006; *Basu et al.,* 2009; *DiFilippo and Brusseau*, 2008] suggest that in some cases mass discharge reduction is proportional to contaminant mass reduction in approximately a 1:1 relationship. Moreover, at most field sites monitoring and remedial activities were initiated 10 to 40 years after the spill, and another study suggests that at aged sites a 1:1 mass discharge to DNAPL mass reduction relationship may be assumed, regardless of initial spill architecture [*Chen and Jawitz*, 2009].

Thus, much work has focused on modeling DNAPL source zones to account for reductions in source strength as DNAPL mass is removed from the source zone. Several analytical models that use either Lagrangian or Eulerian methods have been developed [*Parker and Park*, 2004; *Falta et al.,* 2005b; *Park and Parker*, 2005; *Jawitz et al.,* 2005; *Christ et al.,* 2006; *Basu et al.,* 2008b; *Zhang et al.,* 2008; *Chen and Jawitz*, 2009; *DiFilippo and Brusseau*, 2011]. These screening-level source depletion models (SDMs) offer methods to evaluate the effects of source depletion and incorporate basic parameters to describe heterogeneous DNAPL contamination, heterogeneous groundwater flow, and the potential correlation between the two [*Basu et al.,* 2008a].

The reducing conditions inherently present in aquifers provide an environment conducive to contaminant reaction processes [*Alexander,* 1999]. These can be abiotic and biotic in nature, breaking down the parent compound to daughter products. Less work has been performed to assess the degradation potential or activity of these processes in aquitards. Most of this work has focused on aquifer decay rates [*Newell et. al.,* 2003]. However, the reducing environment extends down into the aquitard and the presence of organic matter in the silt and clay may foster increased degradation. A recent study in Japan determined that the dechlorination of PCE by bacteria can occur in an organic-rich clayey aquitard, and that the aquitard may plan an important role in natural attenuation in the adjacent aquifer [*Takeuchi et al.,* 2011].

Another potential component of aquitard hydrology is vertical advection through leakage. Vertical gradients can cause very slow groundwater flow through an aquitard either in downward or upward direction depending on the direction of the gradient. The gradient can be natural due to head pressure or induced by well pumping. A recent study in Australia determined groundwater flux through the regional aquitard to be ~$8x10^{-9}$ – $8x10^{-6}$ m d^{-1} [*Gardner et al.,* 2012]. Groundwater leakage through confining units has also been studied in the context of lake bed losses [*Annable et al.,* 1996; *Motz,* 2010], however research on contaminant transport through confining units has been less common. Most of the research has been focused on landfill liner leakage [*Johnson et al.,* 1989; *Rubin and Rabideau*, 2000; *Foose et al.,* 2003]. Johnson et al., [1989] determined that diffusion was the dominant transport mechanism for clay liner with an average downward linear velocity of a ~$5x10^{-6}$ m d^{-1}. More focus had been on the groundwater and contaminant flow through the fractures in clay aquitards [*Harrison*

et al., 1992; *Parker et al.,* 1996 ; *Parker and Chapman*, 2005]. The complexity of studying this phenomenon and the ability to sample in aquitards without compromising their integrity to verify computer and laboratory studies with field data may be a reason.

Focus of This Work

The work reported here explores the relationship between source depletion dynamics and diffusive transport in and out of low conductivity media using one dimensional analytical methods as a potential screening level tool for site assessment. An analytical SDM was utilized to provide a time-varying boundary condition for the 1D diffusion model with a semi-infinite domain. Specifically, the work reported herein used the power law model [*Rao et al.,* 2002*; Rao and Jawitz,* 2003*; Zhu and Sykes,* 2004*; Falta et al.,* 2005a; *Falta et al.,* 2005b] to create a temporally variable boundary condition. Since diffusion is a gradient driven phenomenon, the changing concentration in the overlying aquifer will influence the amount of contaminant mass driven into the aquitard and its subsequent release. The potential for plume persistence due to back diffusion is dependent on two factors: (1) the contaminant mass stored in the aquitard due to loading during forward diffusion, and (2) the rate at which the contaminant is released during back diffusion (i.e., the magnitude of contaminant flux from the aquitard). Thus, hydrogeologic and contaminant parameters that affect mass loading to and release from the aquitard were examined. The initial results of aquitard diffusion, mass storage, mass flux, with and without source remediation were recently published [*Brown et al.,* 2012]. The parameters studied in this work include those influencing the source zone dissolution and those influencing contaminant transport in the aquitard including the diffusion coefficient, advection in the low permeability unit, decay rates in the aquitard, and the influence of remedial activities on the source zone.

CHAPTER 2
ONE DIMENSIONAL MODEL DEVELOPMENT

One Dimensional Model for Diffusion

Dimensionless Source Depletion

Our conceptual model begins with a DNAPL source zone in an aquifer, shown in Figure 2-1. Media heterogeneity in the aquifer will cause high and low groundwater velocities and an uneven DNAPL distribution on a local scale. Thus, as a screening-level approximation, we focus on the large-scale, flux-averaged concentration $C(t)$ [ML^{-3}] leaving the source zone across a control plane with cross sectional area A_{SZ} [L^2]. The SDM chosen to represent this time variable concentration is based on a mass balance in the source zone with source depletion by dissolution only:

$$\frac{dM(t)}{dt} = -qA_{SZ}C(t) \tag{2-1}$$

where M is the mass of the contaminant in the source zone [M], t is time [T], and q is the groundwater flux [LT^{-1}]. *Zhu and Sykes* [2004] and *Falta et al.,* [2005a] provide solutions for Eq. 2-1 when M is related to C using a power-law expression,

$$\frac{C(t)}{C_0} = \left[\frac{M(t)}{M_0}\right]^{\Gamma} \tag{2-2}$$

where C_0 is the initial, flux-averaged concentration crossing the source zone control plane [ML^{-3}], M_0 is the initial mass of the contaminant in the source zone [M], and Γ is a unit less empirical parameter that accounts for flow field heterogeneity, DNAPL distribution, and the correlation between the two [*Falta et al.,* 2005a]. Special cases of interest include: $\Gamma = 0$, which represents the constant concentration source; $\Gamma = 0.5$ which represents linear source decay; and $\Gamma = 1.0$, which represents exponential source

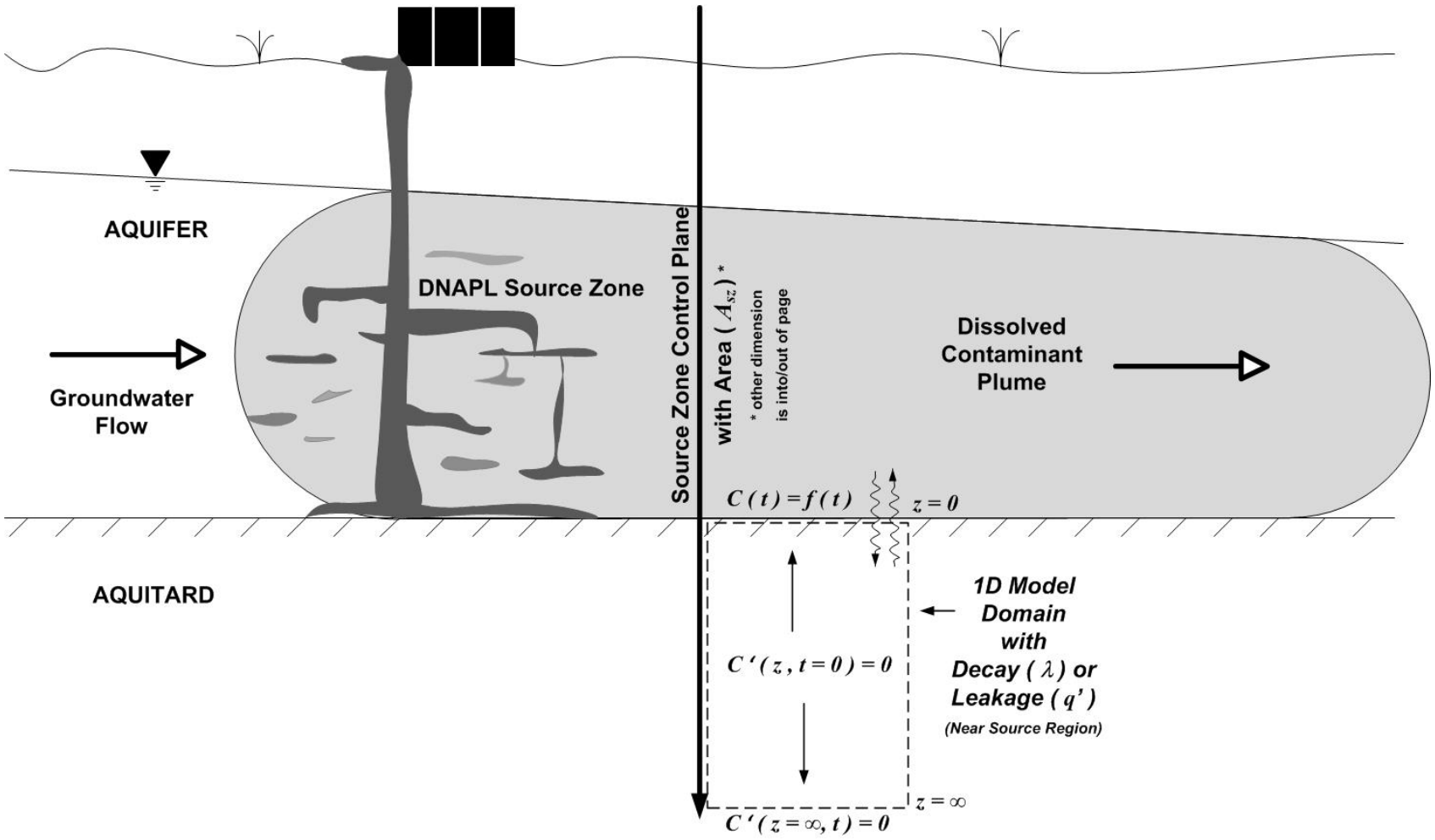

Figure 2-1. Conceptual diagram of the model.

Note: The diagram consists of a DNAPL source zone, the dissolved contaminant plume (gray) with a flux-averaged concentration $C(t)$ crossing the source zone control plane A_{SZ}, and 1D domain with diffusion, leakage, and decay (dashed box) - an underlying, near source, semi-infinite aquitard with a time variable upper boundary $C(t)$.

decay. Using the definitions provided in Table 2-1, equations (1) and (2) can be expressed in dimensionless form as

$$\frac{d\mu(\tau)}{d\tau} = -\beta\chi(\tau) \quad , \tag{2-3}$$

and

$$\chi(\tau) = \left[\mu(\tau)\right]^{\Gamma} \quad , \tag{2-4}$$

where the source to aquitard mass transfer coefficient is β [-] as defined in Table 2-1.

Table 2-1. Definitions of Dimensionless Variables

Source zone mass and concentration	$\mu = \frac{M}{M_0}$; $\chi = \frac{C_w}{C_0}$
Aquitard depth, time and concentration	$\zeta = \frac{z}{\sqrt{A_{SZ}}}$; $\tau = \frac{D_s' t}{A_{SZ} R'}$; $\chi' = \frac{C_w'}{C_0}$
Source to aquitard mass transfer coefficient	$\beta = \psi \cdot \sigma$; $\psi = \frac{q A_{SZ} C_0}{M_0}$; $\sigma = \frac{A_{SZ} R'}{D_s'}$
Post-remedial source mass and concentration	$\mu_R = (1-X)\mu(\tau_R)$; $\chi_R = \left[(1-X)\mu(\tau_R)\right]^{\Gamma}$
Post-remedial source to aquitard mass transfer coefficient	$\beta_R = \psi_R \cdot \sigma$; $\psi_R = \psi \cdot \frac{\chi_R}{\mu_R}$

The term β represents the relative extent to which mass is transferred from the source to the aquitard, and is the product of the source decay function ψ [T^{-1}] given by *Zhu*

and Sykes [2004], and a new variable defined here as the aquitard diffusion timescale σ [T] (Table 1). Consequently, β couples source dissolution processes in ψ and effective diffusional processes in σ. A low β represents slow source zone dissolution and/or low aquitard retardation where the plume concentration remains high for a longer time, while a high β represents rapid source dissolution and/or high aquitard retardation. The soil diffusion coefficient D_s' and the retardation factor R' in the aquitard are used in σ and τ (Table 2-1), and will be discussed in more detail in the next section.

Substitution of Eq. 2-4 into Eq. 2-3, along with an initial condition of $\mu(\tau = 0) = 1.0$, allows for solutions of $\chi(\tau)$ and $\mu(\tau)$ following methods similar to those presented by either *Zhu and Sykes* [2004] or *Falta et al.,* [2005a]:

$$\chi(\tau) = \left[(\Gamma - 1)\beta\tau + 1 \right]^{\frac{\Gamma}{(1-\Gamma)}} \quad , \tag{2-5a}$$

and

$$\mu(\tau) = \left[(\Gamma - 1)\beta\tau + 1 \right]^{\frac{1}{(1-\Gamma)}} \quad . \tag{2-5b}$$

As $\Gamma \to 1$ the limit of Eq. 2-5a and Eq. 2-5b approach

$$\chi(\tau) = \mu(\tau) = e^{-\beta\tau} \quad , \tag{2-5c}$$

[*Abramowitz and Stegun*, 1970]. Detailed derivations for Eq. 2-5a, Eq. 2-5b, and Eq. 2-5c can be found in the Appendix.

The simple screening level SDM (Eq. 2-4, 2-5a, 2-5b, and 2-5c) is a dimensionless form of the equations utilized in the Remediation Evaluation Model for Chlorinated Solvents (REMChlor) [*Falta et al.,* 2007; *Falta*, 2008]. It assumes that

groundwater velocity is one-dimensional and uniform, that contaminant discharge is described as a power function of source mass, and that the power function exponent is invariant over time. While source-zone contaminant decay could be incorporated into the SDM (e.g., *Falta et al.* [2005a] and *Falta et al.* [2007]), we assume this factor is insignificant. Finally, changes in the flux-averaged concentration leaving the source due to lateral or longitudinal dispersion and decay are neglected, and the SDM is therefore considered to represent the aquifer concentration above the aquitard. This assumption is considered appropriate in the region immediately down gradient of the source zone.

Dimensionless Diffusion

The model represents a 1D aquitard, semi-infinite domain with zero concentration at infinite depth, zero concentration initially throughout the domain and an imposed time variable concentration boundary condition at the surface (Figure 2-1). The location of the aquitard is immediately down gradient of the DNAPL source zone, above or below the near source aquifer region; however, an underlying aquitard was chosen as defined by the z direction (Figure 2-1). The upper boundary condition is be represented by the flux-averaged concentration of dissolved contaminant leaving the DNAPL source zone, Eq. 2-5a or Eq. 2-5c. The system is governed by Fick's 2nd law of diffusion,

$$R'\frac{\partial C'}{\partial t} = D_s'\frac{\partial^2 C'}{\partial z^2} \quad , \tag{2-6}$$

where R' is the retardation factor in the aquitard [-], C' the contaminant concentration [ML^{-3}], D_s' is the effective diffusion coefficient [L^2T^{-1}]:

$$D_s' = \frac{D_w}{\phi} \quad , \tag{2-7}$$

where D_w is the water diffusion coefficient and ϕ is the tortuosity of the medium [-]. The value of ϕ was held constant for this study but there is likely considerable variability in the tortuosity of different aquitards and even within the same aquitard. To assess the worst case scenario, this value was kept low to model higher effective diffusion. The total aquitard concentration C_T' [ML^{-3}] can be represented by

$$C_T' = \rho_b C_S' + \theta_w C_w' \quad , \tag{2-8}$$

where ρ_b is the aquitard bulk density [ML^{-3}], C_S' is the aquitard solid phase concentration [M/M], θ_w is the aquitard volumetric water content [-], and C_w' is the aquitard water concentration [ML^{-3}]. Assuming equilibrium, reversible, and linear partitioning of the contaminant between the aquitard pore water and solid media, with

$$K_d' = \frac{C_S'}{C_w'} \quad , \tag{2-9a}$$

$$\theta_w = \eta S_w \quad , \tag{2-9b}$$

and

$$R' = 1 + \frac{\rho_b' K_d'}{\eta} \quad , \tag{2-9c}$$

where ρ_b' is the media bulk density [ML^{-3}], η is the porosity of the aquitard [-], S_w is the aquitard moisture content (S_w = 1.0 for a saturated medium), and K_d' distribution coefficient in the aquitard [LM^{-3}], for saturated conditions, Eq. 2-2 becomes

$$C_T' = \eta C_w' R' \quad . \tag{2-10}$$

Transforming Eq. 2-6 using the dimensionless terms in Table 2-1, Fick's 2nd Law becomes

$$\frac{\partial \chi'}{\partial \tau} = \frac{\partial^2 \chi'}{\partial \zeta^2} \quad . \tag{2-11}$$

A solution for Eq. 2-11 in the Laplace domain is

$$\bar{\chi}'(\zeta, p) = C_1 \left\{ \exp\left[-\zeta \sqrt{p} \right] \right\} . \tag{2-12}$$

With boundary conditions of

$$\chi'(\zeta = 0, \tau \geq 0) = f(\tau) \quad , \tag{2-13a}$$

and

$$\chi'(\zeta = \infty, \tau \geq 0) = 0 \quad , \tag{2-13b}$$

and an initial condition of

$$\chi'(0 < \zeta < \infty, \tau = 0) = 0 \quad , \tag{2-13c}$$

Eq. 2-12 becomes

$$\bar{\chi}'(\zeta, p) = \bar{\chi}(p) \left\{ \exp\left[-\zeta \sqrt{p} \right] \right\} \quad . \tag{2-14}$$

The Laplace Inversion is in the form of

$$L^{-1}\left\{ \exp\left(-\zeta \sqrt{p} \right) \right\} = \frac{\zeta}{2\sqrt{\pi \tau^3}} \exp\left(-\frac{\zeta^2}{4\tau} \right) \quad , \tag{2-15}$$

Abramowitz & Stegun [1970]. Thus, a general solution to Eq. 2-11 is

$$\chi'(\zeta, \tau) = \frac{\zeta}{2\sqrt{\pi}} \int_0^\tau f(\gamma) \frac{1}{\sqrt{(\tau - \gamma)^3}} \exp\left(-\zeta^2 \Big/ 4(\tau - \gamma) \right) d\gamma \quad . \tag{2-16}$$

The upper boundary condition of the aquitard can be represented by a function $f(t)$ that imposes a time variable concentration, represented by the SDM in Eq. 2-5a or Eq. 2-5c. The SDM equation is substituted for $f(\gamma)$ in Eq. 2-16 to convert the general solutions to a specific one. The dimensioned concentration is:

$$C'_w(t) = \chi'(\tau) C_0 \qquad \text{at} \quad \tau = \frac{D_s' t}{A_{SZ} R'} \qquad , \tag{2-17a}$$

and

$$C'_T(t) = \chi'(\tau) \eta C_0 R' \qquad . \tag{2-17b}$$

The resulting specific solution was evaluated with MathCAD™ 15.0, an engineering calculations software program. Other analytical solutions of Eq. 2-11 for specific cases of $\Gamma = \{0,\ 0.5,\ 1\}$ in Eq. 2-4 have been previously published [*Crank*, 1975; *Bear et al.*, 1994]. These solutions were used for model verification and are available in the Appendix. This solution considers diffusion and sorption in the aquitard. More complex conditions will be explored in the next section.

Equation 2-16 is fully dimensionless; is applied to a single-layer semi-infinite aquitard; and employs the convolution theorem, as did *Booker and Rowe* [1987] and *Liu and Ball* [1998]. Several 1D analytical solutions have been used in the study of finite thickness landfill liner contaminant transport, but these use constant concentration boundaries and usually include a leakage term for vertical flow in their governing equation [*Rubin and Rabideau*, 2000; *Foose et al.*, 2001]. In a recent study, *Chen et al.*, [2009] developed a 1D analytical solution with a time changing boundary condition and applied it to diffusion and mass flux through a multi-layer landfill liner. This solution used the separation of variable method instead of the Laplace transform method. While Eq. 2-16 also determines the concentration profiles like previous studies, this work moves into a risk framework by focusing on the mass storage and mass release out of the aquitard resulting from time variable DNAPL sources and source remediation as demonstrated in the next few sections.

The model for diffusion in the aquitard contains several simplifying assumptions. The groundwater flow is assumed to be large enough that diffusion from the aquitard does not influence the aquifer concentration (i.e. no feedback to the concentration gradient). All aquitard properties were assumed to be homogeneous, which is adequate for this screening level model, but in reality properties like ϕ and η, thus D_s' may be variable. Permanent sequestration and decay in the aquitard are not considered, but may both occur in a field setting. The results presented are conservative in that they represent the worst case risk due to flux from the aquitard. In a real system, the concentration re-entering the aquifer from the aquitard would be reduced by aquifer dispersion and biodecay.

Dimensionless Mass Storage and Mass Flux

Aquitard contaminant mass and flux are important to assess the risk and significance of back diffusion from the aquitard. The dimensionless mass per unit area in the aquitard $\mu'(\tau)$ can be determined for any Γ or β through integration of dimensionless flux $\varphi'(\tau)$ through dimensionless time,

$$\mu'(\tau) = \int_0^{\tau} \varphi'(\gamma)\, d\gamma \quad , \tag{2-18a}$$

by integration of dimensionless concentration through dimensionless space,

$$\mu'(\tau) = \int_0^{\infty} \chi'(\zeta, \tau) d\zeta \quad , \tag{2-18b}$$

or integration of dimensionless concentration in dimensionless space in the Laplace domain and application of the convolution method,

$$\mu'(\tau) = \int_0^{\tau} f(\gamma) \left\{ \frac{1}{\sqrt{\pi(\tau - \gamma)}} \right\} d\gamma \quad . \tag{2-18c}$$

The dimensioned mass is

$$M'(t) = \mu'(\tau) \eta C_0 R' \sqrt{A_{sz}} \quad . \tag{2-19}$$

The integral in Eq. 2-18a and Eq. 2-18c were evaluated analytically and Eq. 2-18b numerically. Equation 2-18a gives μ' as a result of loading when using the dimensionless time at which back diffusion starts τ_{BD} as the upper integration bound and zero as the lower bound. To determine the mass that has left the aquitard for $\tau > \tau_{BD}$, the lower integration bound is τ_{BD}, and the upper is the final τ of interest. Calculations of μ' were verified with previously published cases for $\Gamma = \{0,\ 0.5,\ 1\}$ and the relative error was zero for Eq. 2-18a and Eq. 2-18c and less than 1 % for Eq. 2-18b.

The flux into or out of the aquitard was derived from the temporal derivative of dimensionless mass per unit area and by Fick's 1st law of diffusion. Integrating both sides of Eq. 2-11 in dimensionless space yields

$$\int_0^{\infty} \left(\frac{\partial \chi'}{\partial \tau} \right) d\zeta = \int_0^{\infty} \left(\frac{\partial^2 \chi'}{\partial \zeta^2} \right) d\zeta \quad , \tag{2-20a}$$

which simplifies to

$$\frac{\partial \mu'}{\partial \tau} = \left| -\frac{\partial \chi'}{\partial \zeta} \right|_{\zeta = 0} \quad , \tag{2-20b}$$

given Eq. 2-18b and the boundary conditions in Eq. 2-13a and Eq. 2-13c. On the left-hand side of Eq. 2-20b is the temporal change in dimensionless mass in the aquitard. At the beginning of time, the flux is instantaneously infinite so a Dirac Delta function is employed, and the dimensionless flux is

$$\varphi'(\tau) = \frac{\mu'(\tau)}{d\tau} = f(0)\cdot\left\{\frac{1}{\sqrt{\pi\tau}}\right\} + \int_0^{\tau} \frac{d}{d\gamma} f(\gamma)\cdot\left\{\frac{1}{\sqrt{\pi(\tau-\gamma)}}\right\} d\gamma \quad . \qquad \text{(2-21a)}$$

On the right-hand side of Eq. 2-20b is the change in concentration across the boundary, $\zeta = 0$, which is also the dimensionless flux

$$\varphi'(\tau) = \int_0^{\tau} f(\gamma)\left\{\frac{2(\tau-\gamma)-\zeta^2}{4\sqrt{\pi(\tau-\gamma)^5}}\cdot\exp\left(-\zeta^2 \Big/ 4(\tau-\gamma)\right)\right\} d\gamma \quad . \qquad \text{(2-21b)}$$

The dimensioned flux is given by

$$J'(t) = \frac{\varphi'(\tau) D_s' C_0}{\sqrt{A_{SZ}}} \quad . \qquad \text{(2-22)}$$

In Eq. 2-21a and Eq. 2-21b, Eq. 2-5a or Eq. 2-5c is substituted into the convolution for $f(\gamma)$. Equation 2-21a evaluated the boundary flux throughout the time scale. However, the convolution solution in Eq. 2-21b does not allow an evaluation at $\zeta = 0$. Thus, a very small value for ζ (i.e., $10^{-3} > \zeta > 10^{-4}$) was used in Eq. 2-21b to approximate the flux at the aquifer/aquitard interface. For example, $\zeta = 4.56x10^{-4}$ corresponds to $z = 2.5$ mm for $A_{SZ} = 30$ m^2. In this work, an interface depth of 2.5 to 3.5 mm was used in Eq. 2-20b. This depth was assumed to be representative of the interface, and justification for this assumption was that $\varphi'(\tau)$ obtained at a depth of 2.5 to 3.5 mm varied less than 5% from $\varphi'(\tau)$ obtained at the interface using previously published analytical solutions for $\Gamma = \{0,\ 1\}$ (see Appendix). Furthermore, finite difference methods were employed for verification purposes as well for $\varphi'(\tau)$ determined by Eq. 2-20a and at the stated depth for Eq. 2-20b for other cases $\Gamma = \{0.5,\ 2\}$. The finite difference approach used Eq. 2-5a for the boundary condition

and solved Eq. 2-11 using a central difference solution to obtain the concentration profiles, as shown in the Appendix as Eq. A-14 [*Grathwohl*, 1998]. The flux into and out of the layer with Eq. 2-20a was verified with numerical differentiation serving as the spatial derivative approximation. With two exceptions, the error was less than 5%. First, at the start of the model, $\chi(\tau = 0) = 1.0$ and $\chi'(\zeta > 0, \tau = 0) = 0$, so the flux is infinitely large at early times thereafter. For a depth of 2.5 to 3.5 mm in the aquitard, neither the convolution nor the finite difference solution could resolve an instantaneous, infinite flux so relative differences were greater than 5 %, however Eq. 2-20a did not have this problem. Second, just before back diffusion initiates $\varphi'(\tau) = 0$ there were larger than 5 % relative errors in model Eq. 2-20b and the finite difference solution in the Appendix (Eq. A-14), in that instant as well. However since the magnitude of the mass flux is so small, this error is negligible.

Finally, it is noteworthy that for this theoretical model, all of the mass that entered the aquitard eventually returned to the aquifer. This seems counter intuitive given the conceptual model of diffusion into a semi-infinite aquitard; however, once back diffusion began, transport of contaminant mass occurred only through back diffusion and downward migration. After the start of back diffusion, the imposed boundary condition at the aquifer/aquitard interface resulted in a concentration gradient that was larger than the concentration gradient at the bottom of the contaminant distribution. Therefore, the flux leaving the aquitard was larger than that driving it downward. The practical implication of this result for sites with conditions similar to those modeled here is that no sequestration of contaminant is expected within the aquitard.

Dimensionless Time

The range of τ for typical field sites needs to be established to define the modeling timescales. Given the definition of τ in Table 2-1, this requires an estimate of the ranges associated with D_s', A_{SZ}, and t. Because τ includes D_s' and R', which contain several media properties shown in Eq. 2-7 and Eq. 2-9c, and a suggested range for A_{SZ} of 10 m^2 to 1000 m^2, for 0.01 $\leq$ t $\leq$ 1,000 years, τ will range from 10^{-9} to 10^{1} in most applications.

There are two key events in time that were evaluated with the model: (1) the dimensionless time that back diffusion begins τ_{BD}, and (2) the dimensionless time that the source is exhausted by dissolution τ^*. At any time after τ_{BD}, contaminant mass leaves the aquitard due to the reversal in the concentration gradient at the aquifer/aquitard interface. Therefore, no additional mass will be loaded into the aquitard for $\tau \geq \tau_{BD}$ and τ_{BD} represents the time of maximum mass storage, $\mu'_{BD} = \mu'(\tau_{BD})$. For the $\Gamma < 1.0$ cases, the back diffusion flux will peak at τ^*, where

$$\tau^* = \begin{cases} \dfrac{-1}{(\Gamma - 1)\cdot\beta} & for \quad 0 \leq \Gamma < 1 \\ \infty & for \quad \Gamma \geq 1 \end{cases} \quad . \qquad (2\text{-}23)$$

For the $\Gamma \geq 1.0$ cases, peak back diffusion flux will occur at some time after τ_{BD}.

Source Removal

The impact of remediation on diffusion in the aquitard can be investigated by modifying the dimensionless SDM Eq. 2-5a and Eq. 2-5b to account for partial source removal following the method of *Falta et al.,* [2005a]. This modification is based on the instantaneous removal of mass fraction X from the remaining source mass by some

remedial process at time τ_R. The relative mass remaining in the source zone at τ_R, prior to the remediation i.e. $\mu(\tau_R)$, is calculated using Eq. 2-5b, and in turn is used to determine the post-remedial initial relative mass μ_R and relative concentration χ_R (Table 2-1). Likewise, these are used to calculate a new post-remedial source decay function λ_R, and a post-remedial source to aquitard mass transfer coefficient β_R (Table 2-1). Consequently, the post-remedial relative concentration and the relative mass remaining in the source zone are

$$\chi(\mathrm{T}_R) = \left[(\Gamma - 1)\beta_R \mathrm{T}_R + \mu_R{}^{(1-\Gamma)} \right]^{\frac{\Gamma}{(1-\Gamma)}} \quad , \tag{2-24a}$$

and

$$\mu(\mathrm{T}_R) = \left[(\Gamma - 1)\beta_R \mathrm{T}_R + \mu_R{}^{(1-\Gamma)} \right]^{\frac{1}{(1-\Gamma)}} \quad , \tag{2-24b}$$

respectively, where T_R is the dimensionless elapsed time after remediation (i.e., $\mathrm{T}_R = \tau - \tau_R$). For the $\Gamma = 1$ case, the remaining mass and post-remedial source concentration are given by

$$\chi(\mathrm{T}_R) = \mu(\mathrm{T}_R) = (1 - X)e^{-\beta_R T_R} \quad . \tag{2-24c}$$

The dimensionless time at which the mass remaining in the source zone after remediation is exhausted by natural dissolution becomes

$$\mathrm{T}_R{}^* = \frac{-\mu_R{}^{1-\Gamma}}{(\Gamma - 1)\beta_R} \quad for \quad 0 \le \Gamma < 1 \quad . \tag{2-25}$$

Because the solution for dimensionless flux, Eq. 2-21a, takes the derivative of the boundary equation used in the convolution, the flux is infinite at the time of

instantaneous source depletion. Integrating the Dirac Delta leads to a Heaviside step function in the post remedial solution for flux

$$\varphi'(\mathrm{T}_R) = \left[f(0) \cdot \left\{ \frac{1}{\sqrt{\pi\tau}} \right\} \right] + \left[\int_0^{\tau} \frac{d}{d\gamma} f(\gamma) \cdot \left\{ \frac{1}{\sqrt{\pi(\mathrm{T}_R - \gamma)}} \right\} d\gamma \right] + \left[H(\mathrm{T}_R - \tau^*) \cdot f(\mathrm{T}_R) - f(\tau^*) \cdot \left\{ \frac{1}{\sqrt{\pi(\mathrm{T}_R - \tau^*)}} \right\} \right] \quad . \qquad (2\text{-}26)$$

These results will be evaluated for parameter response in Chapter 3.

One Dimensional Model for Diffusion with Decay and Leakage

Dimensionless Diffusion with Decay and Leakage

An aquitard may have vertical gradients causing leakage and may degrade aqueous phase contaminants through reaction processes. The vertical gradient created by pumping can influence the amount of mass loaded into the aquitard compared to diffusion alone. Referring back to Figure 2-1, the elements of leakage and decay were added, and the 1D solutions for concentration, mass, and flux were derived.

The model development, including these additional factors, begins with conservation of mass:

$$\frac{\partial C_T'}{\partial t} + \nabla \cdot J_T' + r = 0 \quad , \qquad (2\text{-}27)$$

where C_T' is the total soil concentration in the aquitard [ML^{-3}], J_T' is total mass flux in/out of the aquitard [$ML^{-2}T^{-1}$], and r is the reaction term in the aquitard [$ML^{-}3T^{-1}$]. Assuming that mass flux occurs only in the aqueous phase, the flux can be expressed by

$$J_T' = q_z' C_w' - \theta_w D_z' \frac{\partial C_w'}{\partial z} \quad , \tag{2-28a}$$

where q_z' is the aquitard advection [LT^{-1}], and D_z' is the hydrodynamic dispersion coefficient in the aquitard [L^2T^{-1}]:

$$D_z' = a_L v_z' + D_s' \quad . \tag{2-28b}$$

where a_L is the dispersivity of the medium [L], v_z' is the seepage velocity [LT^{-1}], and D_s' is the effective diffusion coefficient [L^2T^{-1}]. The value a_L was held at 0.5 to ensure a reasonably large effect of advection in the dispersion coefficient. The seepage velocity for a saturated medium is defined as

$$v_z' = \frac{q_z'}{\theta_w} \quad , \tag{2-28c}$$

Contaminant decay is often represented by r a reaction term [$ML^{-3}T^{-1}$]:

$$r = \theta_w \lambda^* C_w' \quad , \tag{2-29a}$$

where λ^* is the effective degradation constant for decay in the aqueous phase only in a saturated medium and is defined as:

$$\lambda^* = \frac{\lambda}{\eta R} \quad , \tag{2-29b}$$

with λ representing the first-order aqueous phase degradation constant in the aquitard [T^{-1}]. Substituting Eq. 2-28a thru Eq. 2-29b into Eq. 2-27, the governing equation for 1D transport of a contaminant in the aquitard considering storage, diffusion, advection, and decay is

$$R' \frac{\partial C_w'}{\partial t} = D_z' \frac{\partial^2 C_w'}{\partial z^2} - v_z' \frac{\partial C_w'}{\partial z} - \lambda^* C_w' \quad . \tag{2-30}$$

This assumes equilibrium, reversible, and linear partitioning of the contaminant between the aquitard pore water and solid media.

Transforming the variables to dimensionless forms in Table 2-2, the dimensionless governing equation for 1D transport of a contaminant in the aquitard with leakage and decay is

$$\frac{\partial \chi'}{\partial \tau} = \frac{\partial^2 \chi'}{\partial \zeta^2} - P_e \frac{\partial \chi'}{\partial \zeta} - \Lambda \chi' \quad . \tag{2-31}$$

Table 2-2. Definitions of Dimensionless Variables with Leakage and Decay

Time	$\tau = \frac{D_z' t}{A_{SZ}}$
Source to aquitard mass transfer coefficient	$\beta = \psi \cdot \sigma \quad ; \psi = \frac{q A_{SZ} C_0}{M_0} \; ; \; \sigma = \frac{A_{SZ}}{D_z'}$
Aquitard Decay	$\Lambda = \frac{\lambda^* A_{SZ}}{D_z'}$
Peclet Number	$P_e = \frac{v_z' \sqrt{A_{SZ}}}{D_z'}$

where the definition of terms are provided in Table 2-2. A solution to in the Laplace domain is

$$\bar{\chi}'(\zeta, p) = C_1 \exp\left\{\frac{\zeta}{2}\left[P_e - \sqrt{P_e^2 + 4(p+\Lambda)}\right]\right\} \quad . \tag{2-32}$$

With the boundary conditions and initial conditions from Eq. 2-13a-c, the solution in the Laplace domain becomes

$$\bar{\chi}'(\zeta, p) = \bar{\chi}(p) \exp\left(\frac{\zeta}{2} P_e\right) \exp\left[-\zeta \sqrt{p + \left(\frac{P_e^2}{4} + \Lambda\right)}\right] \quad , \tag{2-33}$$

which is in the form of Eq. 2-15. Using the Delay Theorem

$$L^{-1}\left\{F\left(p+\left(\frac{P_e^2}{4}+\Lambda\right)\right)\right\}=L^{-1}\left\{F\left(p\right)\right\}\cdot\exp\left[-\left(\frac{P_e^2}{4}+\Lambda\right)\tau\right] \quad , \qquad (2\text{-}34)$$

[Abramowitz & Stegun, 1970], and applying the convolution principle, a general solution can be written as:

$$\chi'(\zeta,\tau)=\exp\left(\frac{P_e}{2}\zeta\right)\frac{\zeta}{2\sqrt{\pi}}\cdot$$

$$\int_0^\tau f(\gamma)\left[\frac{1}{\sqrt{(\tau-\gamma)^3}}\exp\left[-\frac{\zeta^2}{4(\tau-\gamma)}\right]\exp\left[-\left(\frac{P_e^2}{4}+\Lambda\right)(\tau-\gamma)\right]\right]d\gamma\,. \quad (2\text{-}35)$$

Dimensionless Mass Storage and Mass Flux with Leakage and Decay

We recognize that a solution for Eq. 2-31 in Laplace space is Eq. 2-33. Integration over the entire domain gives

$$\bar{\mu}'(p)=\int_0^\infty \bar{\chi}'(\zeta,p)\,d\zeta=\bar{\chi}(p)\cdot\frac{1}{\sqrt{p+\left(\frac{P_e^2}{4}+\Lambda\right)}-\frac{P_e}{2}} \quad . \qquad (2\text{-}36)$$

The Laplace Inversion is in the form of

$$L^{-1}\left\{\frac{1}{\sqrt{p}+a}\right\}=\frac{1}{\sqrt{\pi\tau}}-a\exp\left(a^2\tau\right)erfc\left(a\sqrt{\tau}\right) \quad , \qquad (2\text{-}37)$$

Abramowitz & Stegun [1970], with $a=-P_e/2$. Applying convolution and delay theorems gives the dimensionless mass per unit area including leakage and decay

$$\mu'(\tau)=\int_0^{\tau} f(\gamma)\left[\left[\frac{1}{\sqrt{\pi(\tau-\gamma)}}+\frac{P_e}{2}\exp\left[\frac{P_e^{\,2}}{4}(\tau-\gamma)\right]\cdot erfc\left(-\frac{P_e}{2}\sqrt{(\tau-\gamma)}\right)\right]\cdot\right.$$

$$\left.\exp\left(-\left[\frac{P_e^{\,2}}{4}+\Lambda\right](\tau-\gamma)\right)\right]d\gamma \qquad . \tag{2-38}$$

The dimensionless mass flux was obtained by taking the temporal derivative of mass by starting with the dimensionless governing Eq. 2-31 and moving decay over to the left-hand-side of the equation. Integrating both sides in dimensionless space yields

$$\frac{\partial\mu'}{\partial\tau}+\Lambda\mu'=\left|-\frac{\partial\chi'}{\partial\zeta}+P_e\chi'\right|_{\zeta=0} \qquad , \tag{2-39}$$

due to Eq. 2-18b and the boundary condition (Eq. 2-13b), where the terms on the left-hand side are the temporal change in dimensionless mass, which in the absence of decay, must be equal to what is coming in or leaving through the interface. In the presence of decay, the second term corrects for the amount degraded in dimensionless time.

Using Eq. 2-36 the terms are grouped $\bar{\chi}(p)\,p$ such that Eq. 2-37 remains applicable, and then the temporal derivative is identical to Eq. 2-38, with the exception that $f(\gamma)$ is substituted by its derivative $\frac{df(\gamma)}{d\gamma}$. For $\gamma=0$ the aquifer concentration makes a step change, such that $\frac{df(\gamma)}{d\gamma}=f(0)\delta(\tau)$ is a Dirac impulse at that time such that

$$\frac{\mu'(\tau)}{d\tau} = f(0)\cdot\left[\frac{-1}{\sqrt{\pi\tau}} + \frac{P_e}{2}\exp\left[\frac{P_e^2}{4}\tau\right]\cdot erfc\left[-\frac{P_e}{2}\sqrt{\tau}\right]\cdot\exp\left(-\left[\frac{P_e^2}{4}+\Lambda\right]\tau\right)\right]+$$

$$+\int_0^{\tau}\frac{df(\gamma)}{d\gamma}\cdot\left[\left(\frac{-1}{\sqrt{\pi(\tau-\gamma)}}\right)+\frac{P_e}{2}\exp\left[\frac{P_e^2}{4}(\tau-\gamma)\right]\cdot erfc\left[-\frac{P_e}{2}\sqrt{(\tau-\gamma)}\right]\right.$$

$$\left.\exp\left(-\left[\frac{P_e^2}{4}+\Lambda\right](\tau-\gamma)\right)\right]d\gamma \qquad . \qquad (2\text{-}40)$$

Therefore the left-hand side of Eq. 2-39 is the dimensionless flux given by the change in dimensionless mass per unit area in the aquitard in dimensionless time,

$$\varphi'(\tau) = \frac{\mu'(\tau)}{d\tau} + \Lambda\mu'(\tau) \qquad , \qquad (2\text{-}41a)$$

And the right-hand side of Eq. 2-39 is the dimensionless flux given by the change in concentration

$$\varphi'(\tau) = \left|-\frac{\partial\chi'}{\partial\zeta} + P_e\chi'\right|_{\zeta=0} \qquad . \qquad (2\text{-}41b)$$

The dimensioned flux is given by

$$J'(t) = \frac{\varphi'(\tau)D_z'C_0}{\sqrt{A_{SZ}}} \qquad . \qquad (2\text{-}42)$$

The solution in Eq. 2-41a will evaluate the dimensionless mass flux over the complete timescale. However, a solution for Eq. 2-41b could not be obtained analytically so the finite difference solution for flux (see the Appendix) was used to verify Eq. 2-41b and resulted in less than 5% error. The solutions for dimensionless mass and flux were also verified with the previous solutions in Chapter 2 by setting $P_e = 0$ and $\lambda' = 0$ with zero error.

Source Removal with Leakage and Decay

The source removal SDM is unaffected by the addition of leakage or decay. However, the solution for dimensionless flux in Eq. 2-40 uses a derivative of the source function $\frac{df(\gamma)}{d\gamma}$. For any case $\Gamma \le 0.5$ where the source is eventually exhausted, or for any case with instantaneous source depletion (e.g. remediation or source isolation), the derivative will be infinite at that time and a Dirac delta function is used $f(\tau^*)\delta(\tau^*)$ and $f(\tau_R)\delta(\tau_R)$, respectively. After integration in the convolution, the Dirac function becomes a Heaviside step function, and the post source depletion flux is

$$\varphi'(\mathrm{T}_R) = \left[\frac{\mu'(\mathrm{T}_R)}{d\tau}\right] + \left[\Lambda\mu'(\mathrm{T}_R)\right] + \left[H(\mathrm{T}_R - \tau_R)\Delta f(\tau_R)\cdot \right.$$

$$\left\{\frac{-1}{\sqrt{\pi(\mathrm{T}_R - \tau_R)}}\cdot \exp\left(-\frac{Pe^2}{4} + \Lambda\right)(\mathrm{T}_R - \tau_R) + \frac{Pe}{2}\cdot \right.$$

$$\left.\left.\exp\left[\frac{Pe^2}{4}(\mathrm{T}_R - \tau_R)\right]\cdot erfc\left(-\frac{Pe}{2}\sqrt{(\mathrm{T}_R - \tau_R)}\right)\right\}\right] \quad . \qquad (2\text{-}43)$$

where $H(\mathrm{T}_R - \tau_R) = \begin{cases} 1, & \mathrm{T}_R \ge \tau_R \\ 0, & \mathrm{T}_R < \tau_R \end{cases}$ is the Heaviside step function, $\Delta f(\tau_R) = f(\mathrm{T}_R) - f(\tau_R)$ is the source function change due to source depletion. These functions can be used to predict concentration profiles and mass flux from aquitards under vertical advection (leakage) and first-order aqueous decay processes.

The simplifying assumptions used in the diffusion with decay and leakage model development included an assumed homogeneity of the aquitard. In fact, aquitard parameters like a_L, v_z', η, and ϕ can be highly variable but for a screening level

model, this assumption is considered appropriate. Furthermore, the use of constant parameters eliminated the potential flow variability due to fractures or highly interconnected pores, which was not the focus of this work.

CHAPTER 3
CONCENTRATION, MASS, AND FLUX RESULTS

Dimensionless Results for Diffusion

Aquitard Concentration Profiles

There are two main parameters that affect the model results: Γ and β. The effects of Γ on the model were investigated first, and then the effects of β were explored. Aquifer and source properties for the set of simulations featured in Figure 3-1 and Figure 3-2 are shown in Table 3-1, representing a hypothetical PCE spill and are similar to those used by *Falta et al.* [2005a]. Aquitard parameters used in these simulations are presented in Table 3-2.

One method to evaluate the effects of source dissolution on aquitard storage and release is to construct profiles of χ' as a function of depth using equation (9). Figure 3-1a illustrates the SDM for $\Gamma = \{0,\ 0.5,\ 1,\ 2\}$ and Figures 3-1b, 3-1c, and 3-1d illustrate the depth profiles of χ' for $\Gamma = \{0.5,\ 1,\ 2\}$, respectively. As Γ increased, the profiles in Figures 3-1b through 3-1d show reduced concentrations in the aquitard for a given time and depth due to the reduced concentration at the aquifer/aquitard boundary. Likewise, the peak of the aquitard concentration χ'_{peak} was reduced with less penetration as Γ increased. For example, at $\tau = 0.0005$, $\chi'_{peak} = \{0.25,\ 0.21,\ 0.15\}$ for $\Gamma = \{0.5,\ 1,\ 2\}$, respectively; and these values of χ'_{peak} occurred at depths of $\zeta = \{0.015,\ 0.014,\ 0.012\}$, respectively.

In Figure 3-2, the χ' depth profiles are shown at specific events in time (i.e., τ_{BD} and τ^*) as a function of Γ and β. The highest concentration in the aquitard is

achieved at τ_{BD}. Figure 3-2a shows that the penetration and magnitude of χ' at $\tau = \tau_{BD}$ decreased as Γ and β increased. For example, with $\beta = 3500$ and at $\zeta = 0.025$, $\chi' = \{0.30,\ 0.18,\ 0.13\}$ for $\Gamma = \{0,\ 1,\ 2\}$, respectively. Likewise, with $\Gamma = 1$ and at $\zeta = 0.025$, $\chi' = \{0.372,\ 0.180,\ 0.042\}$ for $\beta = \{500,\ 3500,\ 11000\}$, respectively. In Figure 3-2b, the concentration profiles at $\tau = \tau^*$ for cases with $\Gamma < 1$ are shown. As Γ increased, concentrations in the aquitard were reduced due to three factors: (1) a more rapid decline in χ, (2) τ_{BD} decreased as Γ increased, resulting in more time for back diffusion to remove mass, and (3) τ^* increased as Γ increased, resulting in more time for downward diffusion of mass.

For $\Gamma = 0$, $\chi = 1.0$ was maintained until τ_{BD}, which occurred at τ^* (and hence $\chi'_{peak} = 1$ at $\zeta = 0$). For the other cases, $\chi'_{peak} = \{0.407,\ 0.202,\ 0.078,\ 0.013\}$. Shown in Figure 4a is the SDM for $\beta = \{500,\ 3500,\ 11000\}$ and $\Gamma = 1$; and in Figures 3b through 3d the resultant χ' depth profiles. Similar to the influence of Γ, χ' decreased as β increased as a result of the more rapid reduction in the concentration gradient. For example, at $\tau = 0.0002$, $\chi = \{0.94,\ 0.49,\ 0.11\}$ for $\beta = \{500,\ 3500,\ 11000\}$, respectively. This resulted in a lower χ' for a given time and depth. At $\tau = 0.0005$ and at a depth of $\zeta = 0.025$, $\chi' = \{0.375,\ 0.181,\ 0.091\}$ for $\beta = \{500,\ 3500,\ 11000\}$, respectively.

To add context to these results in terms of actual site conditions, the dimensionless results in Figure 3-1 were converted to dimensioned time and space using our hypothetical PCE site values (Tables 3-1 and 3-2).

Table 3-1. Aquifer parameters used in the model for DNAPL source dissolution.

	C_0 (mg l^{-1})	M_0 (kg)	q (m d^{-1})	A_{SZ} (m^2)	ψ (d^{-1})
Fig 2,3,5a,6,7a-b,7e-f	150	1620	0.0548	30	1.52 $x10^{-4}$
Fig 3,4,5b,6,7c-d	150	1620	0.00782	30	2.19 $x10^{-5}$
			0.0548		1.52 $x10^{-4}$
			0.172		4.78 $x10^{-4}$

Table 3-2. Aquitard media values used in model for diffusion.

	$D(PCE)$ (m^2 d^{-1})	ϕ	ρ_b (l kg^{-1})	K_d (g ml^{-1})	η	R'	D_s'/R' (m^2 d^{-1})	σ (d)
Fig 2,3,4,5a,6,7a-d	1.46 $x10^{-5}$	1.4	1.2	2.6	0.45	8.0	1.30 $x10^{-6}$	2.30 $x10^{7}$
Fig 3,4,5b,6,7e-f	1.46 $x10^{-5}$	1.4	1.25	0.04	0.35	1.14	9.13 $x10^{-6}$	3.28 $x10^{6}$
			1.2	2.6	0.45	8.0	1.30 $x10^{-6}$	2.30 $x10^{7}$
			1.1	12.1	0.55	25.1	4.15 $x10^{-7}$	7.22 $x10^{7}$

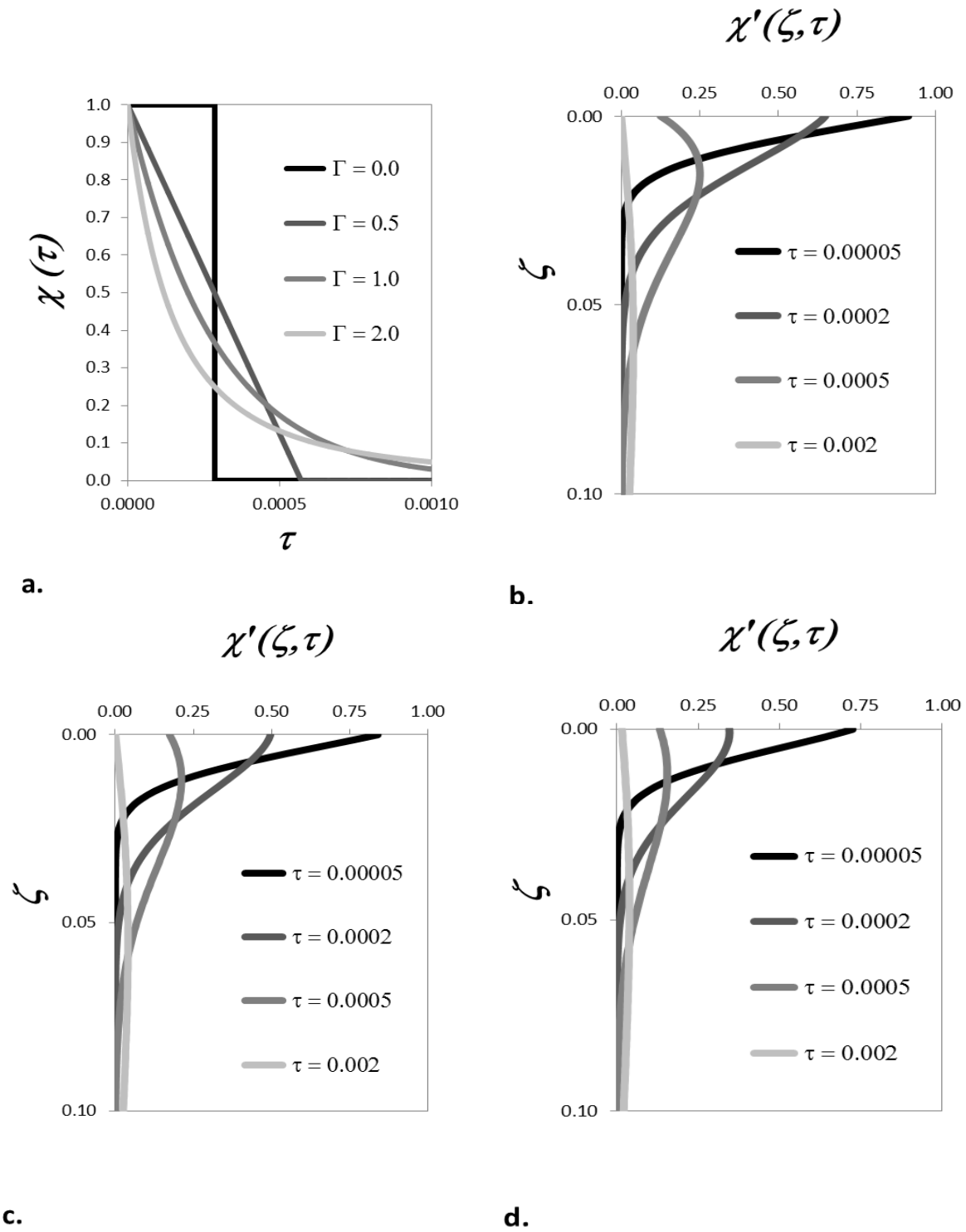

Figure 3-1. SDM and resultant χ' depth profiles for $\beta = 3500$ and $\Gamma = \{0,\ 0.5,\ 1,\ 2\}$.

Note: (a) SDM as a function of Γ for $\Gamma = \{0,\ 0.5,\ 1,\ 2\}$ and $\beta = 3500$. χ' depth profiles in the aquitard are shown for (b) $\Gamma = 0.5$, (c) $\Gamma = 1$, (d) $\Gamma = 2$.

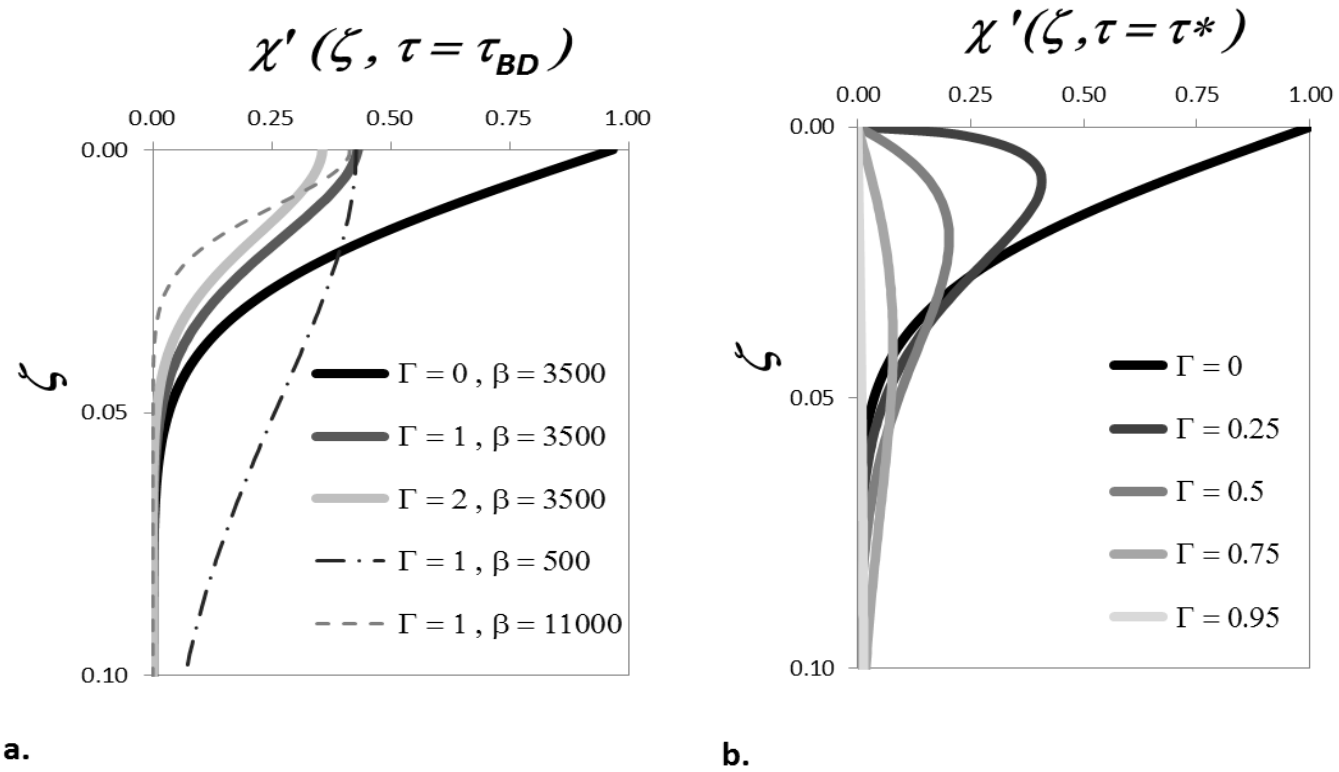

Figure 3-2. χ' depth profiles when back diffusion begins and source is exhausted.

Note: (a) χ' depth profiles are shown at the time back diffusion begins, τ_{BD}, as a function of Γ (solid lines) with $\beta = 3500$; and as a function of β (dashed lines) with $\Gamma = 1$. (b) χ' depth profiles are shown at the time the source is exhausted, τ^* as a function of Γ.

Results are reported as soil concentrations similar to previous back diffusion field studies, which is the sum of the mass in solution and the sorbed mass. For illustration, at $t = 31.6$ yr $(\tau = 0.0005)$, $C'_{peak} = \{113,\ 95,\ 70\}$ mg kg^{-1} which occurred

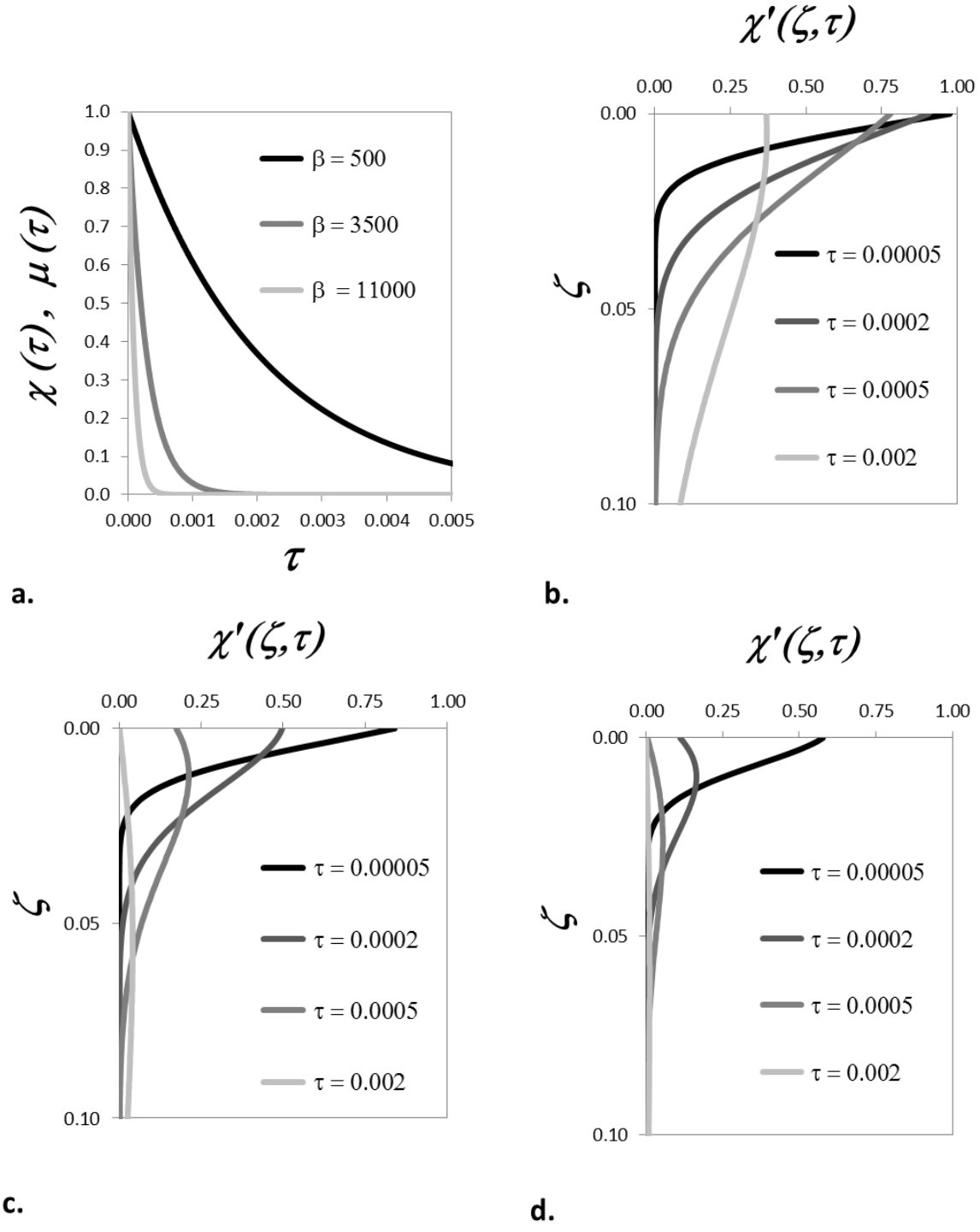

Figure 3-3. SDM and resultant χ' depth profiles for $\Gamma = 1$.

Note: (a) SDM as a function of β for $\beta = \{500,\ 3500,\ 11000\}$ and $\Gamma = 1$. χ' depth profiles are shown for (b) $\beta = 500$, (c) $\beta = 3500$, and (d) $\beta = 11000$.

at depths of $z = \{0.08,\ 0.07,\ 0.06\}$ m for $\Gamma = \{0.5,\ 1,\ 2\}$, respectively. Evaluating the influence of β on concentration in dimensioned time and space, however, is not as straight forward. At $z = 0.14$ m $(\zeta = 0.025)$ and $t = 31.6$ yr $(\tau = 0.0005)$, the total soil concentration (aqueous and solid phase) $C_T' = \{169,\ 82,\ 25\}$ mg kg^{-1} for $\beta = \{500,\ 3500,\ 11000\}$, respectively; where values of β were obtained considering $q = \{0.0078,\ 0.055,\ 0.17\}$ m d^{-1}, respectively, $R' = 8.0$, and all other parameters defined as shown in Table 3-1 and Table 3-2. However the same dimensionless profiles for $\beta = \{500,\ 3500,\ 11000\}$ occur when β results from $R' = \{1.14,\ 8.0,\ 25.1\}$, respectively, $q = 0.0548$ m d^{-1}, and all other parameters equal to the same previous values (Tables 3-1 and 3-2). These values of R may occur, for example, considering typical properties associated with sandy-silt, silt, and silty-clay aquitards. Because τ is a function of R', the results at $\tau = 0.0005$ in dimensioned time occur at $t = \{4.5,\ 32,\ 99\}$ yr for $R' = \{1.14,\ 8.0,\ 25.1\}$, respectively. Consequently, at the same depth of $z = 0.14$ m$(\zeta = 0.025)$, $C_T' = \{24,\ 82,\ 95\}$ mg kg^{-1}, for $R' = \{1.14,\ 8.0,\ 25.1\}$ respectively, demonstrating an increase in total mass as β increased due to sorption. Thus, increasing Γ decreased the aquitard contaminant concentrations and the depth of contaminant penetration. Likewise, increasing β by increasing ψ, decreased aquitard contaminant concentrations and the depth of contaminant penetration. However, when β increased due to an increase in σ (via increased R'), solid phase concentrations increased (increasing total concentrations), but the contaminant penetration depth decreased.

Aquitard Mass Storage

The risk of back diffusion is dependent on the contaminant mass present in the aquitard at any given point in time. As expected from the results in Figure 3-1, as Γ increased, the amount of mass stored in the aquitard decreased. Specifically, using equation (10b) to integrate the χ' depth profiles in Figure 3-1 for $\tau = 0.0005$, $\mu' = \{0.01,\ 0.009,\ 0.007\}$ for $\Gamma = \{0.5,\ 1,\ 2\}$, respectively. As Γ increased, less mass entered the aquitard due to the more rapid decrease in source concentration and thus a reduced diffusion gradient. At later times most of the mass in the aquitard had been released back to the aquifer, so the profiles were flat and the dimensionless mass remaining was less variable. For example, at $\tau = 0.002$, $\mu' = \{0.0038,\ 0.0039,\ 0.0039\}$ for $\Gamma = \{0.5,\ 1,\ 2\}$, respectively. Higher μ' in the latter two cases results from higher concentrations at the boundary for longer durations (e.g., Figure 3-1a for $\Gamma \geq 1$), reducing the back diffusion gradient, which in turn yields slightly more dimensionless mass at this point in time.

To evaluate the maximum mass storage μ'_{BD}, the χ' depth profiles at τ_{BD} (Figure 3-2a) were integrated using Eq. 2-18c, and the results are shown in Figure 3-4a as a function of Γ and in Figure 3-4b as a function of β. As Γ increased from 0 to 10, μ'_{BD} decreased from 0.019 to 0.0039. Likewise, as β increased from 250 to 11000, μ'_{BD} decreased from 0.039 to 0.006. Figure 3-4a illustrates the error that might occur in estimates of μ'_{BD} when assuming $\Gamma = 0$, as is often done, for those sites with characteristics better represented by $\Gamma > 0$. As further illustration of this point, Table 3-

3 lists the relative reduction in μ'_{BD}, defined as $1-\left[\mu'_{BD}(\Gamma)\Big/\mu'_{BD}(\Gamma=0)\right]$, as a function of Γ. The relative reduction in maximum stored mass ranged from 36 to 60% for $0.5\le\Gamma\le 2$. Thus, while the $\Gamma=0$ case is often used as a conservative approach, it will likely over predict the aquitard stored mass, thus increasing the perceived risk of back diffusion, if this assumption is not valid.

Table 3-3. Relative reduction in maximum mass stored in aquitard, $\beta=3500$.

Γ	$1-\left[\mu'_{BD}(\Gamma)\Big/\mu'_{BD}(\Gamma=0)\right]$
0.0	0.00
0.25	0.25
0.5	0.36
0.75	0.43
1.0	0.48
1.25	0.52
2.0	0.60
4.0	0.71
10.0	0.81

Longevity and Hysteresis

Contaminated site diffusion processes are hysteretic because they are gradient driven, and loading occurs much more rapidly than release. To investigate this behavior, τ_{BD} is plotted as a function of Γ and β in Figure 3-5. Starting at $\Gamma=0$, τ_{BD} increased to its peak at $\Gamma=0.25$, then decreased as Γ increased (Figure 3-4a). In general, as Γ increases, the source-zone architecture results in a reduced forward concentration gradient at the aquifer-aquitard interface, which in turn results in an earlier back diffusion time. When $\Gamma\ge 1$ the source, in theory, is never completely exhausted by dissolution; consequently, back diffusion lasts for an infinitely long time.

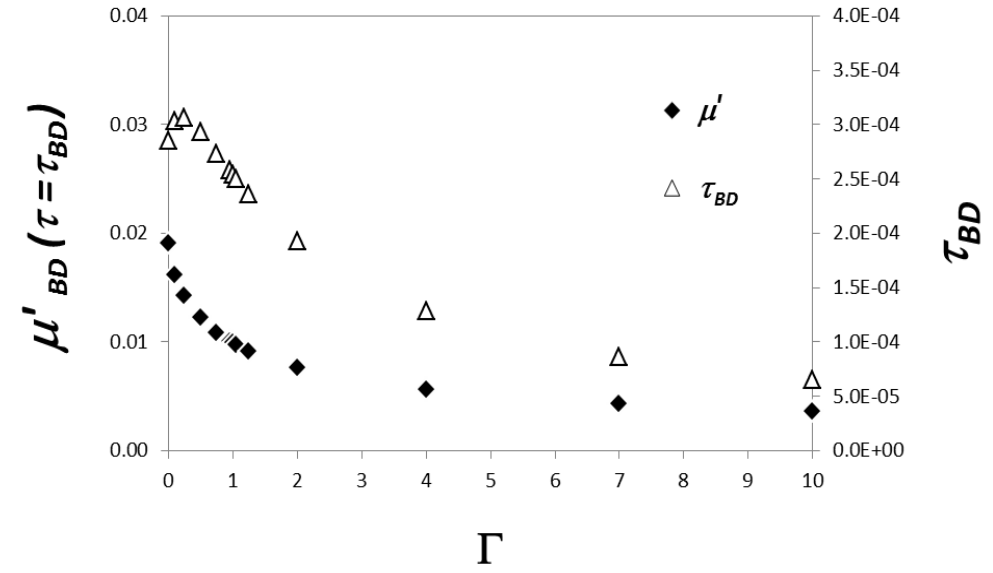

a.

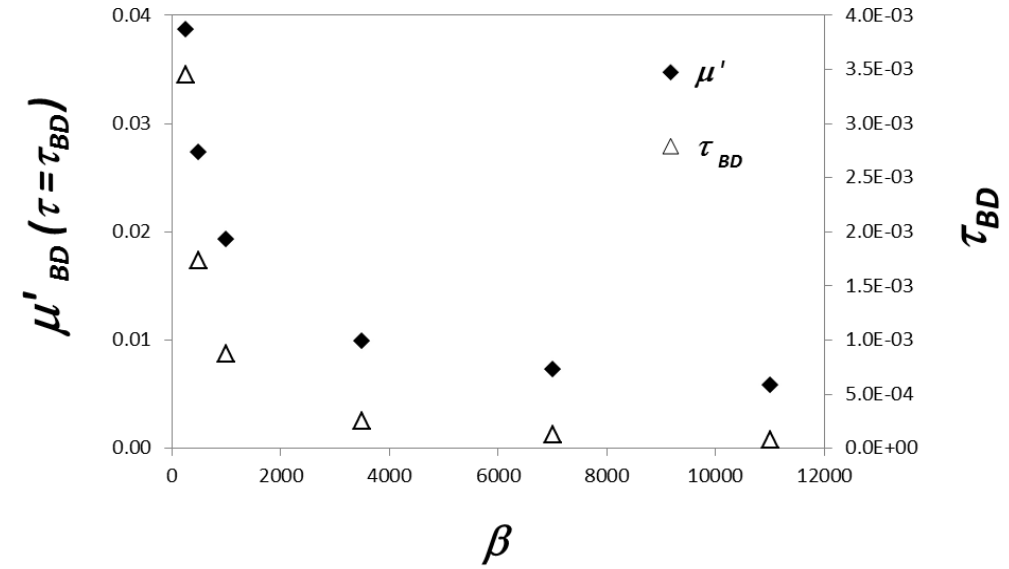

b.

Figure 3-4. Maximum mass stored in the aquitard.

Note: (a) Maximum mass stored in the aquitard (μ'_{BD}) and τ_{BD} as a function of Γ, $\beta = 3500$. (b) μ'_{BD} and τ_{BD} as a function of β, $\Gamma = 1$.

Similar to Γ, as β increases, back diffusion begins earlier (Figure 3-4b). When β was increased by more rapid source dissolution, back diffusion flux initiated earlier

and less mass was loaded into the aquitard. However, if β was increased due to increased aquitard sorption only, τ_{BD} decreased, but that value corresponded to the same dimensioned time since τ is also a function of R (Table 2-1). Thus, aquitard sorption has no effect on the time when mass loading into the aquitard ends

The hysteresis of contaminant mass loading and release is shown in Figure 3-5, where the relative mass in the aquitard is plotted as a function of τ for $\Gamma = \{0.5,\ 1,\ 2\}$ and $\beta = 3500$, and as a function of τ for $\Gamma = 1$ and $\beta = \{500,\ 11000\}$. Relative mass in these figures was scaled to μ'_{BD} for each specific case. As τ increased, the contaminant mass was loaded relatively rapidly into the aquitard due to the high concentration gradients, peaked at the start of back diffusion, and was slowly released thereafter. This hysteretic behavior is demonstrated in the linear scale overlay. Overall, Γ had a minimal effect on the timescale of the loading and release of mass in the aquitard, while β had a stronger influence in the model results. As β decreased, both the loading and release times increased.

Aquitard Source Functions

A convenient means to evaluate the risk of contaminant source mass in subsurface systems is through source functions, defined as the relative relationship between contaminant flux and mass (e.g., *Rao et al*., [2002]). Likewise, aquitard source functions can be defined as the relationship between the relative back diffusion flux and the contaminant mass in the aquitard. Aquitard source functions were constructed by converting μ' and φ' to dimensioned values using Eq. 2-19 and Eq. 2-22, respectively where $M'(t)$ is aquitard mass per unit area [ML^{-2}] and $J'(t)$ is back diffusion flux

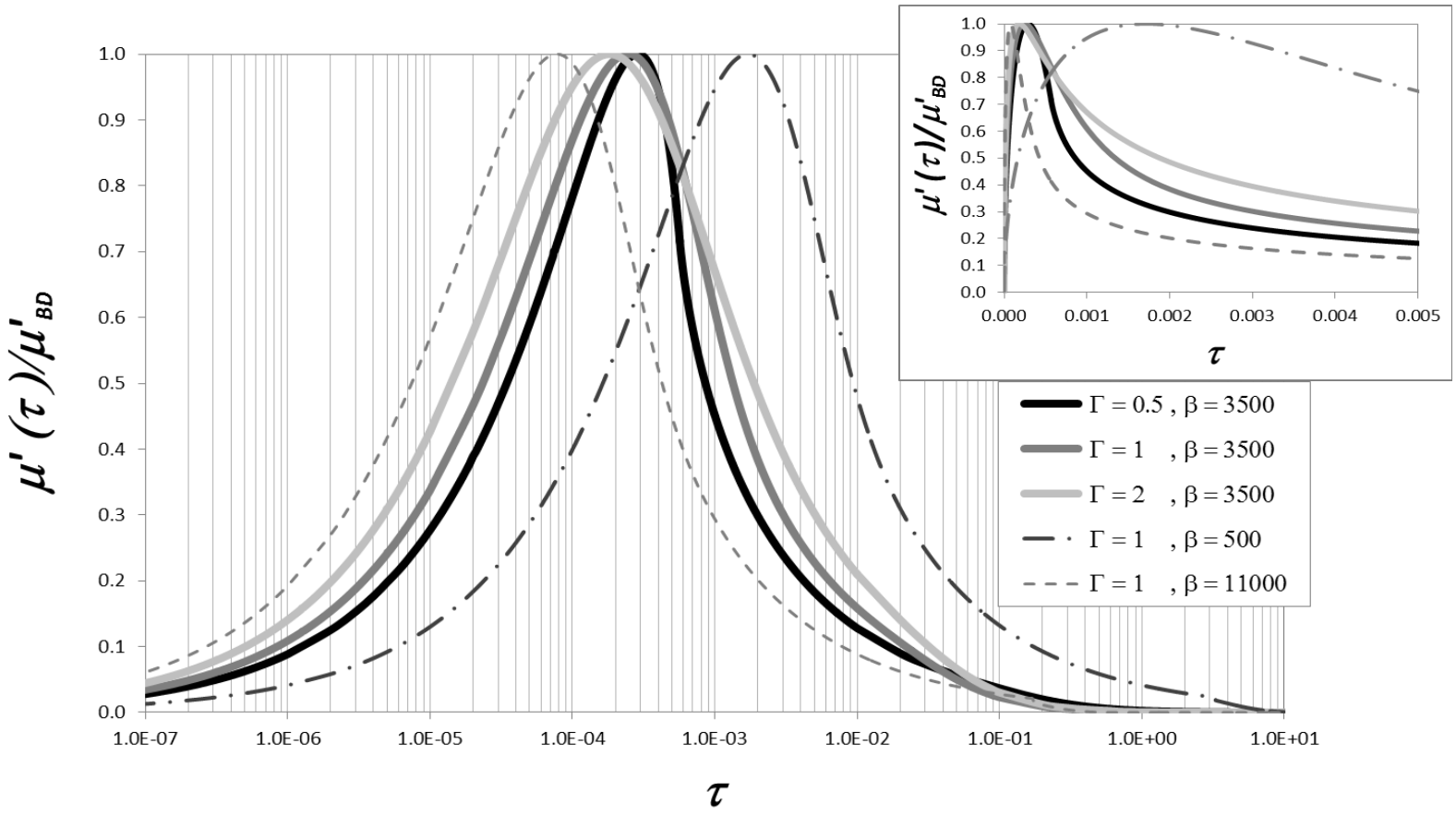

Figure 3-5. Relative mass in the aquitard as a function of τ.

Note: Relative mass in the aquitard as a function of τ in log scale for $\Gamma = \{0.5,\ 1,\ 2\}$ (solid lines), $\beta = 3500$; and as a function of τ in log scale for $\beta = \{500,\ 11000\}$ and $\Gamma = 1$ (dashed lines); overlay is plotted in a linear time scale.

[$ML^{-2}T^{-1}$]. Aquitard source functions are shown in Figure 3-6 as a function of Γ and β, along with the corresponding dimensioned times series for M' (dashed lines) and J' (solid lines). The ratio M_0/A_{SZ} was used to normalize M', while $J_0 = qC_0$ was used to normalize J'. Temporal progression can also be followed in the aquitard source functions themselves, which begin at τ_{BD} on the right, and increases in time from there to the left.

Figure 3-6a presents aquitard source functions for $\Gamma = \{0,\ 0.5,\ 1,\ 2\}$ and $\beta = 3500$, and illustrates three distinct shapes. For $\Gamma = 0$, the boundary concentration jumped from $\chi(\tau < \tau^*) = 1.0$ to $\chi(\tau \geq \tau^*) = 0$ instantaneously, resulting in an infinite flux at $\tau = \tau^* = \tau_{BD}$. In contrast, the back diffusion flux peaked after τ_{BD} for cases with $\Gamma > 0$ because the concentration in the aquitard and the SDM boundary were equal at τ_{BD}, resulting in no flux. For cases with $0 < \Gamma < 1.0$ (as illustrated by $\Gamma = 0.5$), a sharp but finite peak occurred when the source was exhausted at τ^*. For $\Gamma \geq 1$ (as illustrated by $\Gamma = 1$ and $\Gamma = 2$), aquitard source functions were more curvilinear paths resulting from the more gradual decay of the DNAPL source-zone flux. An important feature evident in Figure 3-6a is that as Γ increased, the relative mass and flux decreased, indicating reduced risk due to back diffusion. Specifically, as Γ increased from 0 to 2, the maximum relative mass decreased from 1.04×10^{-3} to 4.3×10^{-4}, respectively; while the maximum relative flux decreased from ∞ to 1.3×10^{-4}, respectively. Moreover, in all cases, the mass per unit area stored in the aquitard was three or more orders of magnitude less than the initial source zone mass per unit area; and the back diffusion flux, with the exception of the $\Gamma = 0$ case, was three or more orders of magnitude less

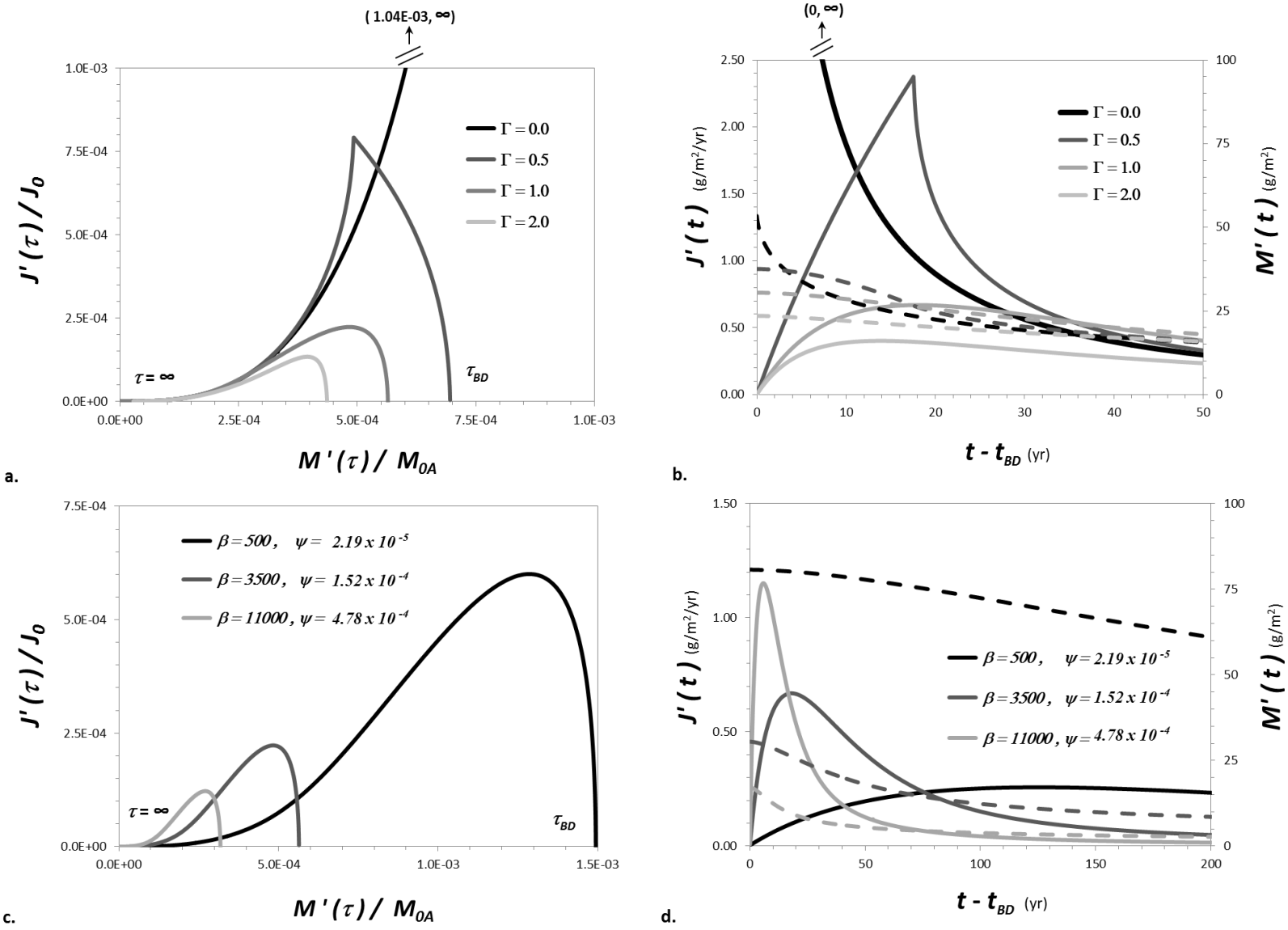

Figure 3-6. Aquitard source functions.

Note: (a) Aquitard source functions for $\Gamma = \{0,\ 0.5,\ 1,\ 2\}$ and $\beta = 3500$. (b) Dimensioned mass storage and mass flux time series for (a). (c) Aquitard source functions for $\beta = \{500,\ 3500,\ 11000\}$ and $\Gamma = 1$, where β is varied by q [m d^{-1}], shown as ψ [d^{-1}]. (d) Dimensioned mass storage and mass flux time series for (c).

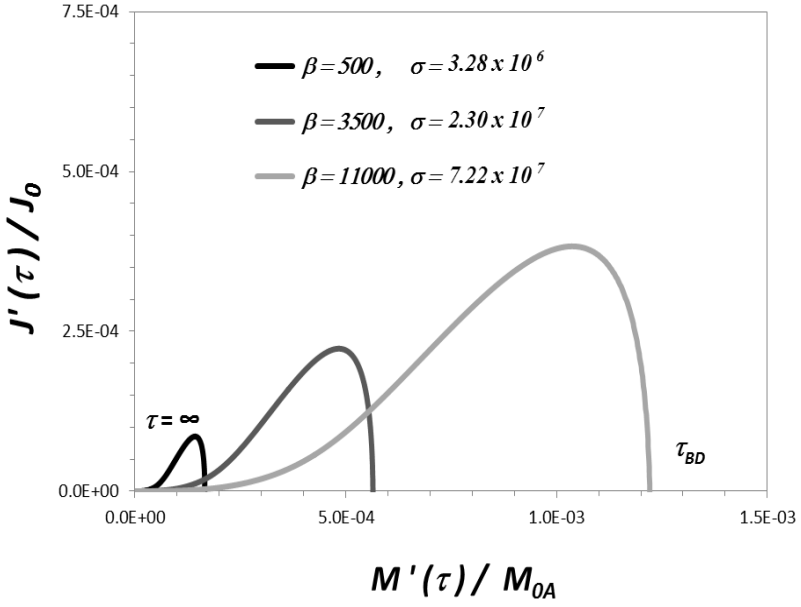

e.

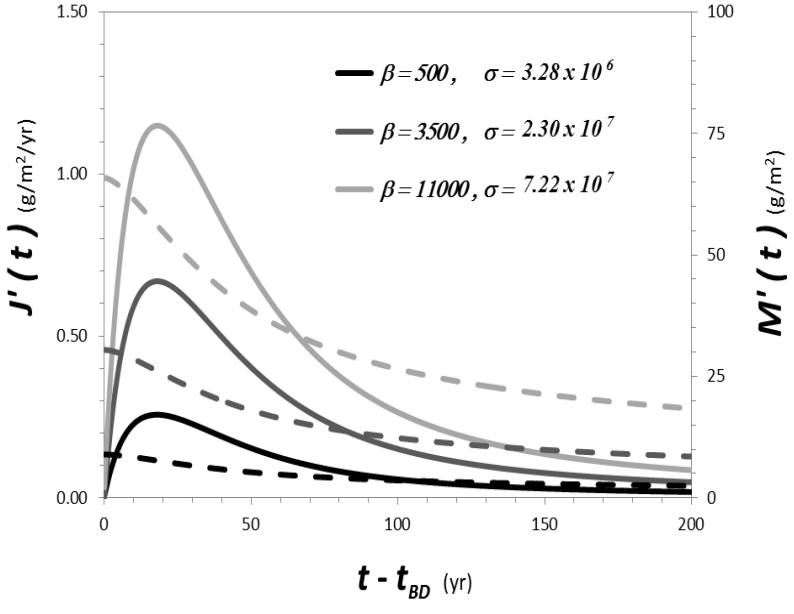

f.

Figure 3-6. Continued.

Note: (e) Aquitard source functions for $\beta = \{500,\ 3500,\ 11000\}$ and $\Gamma = 1$, where β is varied by R', shown as σ [d]. (f) Dimensioned mass storage and mass flux time series for (e). Dashed lines are mass (M', right y-axis), solid lines are flux (J', left y-axis).

than the initial source zone flux.

The results from Figure 3-6a were converted to dimensioned flux (solid lines) and dimensioned mass per unit area

(dashed lines), and plotted as a function of elapsed dimensioned time from the start of back diffusion (Figure 3-6b). Similar to the results in Figure 3-6a, as Γ increased the peak mass and mass flux decreased. The rates of decrease, however, varied as a function of Γ. For example, within the first ten years after t_{BD}, the order of J' as a function of Γ was: $J'|_{\Gamma=0} > J'|_{\Gamma=0.5} > J'|_{\Gamma=1} > J'|_{\Gamma=2}$. By 250 years after t_{BD} (offscale in Figure 3-6b), the order was reversed, and $J' < 0.05$ g m^{-2} yr^{-1} for all cases of Γ. Additionally, comparing the $\Gamma = 0$ result to that of $\Gamma = 1$, 10 years after t_{BD} the back diffusion flux was 68 % greater for $\Gamma = 0$, than for a site with $\Gamma = 1$. However, 100 years after τ_{BD}, $\Gamma = 0$ resulted in 30 % less flux than $\Gamma = 1$. This is due to the more rapid removal of mass by the increased flux in the $\Gamma = 0$ case at earlier times.

Since $\beta = \psi \cdot \sigma$, the effect of β on aquitard source functions was investigated by separately exploring the impacts of ψ and σ. In Figure 3-6c, aquitard source functions are shown for $\Gamma = 1$ and $\beta = \{500,\ 3500,\ 11000\}$. These values of β correspond to $\psi = \{2.19\text{x}10^{-5},\ 1.52\text{x}10^{-4},\ 4.78\text{x}10^{-4}\}$ d^{-1}, and were generated using $q = \{0.0078,\ 0.055,\ 0.17\}$ m d^{-1}, and the other parameters as shown in Table 3-1. As β increased from $\beta = 500$ ($\psi = 2.19x10^{-5}$ d^{-1}) to $\beta = 11000$ ($\psi = 4.78\text{x}10^{-4}$ d^{-1}), the maximum relative mass decreased from $1.5x10^{-3}$ to $3.2x10^{-4}$, and the maximum relative flux decreased from $6.0x10^{-4}$ to $1.2x10^{-4}$. Moreover, in all cases the aquitard mass per unit area and flux were at least three orders of magnitude less than the source mass per unit area and flux. Similar results are expected for changes in C_0 and M_0 that lead to an

increase in ψ and hence β. Variations in A_{SZ} affect ψ, σ, and τ; and the resulting impacts on aquitard mass and flux are more complex and not shown here.

Figure 3-6d shows the dimensioned time series for M' and J' corresponding to the dimensionless data in Figure 3-6c. Comparison of Figures 3-6c and 3-6d for $\beta = 500$ ($\psi = 2.19x10^{-5}$ d^{-1}) indicated that while this case has the highest relative flux, it had the lowest dimensioned flux. This was due to the fact that J' is normalized to a low initial source flux resulting from the low groundwater velocity in this case. Comparing the case of $\beta = 500$ ($\psi = 2.19x10^{-5}$ d^{-1}) to the others shown in Figure 3-6d, the source dissolved more slowly, which generated a stronger forward diffusion gradient over a longer time and reduced the gradient for back diffusion. Thus, the $\beta = 500$ ($\psi = 2.19x10^{-5}$ d^{-1}) case had the greatest M' and the lowest J' for $t > t_{BD}$. This illustrates a case where there may be a large amount of mass in the aquitard, but the back diffusion flux is low, resulting in low, but perhaps prolonged risk. Conversely, $\beta = 11000$ ($\psi = 4.78x10^{-4}$ d^{-1}) represents a site with a high q, that dissolves the source more rapidly, resulting in less mass within the aquitard, but higher back diffusion flux (Figure 3-6d). This represents a greater short-term risk, but a lower long-term risk. Finally, it is worth noting that the magnitude of the mass storage in Figure 3-6d is in the same range as that calculated by *Chapman and Parker* [2005] for an industrial site in Connecticut.

Changes in retardation factors associated with changes in aquitard media are evaluated in the aquitard source functions shown in Figure 3-6e for $\Gamma = 1$ and $\beta = \{500,\ 3500,\ 11000\}$. These values of β correspond to

$\sigma = \{3.28\text{x}10^{6},\ 2.30\text{x}10^{7},\ 7.22\text{x}10^{7}\}$ d, and represent the dissolution of a PCE source over silty-sand $(R' = 1.14)$, silt $(R' = 8.0)$, and silty-clay $(R' = 25.1)$ aquitards, with the modeling parameters shown in Table 3-2. The results showed that as R' increased (and hence β), additional mass was stored in the aquitard (on the solid phase as expected). Perhaps less obvious however is the result that the maximum relative flux likewise increased due to the additional sorbed mass. In Figure 3-6f, the time series for M' and J' are shown for the model results in Figure 3-6e. Increasing σ (and hence β) due to increased retardation increased both M' and J', even though the penetration depth was reduced (see Figure 3-3).

Dimensionless Results for Diffusion with Decay

Aquitard Concentration Profiles

To investigate the effect of aquitard contaminant decay, a conservative approach was used starting with λ' values two to three orders of magnitude less than the published range for TCE (1.0x10^{-2} to 1.0x10^{-3} d^{-1}) in an aquifer [*Newell et al.,* 2002]. Furthermore, only aqueous phase was considered and the decay rate was assumed to be constant. The range of λ' selected $\lambda' = \{0,\ 1.0\text{x}10^{-5},\ 2.5\text{x}10^{-5}\}$ d^{-1}, which yields dimensionless decay coefficients of $\Lambda = \{0,\ 72,\ 180\}$ for a low $R' = 1.14$. However, for sites with higher sorption, the λ' required to exhibit similar parent reductions was zero to two orders of magnitude less than the published range, where $\lambda' = \{0,\ 5.0\text{x}10^{-4},\ 1.0\text{x}10^{-3}\}$ d^{-1}, yields dimensionless decay coefficients of $\Lambda = \{0,\ 400,\ 800\}$ for $R' = 8.0$. The cases with decay were compared to the original

baseline cases without decay ($R'=1.14, \beta=500; R'=8.0, \beta=3500$). The values of the parameters used in aquitard diffusion modeling with decay are shown in Table 3-4.

Table 3-4. Dimensionless values used in decay modeling.

Γ	1	1	1	1	1	1
β	500	500	500	3500	3500	3500
η	0.35	0.35	0.35	0.45	0.45	0.45
R'	1.14	1.14	1.14	8.0	8.0	8.0
λ'(d^{-1})	0	1.0×10^{-5}	2.5×10^{-5}	0	5.0×10^{-4}	1.0×10^{-3}
Λ	0	72	180	0	400	800

The starting value of β is the same as Chapter 2 since the values of ψ and σ are the same, but since there is a definition change in σ (Table 3-1). Three dimensionless variables τ, σ, and Λ now contain D_z' instead of D_s'. As before, both τ and σ contain R' (Table 2-1).

Using Eq. 2-35, χ' profiles were created to represent a $\Gamma=1$ site without sorption ($R'=1.14, \beta=500$) with and without decay in the aquitard in Figure 3-7. Comparing the no decay case (Figure 3-7a) to those with decay (Figures 3-7b-c), the aquitard concentrations were reduced by decay, especially in the later times. In early times (black lines, 5 yrs) the effect of decay was not apparent. However, as time increased, the effect of decay χ' increased in the later times (progressively lighter gray lines, 25, 30, 50 and 75 years after spill). The concentration reductions were slightly visible in the reduction in the peak magnitude (i.e. flattening of the peaks in the profiles) in Figures 3.7b-c. However, the slight differences in these profiles can lead to more observable changes in mass and flux that will be explored in Table 3-5. In Figure 3-8, several times for the different decay rates were isolated. The flattening of the concentration profiles as the decay rate increased was most visible at 25 (Figure 3-8b),

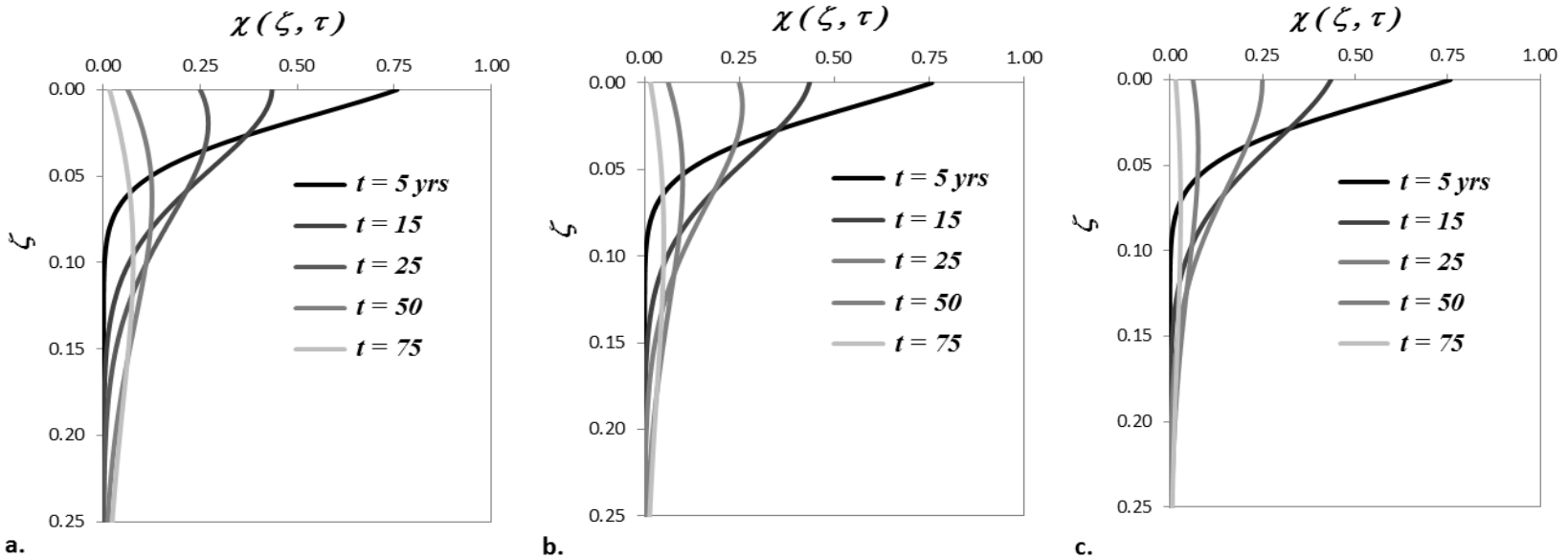

Figure 3-7. χ' depth profiles for diffusion ($R'=1.14, \beta=500$) with decay $\Lambda=\{0,\ 72,\ 180\}$.

Note: χ' depth profiles are shown for 5, 15, 25, 50, and 75 years with aquitard aqueous decay (a) $\Lambda=0$, (b) $\Lambda=72$, (c) $\Lambda=180$.

Table 3-5. Summary of results for diffusion with decay modeling, $R'=1.14, \beta=500$.

Λ	$M'(t)$ mg m^{-2}					$J'(t)$ mg m^{-2} d^{-1}				
	5 yrs	25	30	50	75	5 yrs	25	30	50	75
0	7272	8470	8037	6314	4850	-3.67	0.63	0.71	0.59	0.35
72	7169	7725	7152	4988	3192	-3.92	0.37	0.46	0.41	0.22
180	7019	6781	6070	3607	1799	-4.25	0.03	0.15	0.21	0.11
			MR					FR		
	5 yrs	25	30	50	75	5 yrs	25	30	50	75
72:0	0.014	0.088	0.110	0.210	0.342	-	0.417	0.346	0.305	0.362
180:0	0.035	0.199	0.245	0.429	0.629	-	0.956	0.782	0.645	0.689

Note: aquitard mass storage and mass flux for $\Lambda = \{0,\ 72,\ 180\}$. Negative flux ($J'$) is loading direction, positive flux is back diffusion flux. Fractional mass reduction (MR) and fractional flux reduction (FR) are compared to $\Lambda = 0$ results. (-) FR indicates back diffusion flux not occurring.

50 (Figure 3-8c), and 75 years (Figure 3-8d) after source initiation. Furthermore, because an increase in Λ decreased χ', it also decreased mass storage and mass flux. The dimensioned mass storage per unit area was calculated using Eq. 2-38 and Eq. 2-19, and the results are shown in Table 3-5. The mass was reduced by the effect of decay in the aquitard, and the effect increased as time progressed. The fractional mass reduction was calculated and shown as MR and it increased accordingly. Table 3-5 summarizes the results of the decay modeling in the case of an aquitard without sorption. For a site represented by $\Gamma = 1, R' = 1.14, \beta = 500$ with an aquitard decay represented by $\Lambda = 72$ ($\lambda' = 1.0\text{x}10^{-5}$ d^{-1}), $MR = \{0.088,\ 0.210\}$ at $t = \{25,\ 50\}$ years after the spill, respectively.

Similarly, the dimensioned back diffusion flux was determined by Eq. 2-41a and Eq 2-42. As dimensionless decay increased, the effect on dimensionless mass flux was more complex however. The early time flux increased and the late flux decreased. The increased rate of decay in the aquitard, acted to lower the concentration in the aquitard, thus increasing the loading gradient and loading flux, J' at 5 years. Conversely, as the source boundary concentration decreased over time and back diffusion began, the reduction of mass in the aquitard due to decay reduced the magnitude of the back diffusion flux, J' at 25 years and later. For a site where $\Gamma = 1$ is representative with decay represented by a rate of $\Lambda = 180$ ($\lambda' = 2.5x10^{-5}$ d^{-1}), $FR = \{0.782,\ 0.645\}$ at $t = \{30,\ 50\}$ years after the initial spill, respectively.

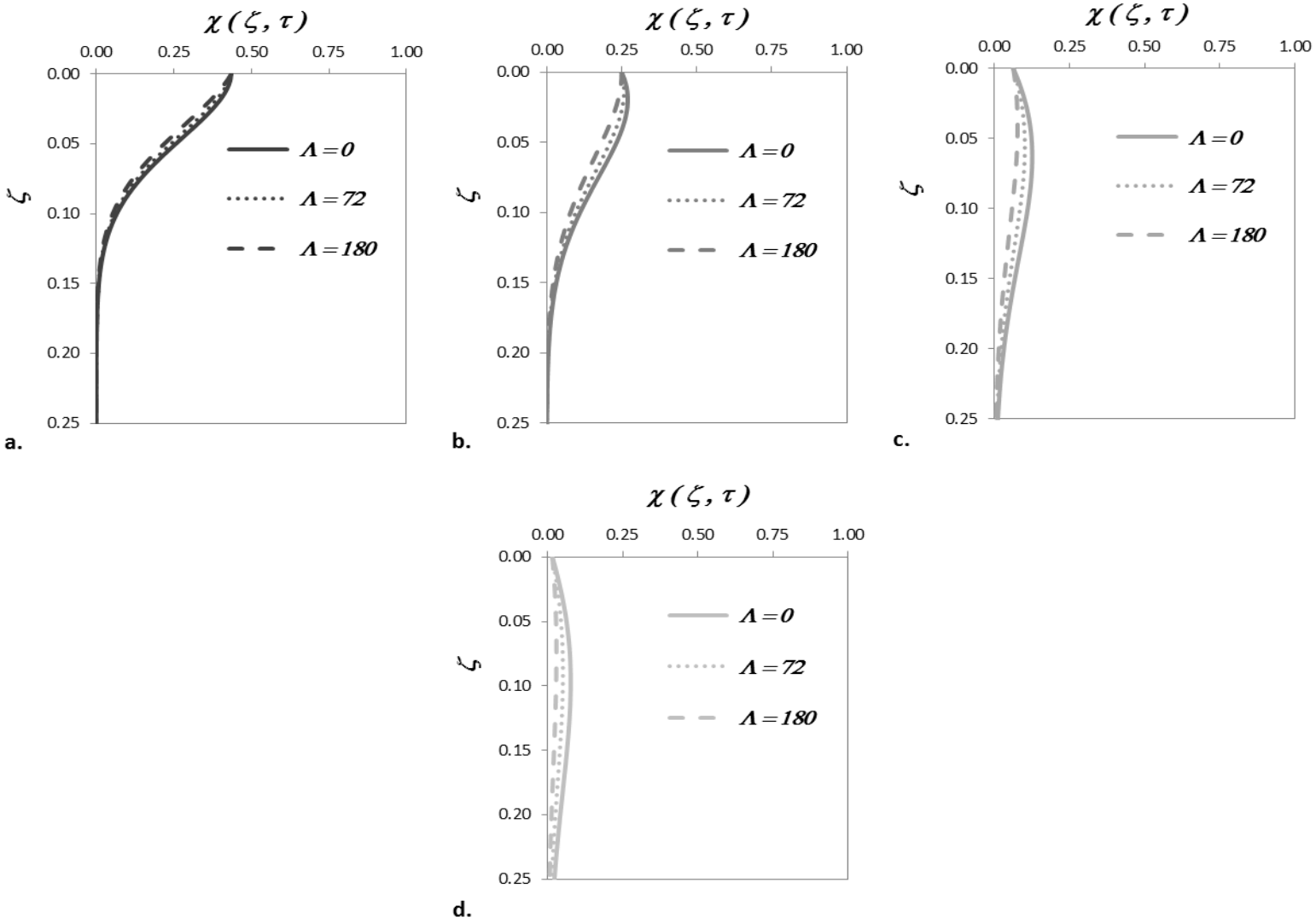

Figure 3-8. χ' depth profiles for diffusion ($R'=1.14, \beta=500$) with decay $\Lambda=\{0,\ 72,\ 180\}$ for specific times.

Note: χ' depth profiles for $R'=1.14$, $\beta=500$, $\Lambda=\{0,\ 72,\ 180\}$; (a) $t=15$, (b) $t=25$, (c) $t=50$, (d) $t=75$ years.

One of the most interesting outcomes here is the reduction of flux and the direction change of flux due to decay. For a site with decay represented by a rate of $\Lambda=180$ ($\lambda'=2.5x10^{-5}$ d^{-1}), the loading flux continued longer than a site without this level of decay. A greater decay rate would in fact eliminate back diffusion entirely (not shown). For a site represented by $\Lambda=360$ ($\lambda'=5.0x10^{-5}$ d^{-1}, not shown), the degradation is large enough to remove enough mass in the aquitard such that the concentration gradient never reverses, and back diffusion does not occur. Overall, flux reductions were achieved by decay in the aquitard proportional to the magnitude of the decay for sites with little or no sorption.

In order to represent a site with sorption ($\Gamma=1, R'=8.0, \beta=3500$) with decay, the coefficients were an order of magnitude greater $\Lambda=\{0,\ 400,\ 800\}$ for $\lambda'=\{0,\ 5.0\text{x}10^{-4},\ 1.0\text{x}10^{-3}\}$ d^{-1}, respectively. Using the same equations, χ' profiles were created to represent a site with and without decay in the aquitard in Figure 3-9. Comparing the no decay case (Figure 3-9a) to those with decay (Figures 3-9b-c) decay acted to reduce the aquitard concentrations, but to a lesser degree than the site without sorption presented in Figures 3-7 and 3-8. Aqueous phase decay had a lesser effect for a site with sorption due to a reduction in availability, since more mass is stored on the solid phase. However, the effect of decay on χ' was still visible. Figure 3-9 shows that χ' decreased in the later times (progressively lighter gray lines, 25, 30, 50 and 75 years after spill). Those peaks were flattened in Figures 3.9b and 3.9c. One thing that stands out compared to the no sorption cases is the magnitude of the y-axis in Figure 3-9. It

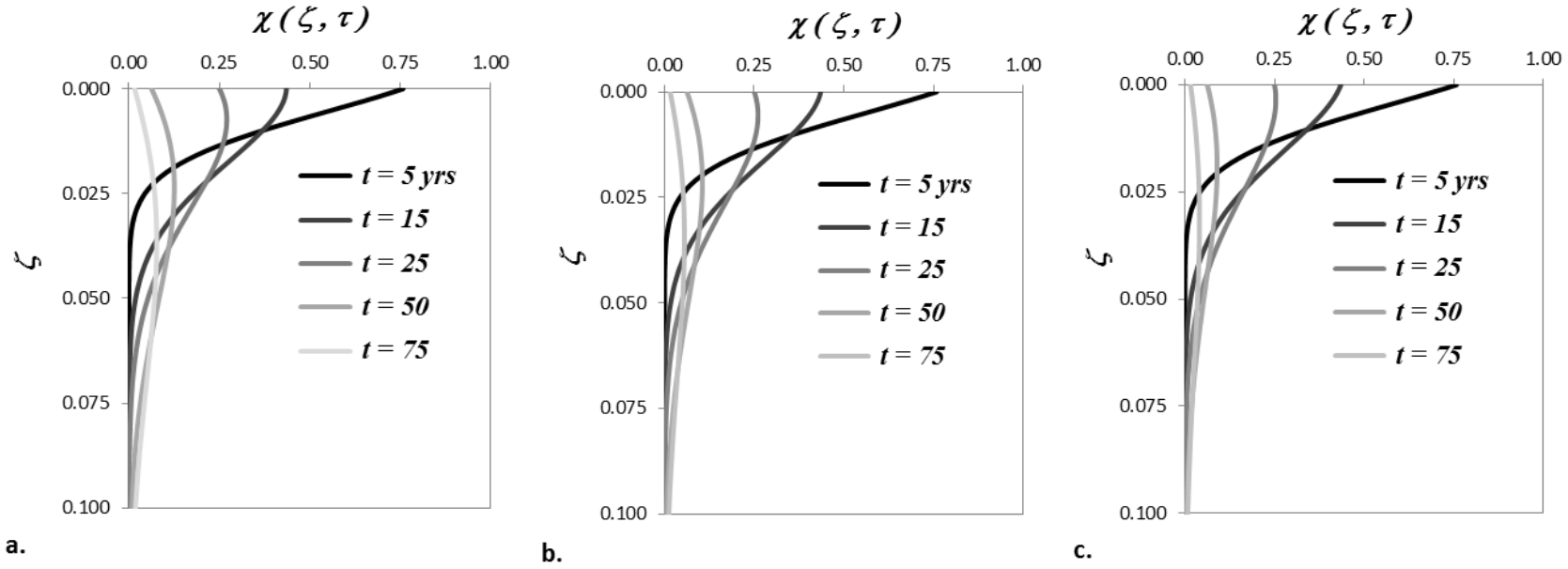

Figure 3-9. χ' depth profiles for diffusion with sorption ($R'=8.0, \beta=3500$) and decay $\Lambda=\{0,\ 400,\ 800\}$.

Note: χ' depth profiles are shown for 5, 15, 25, 50, and 75 years with aquitard aqueous decay (a) $\Lambda=0$, (b) $\Lambda=400$, (c) $\Lambda=800$.

Table 3-6. Summary of results for 1D decay modeling with sorption, $R'=8.0, \beta=3500$.

Λ	$M'(t)$ mg m^{-2}					$J'(t)$ mg m^{-2} d^{-1}				
	5 yrs	25	30	50	75	5 yrs	25	30	50	75
0	24777	28886	27417	21548	16554	-9.887	1.607	1.830	1.541	0.915
400	24498	26854	24991	17868	11875	-10.343	1.077	1.330	1.164	0.644
800	24225	25029	22864	14959	8664	-10.794	0.583	0.874	0.850	0.449
			MR					FR		
	5 yrs	25	30	50	75	5 yrs	25	30	50	75
400:0	0.011	0.070	0.088	0.171	0.283	-	0.330	0.273	0.245	0.296
800:0	0.022	0.134	0.166	0.306	0.477	-	0.637	0.523	0.448	0.510

Note: Aquitard mass storage and mass flux for cases with $\Lambda = \{0,\ 400,\ 800\}$. Negative flux ($J'$) is loading direction, positive is back diffusion flux. Fractional mass reduction (MR) and fractional flux reduction (FR) are compared to $\Lambda = 0$. (-) indicates back diffusion flux not occurring.

goes from $\zeta = 0.000$ to $\zeta = 0.100$, whereas in Figures 3-7 and 3-8, the Y-axis ranged from $\zeta = 0.00$ to $\zeta = 0.25$. This is due to reduction of penetration depth by sorption shown previously in Figure 3-3. When the later times were isolated for specific times for the different decay rates $\Lambda = \{0,\ 400,\ 800\}$ (Figure 3-10), χ' reductions were more easily observable at 25 (Figure 3-10b), 50 (Figure 3-10c), and 75 years (Figure 3-10d).

In Table 3-6, the dimensioned mass per unit area and dimensioned mass flux are shown for the representative site ($\Gamma = 1, R' = 8.0, \beta = 3500$). The additional mass, when compared to the results in Table 3-5, was due to solid phase storage. The trends were similar to the cases without sorption. As the decay rate increased and time increased, mass storage was reduced. Additionally, the loading mass flux increased with increased decay and decreased during back diffusion. In Table 3-5, a $MR = \{0.070,\ 0.171\}$ were achieved at $t = \{25,\ 50\}$ years after the spill, respectively for a site represented by $\Gamma = 1, R' = 8.0, \beta = 3500$ with decay of $\Lambda = 400$ ($\lambda' = 5.0\text{x}10^{-4}$). For the same site with a decay rate of $\Lambda = 800$ ($\lambda' = 1.0\text{x}10^{-3}$), $MR = \{0.134,\ 0.306\}$ were achieved at $t = \{25,\ 50\}$ years.

Similar to the no sorption case, the loading J' increased as Λ increased (shown at 5 yrs). Sorption acted to remove mass from the aqueous phase as it penetrated the aquitard. This reduced the aqueous concentration in the aquitard increasing the inward gradient. After back diffusion began, decay acted to reduce the mass flux from the

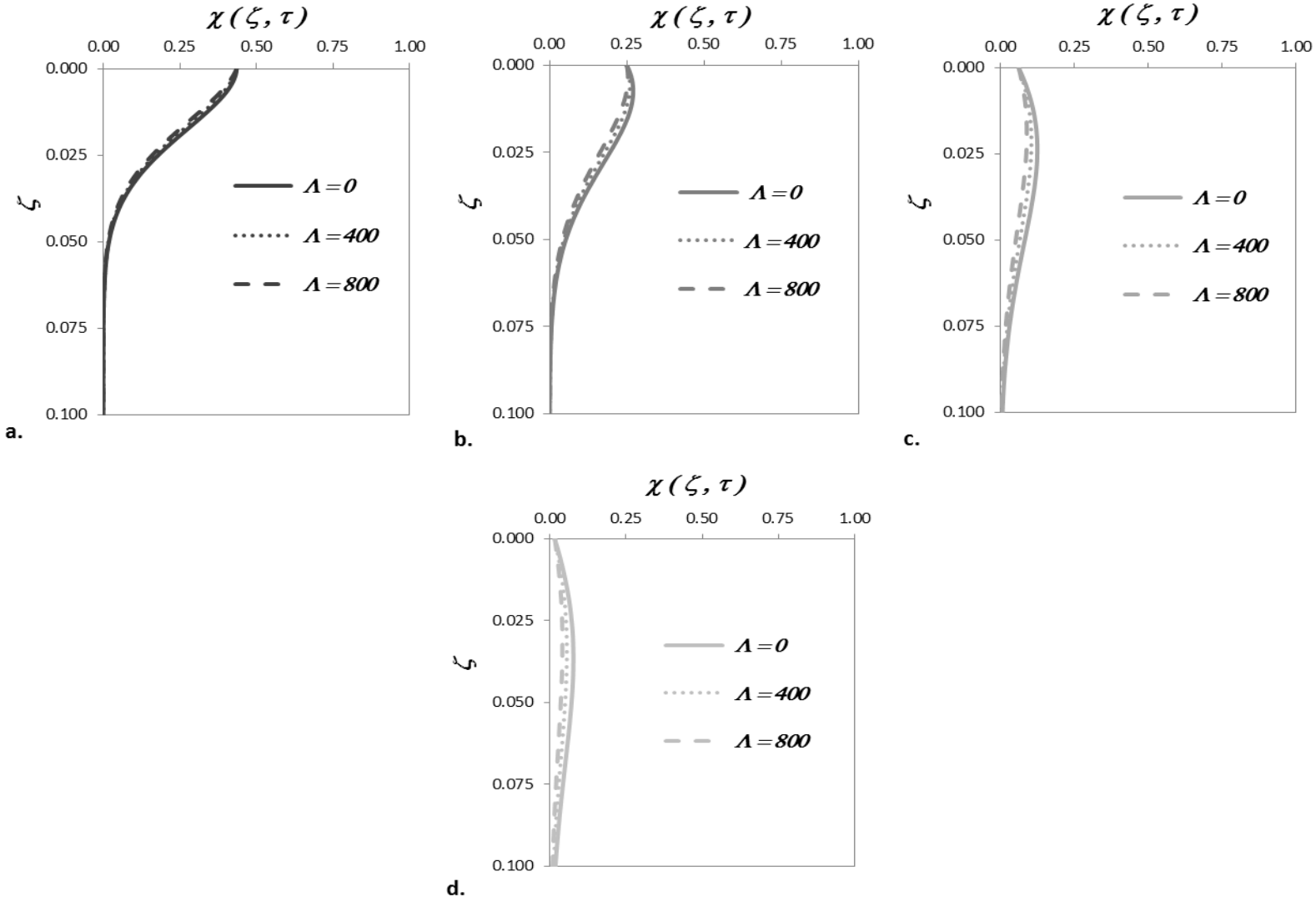

Figure 3-10. χ' depth profiles for diffusion with sorption ($R'=8.0, \beta=3500$) and decay $\Lambda=\{0,\ 400,\ 800\}$ for specific times.

Note: χ' depth profiles for $R'=8.0, \beta=3500$, $\Lambda=\{0,\ 400,\ 800\}$; (a) $t=15$, (b) $t=25$, (c) $t=50$, (d) $t=75$ years.

aquitard. Looking at Table 3-5, for a decay rate of $\Lambda=400$ ($\lambda'=5.0\text{x}10^{-4}$), $FR=\{0.273,\ 0.296\}$ at $t=\{30,\ 50\}$ years. Likewise, a site represented with a decay rate of $\Lambda=800$ ($\lambda'=1.0\text{x}10^{-3}$), the $FR=\{0.523,\ 0.510\}$ at $t=\{30,\ 75\}$ years. This larger decay rate used in the site with sorption is still at the low end of the published range for TCE [*Newell et al.,* 2002].

Aquitard Source Functions for Diffusion with Decay

Aquitard source functions were generated to compare the effect of decay on mass loading and back diffusion flux in Figure 3-11a, for $\beta=500$ with $\Lambda=\{0,\ 72,\ 180\}$. In Figure 3-11a, the relative flux and the relative mass in the aquitard were increasingly reduced as Λ increased (progressively lighter gray lines) compared to the no decay site (black line). The maximum mass storage reduction was evident by the location of $M'(t)/M_{OA}$ at τ_{BD}. Back diffusion began at lower total mass as Λ increased. Likewise, the peak of back diffusion flux was reduced as Λ increased, and the slope of the flux decline was reduced, demonstrated by the flattening effect on the aquitard source functions as Λ increased. As expected, similar to the previous aquitard source functions (Figure 3-6), the relative mass and flux in the aquitard were very low values, shown by the magnitude of the x and y-axes. The dimensioned mass storage and flux were 4-5 orders of magnitude less than the initial source zone mass and flux.

The dimensioned mass per unit area and the dimensioned flux time series are shown in Figure 3-11b for $\beta=500$ with $\Lambda=\{0,\ 72,\ 180\}$. The mass storage per unit area in the aquitard is shown on the right vertical axis. The no decay site ($\Lambda=0$) is the

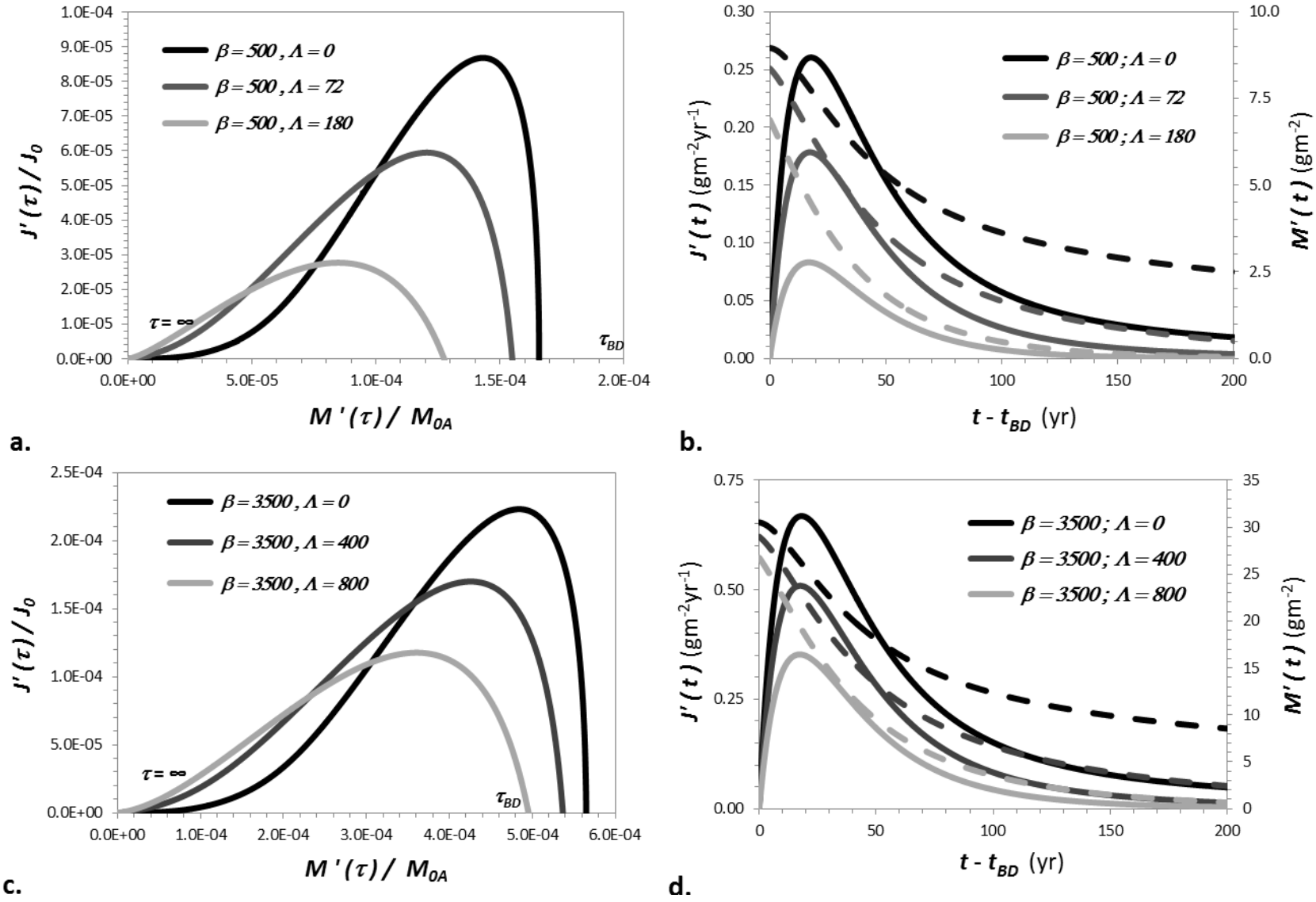

Figure 3-11. Aquitard source functions with decay and $M'(t)$ and $J'(t)$ for $\beta = 500$ and $\beta = 3500$.

Note: (a) Aquitard source functions for $R' = 1.14, \beta = 500$ with $\Lambda = \{0,\ 72,\ 180\}$. Temporal progression is from right to left, from τ_{BD} to $\tau = \infty$. (b) Dimensioned mass storage $M'(t)$ and back diffusion flux $J'(t)$ time series for (a). (c) Aquitard source functions for $R' = 8.0, \beta = 3500$ with $\Lambda = \{0,\ 400,\ 800\}$. (d) Dimensioned mass storage $M'(t)$ and back diffusion flux $J'(t)$ time series for (c).

black dashed line and increasing decay, $\Lambda = \{72,\ 180\}$, is shown by progressively lighter gray dashed lines. The magnitude of the maximum mass storage, where the dashed lines meet the left vertical axis, decreased as Λ increased ; $M'_{\max} = \{8.95,\ 8.06,\ 6.91\}$ g m^{-2} for $\Lambda = \{0,\ 72,\ 180\}$. Similarly, as decay increased, the remaining mass at the end of the simulation (200 years) was reduced. The flux (solid lines) peaked at $t_{peak} = \{17.8,\ 17.4,\ 16.9\}$ years for $\Lambda = \{0,\ 72,\ 180\}$, at a magnitude of $J'_{peak} = \{0.26,\ 0.18,\ 0.08\}$ g m^{-2} yr^{-1} respectively. The source dissolution was unchanged by different aquitard conditions, but increasing Λ in the aquitard increased the loading flux. However, it reduced magnitude of the peak and slightly reduced the time of the peak. After peak flux, the slope of the flux decreased as Λ increased (solid progressively lighter gray lines) compared to the no decay site (solid black line).

For sites with aquitard sorption, the effect of Λ is shown in Figure 3-11c with aquitard source functions for $R' = 8.0, \beta = 3500$. The relative mass storage and the relative back diffusion flux were greater than the no sorption sites shown in Figure 3-9, and demonstrated reduction in mass and flux as Λ increased. The maximum relative mass on the x-axis at τ_{BD} decreased as Λ increased (lighter gray lines) and the peak flux decreased accordingly, compared to the no decay site (black line). Looking at the dimensioned mass and flux time series shown in Figure 3-11d,

$M'_{\max} = \{30.5,\ 29.4,\ 28.4\}$ g m^{-2} for $\Lambda = \{0,\ 400,\ 800\}$. The flux (solid lines) peaked at $t_{peak} = \{18.0,\ 17.5,\ 17.3\}$ years for $\Lambda = \{0,\ 400,\ 800\}$, at a magnitude of $J'_{peak} = \{0.67,\ 0.51,\ 0.35\}$ g m^{-2} yr^{-1} respectively. The flux slope was steeper as flux approached its peak and during the early times after peak flux, compared to the no sorption modeling.

If $R' = 25.1$, the decay rate would have to be another order of magnitude larger ($\Lambda = 360$) to produce a similar result (not shown). Because the equations only consider aqueous phase decay, the effect of degradation is reduced in the model for sites with sorption. The model can be modified to add solid phase decay to calculate bulk decay as desired.

Dimensionless Results for Diffusion with Leakage

Aquitard Concentration Profiles

Some sites have a leaky aquitard where vertical groundwater gradients induce seepage thru the aquitard. The effects of leakage on aquitard storage and flux were investigated using the parameter values in Table 3-7.

Table 3-7. Parameter values used in aquitard diffusion with leakage modeling.

Γ	1	1	1	1	1	1
β	500	296	1590	3500	2883	7500
η	0.35	0.35	0.35	0.45	0.45	0.45
R'	1.14	1.14	1.14	8.0	8.0	8.0
q'(md^{-1})	0	5.0x10^{-6}	-5.0x10^{-6}	0	5.0x10^{-6}	-5.0x10^{-6}
D_z'(m^{2}d^{-1})	1.04x10^{-5}	1.60x10^{-5}	4.86x10^{-6}	1.04x10^{-5}	1.76x10^{-5}	3.72x10^{-6}
P_e	0	4.5	-23.9	0	3.8	-12.5

Note: Top section is aquifer parameters, bottom section is aquitard parameters.

A conservative value of 5.0×10^{-6} m d^{-1} for leakage was used in this effort which is in the range for clay landfills [*Johnson et al.,* 1998] and a regional aquitard in Australia [*Gardner et al.,* 2012]. Because β incorporates D_z' in σ (Table 2-2), the value of β changes with magnitude and direction of q_z'.

In Figure 3-12, the χ' profiles are shown for a $\Gamma = 1$ site without significant sorption ($R' = 1.14$) with leakage in both the upward and downward directions. In Figure 3-12a, a site with no leakage is used for comparison to a site with a downward leakage in Figure 3-12b, and a site with upward leakage in Figure 3-12c. The most noticeable difference is in the depth of penetration of mass into the aquitard. Downward leakage ($P_e = 4.5, \beta = 296$) in Figure 3-12b results in χ'_{peak} at $\zeta = 0.035$ at 25 years and $\zeta = 0.100$ at 50 years. For a site without leakage χ'_{peak} occurs at $\zeta = 0.020$ at 25 years and $\zeta = 0.063$ at 50 years (Figure 3-12a). Conversely, upward leakage ($P_e = -23.9, \beta = 1590$) in Figure 3-12c results in χ'_{peak} at $\zeta = 0.000$ at 25 years and $\zeta = 0.018$ at 50 years. Thus, upward leakage can reduce or delay back diffusion.

Figure 3-13, a comparison of each specific time for the three sites modeled in Figure 3-12 is presented for $P_e = 0$ (solid lines), $P_e = 4.5$ (dotted lines), and $P_e = -23.9$ (dashed lines). The differences in the χ' depth profiles are highly visible in this format with the greatest differences occurring in the 15 through 50 year profiles. Fifteen years is good predictor of site back diffusion potential because it is essentially a snapshot of the when the back diffusion flux is the greatest (Figure 3-13b). At other times, the flux is either loading (5 years, Figure 3-13a), releasing but very slowly (18-20

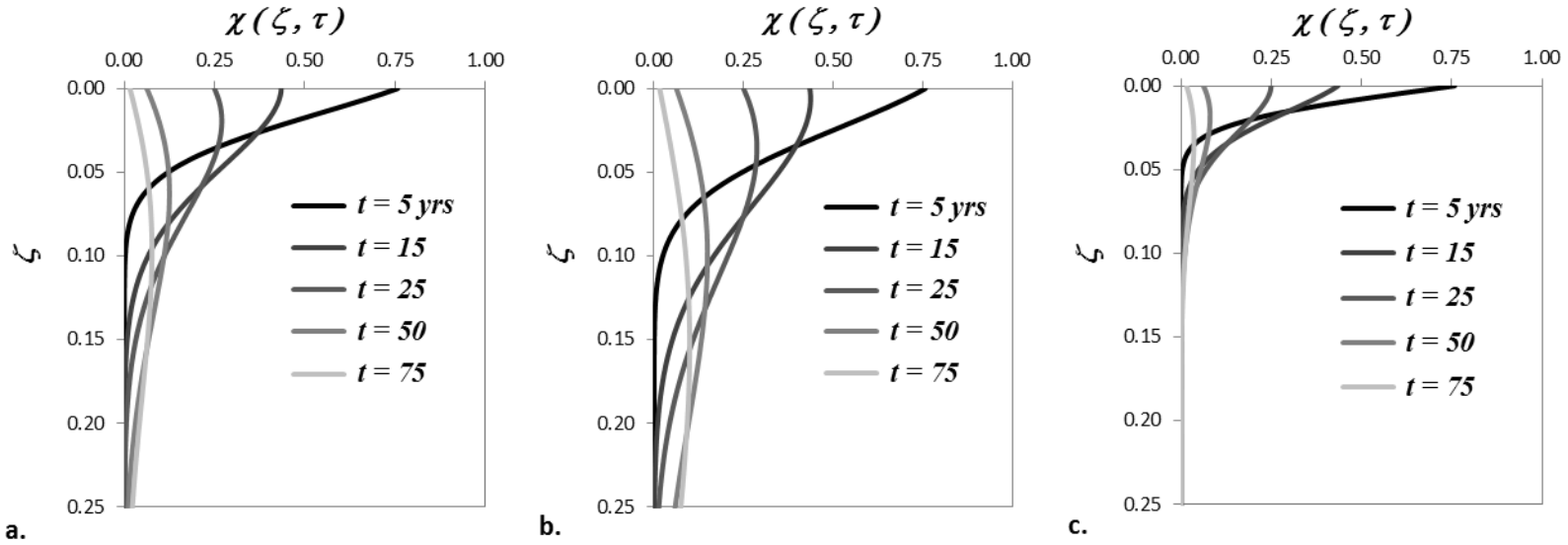

Figure 3-12. χ' depth profiles for diffusion ($R' = 1.14$) with leakage $\beta = \{500,\ 296,\ 1590\}$, $P_e = \{0,\ 4.5,\ -23.9\}$.
Note: χ' depth profiles are shown for 5, 15, 25, 50, and 75 years with aquitard leakage (a) $P_e = 0$, $\beta = 500$; (b) $P_e = 4.5$, $\beta = 296$; (c) $P_e = -23.9$, $\beta = 1590$.

Table 3-8. Summary of results for diffusion modeling with leakage, $R' = 1.14$.

P_e	$M'(t)$ mg m^{-2}					$J'(t)$ mg m^{-2} d^{-1}				
	5 yrs	25	30	50	75	5 yrs	25	30	50	75
0	7272	8470	8037	6314	4850	-3.67	0.63	0.71	0.59	0.35
4.5	10055	12966	12578	10738	9034	-4.01	1.04	1.08	0.80	0.44
-23.9	3516	3173	2837	1748	987	-2.96	-0.02	0.10	0.19	0.13
			MR					FR		
	5 yrs	25	30	50	75	5 yrs	25	30	50	75
4.5:0	-0.383	-0.531	-0.565	-0.701	-0.863	-	-0.648	-0.523	-0.358	-0.279
-23.9:0	0.517	0.625	0.647	0.723	0.796	-	-	0.858	0.670	0.628

Note: aquitard mass storage and mass flux for $\beta = \{500,\ 1590,\ 296\}$, $P_e = \{0,\ 4.5,\ -23.9\}$. Negative flux ($J'$) is loading direction, positive flux is back diffusion flux. Fractional mass reduction (MR) and fractional flux reduction (FR) are compared to $P_e = 0$ results. (-) MR indicates an increase in stored mass, (-) FR indicates back diffusion flux not occurring when no number follows the (-) and increase in flux otherwise.

years, not shown), or negligible (75 years, Figure 13e). For the example site modeled here, a greater upward leakage would prevent any back diffusion flux from occurring, and a lower leakage has a lesser effect where the non-leaky model may be an appropriate approximation. A summary of the results of aquitard diffusion with leakage and without sorption are presented in Table 3-7. The presence of downward leakage ($P_e = 4.5, \beta = 296$) not only leads to deeper penetration, but also results in significantly more mass stored. The mass increase was $MR = \{-0.531,\ -0.701\}$ at $t = \{25,\ 50\}$ years respectively, compared to the $P_e = 0, \beta = 500$ site. On the other hand, a site represented by upward leakage ($P_e = -23.9, \beta = 1590$) demonstrated $MR = \{0.625,\ 0.723\}$ at $t = \{25,\ 50\}$. Mass flux showed a similar trend. The loading flux ($t = 5$ years) increased with $P_e = 4.5$ and decreased with $P_e = -23.9$. Similarly, during back diffusion, J' increased with downward leakage while it decreased with upward leakage. The $FR = \{-0.648,\ -0.358\}$ at $t = \{25,\ 50\}$ years compared to the $P_e = 0$ site. Upward leakage resulted in significant decreases in back diffusion flux with back diffusion was not occurring at $t = 25$ years, and $FR = \{0.858,\ 0.628\}$ at $t = \{30,\ 75\}$ years.

To investigate the effects of aquitard diffusion with leakage on a site with sorption ($R = 8.0$), χ' depth profiles were generated and are shown in Figure 3-14. Leakage did not have as great effect compared to the non-sorption site (Figures 3-11 and

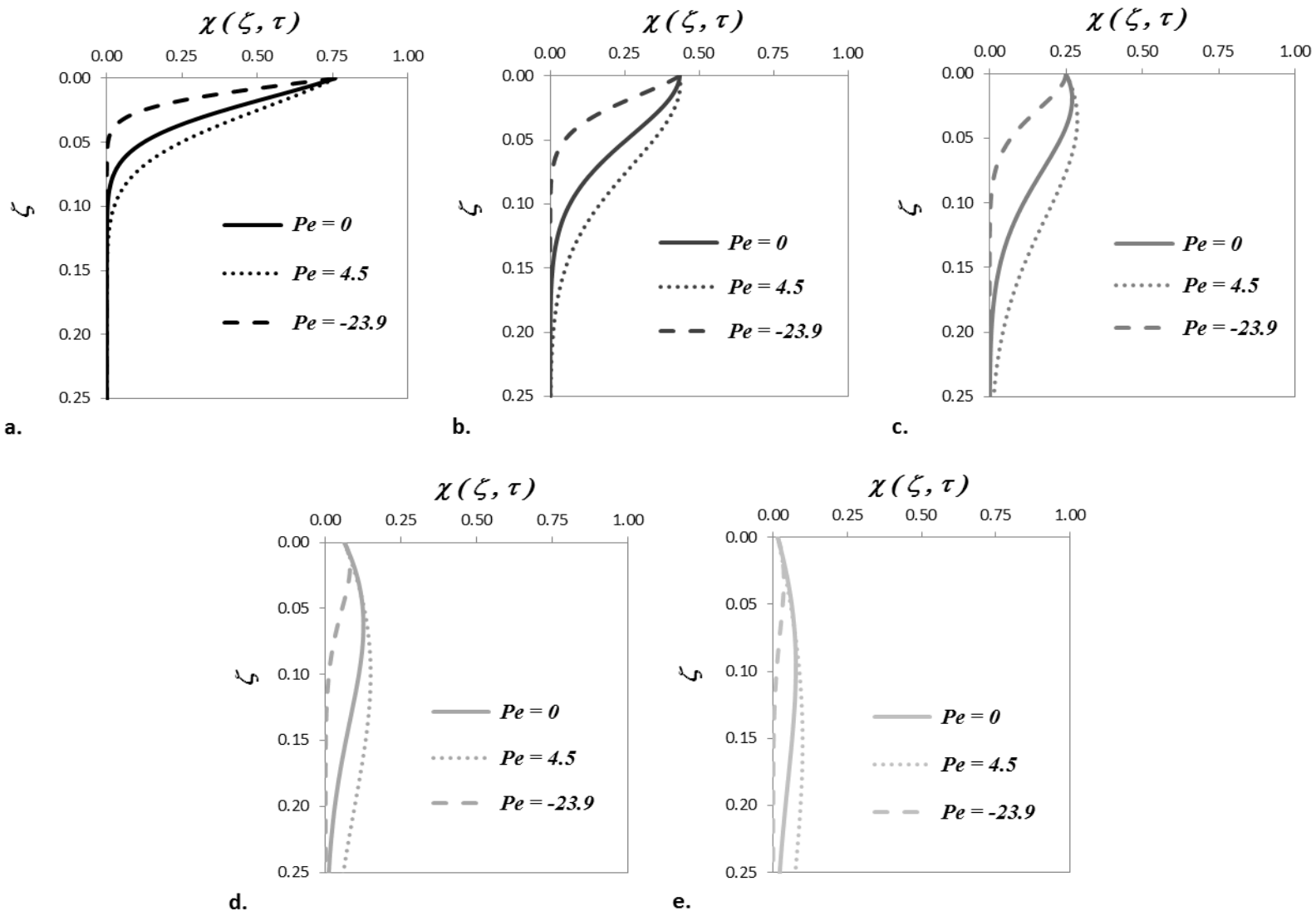

Figure 3-13. χ' depth profiles for diffusion ($R = 1.14$) with leakage ; $P_e = \{0,\ 4.5,\ -23.9\}$ for specific times.

Note: χ' depth profiles for $R'=1.14$, $P_e=\{0,\ 4.5,\ -23.9\}$; (a) $t=5$, (b) $t=15$, (c) $t=25$, (d) $t=50$, (e) $t=75$ years.

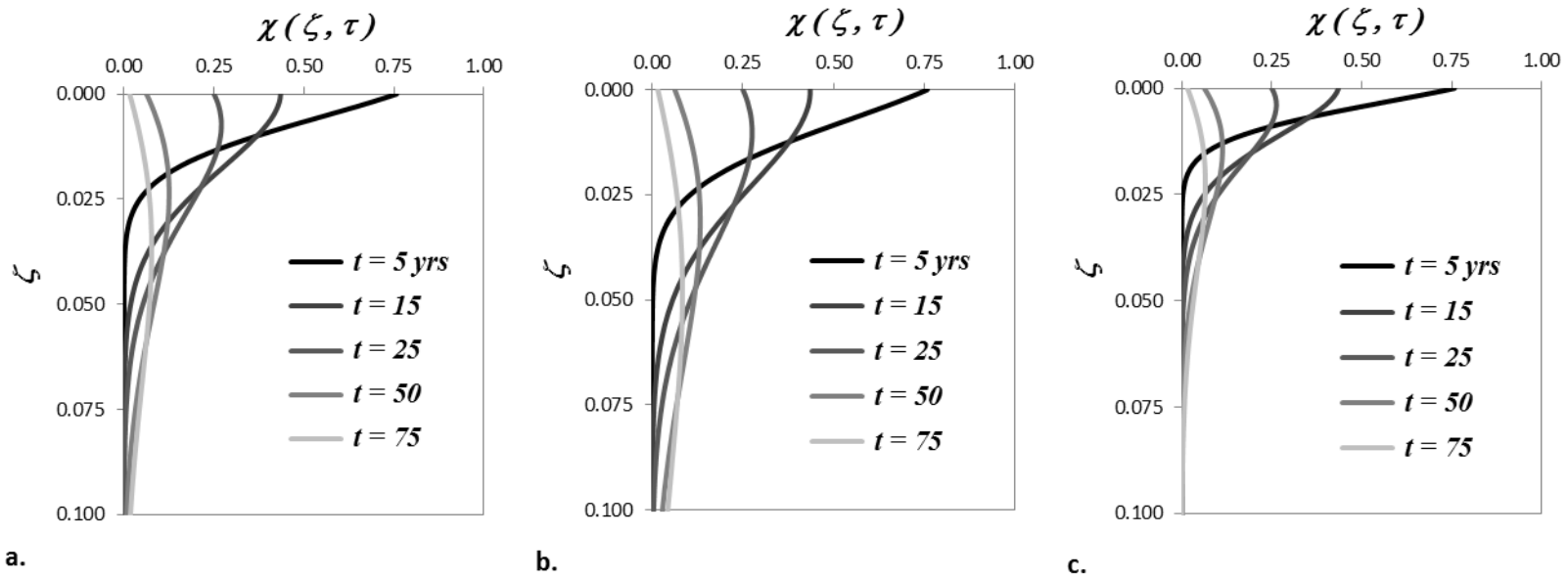

Figure 3-14. χ' depth profiles for diffusion with sorption ($R'=8.0$) and leakage ; $P_e=\{0,\ 3.8,\ -12.5\}$.
Note: χ' depth profiles are shown for 5, 15, 25, 50, and 75 years with aquitard leakage (a) $\beta=3500$, $P_e=0$;
(b) $\beta=2883$, $P_e=3.8$; (c) $\beta=7500$, $P_e=-12.5$.

Figure 3-12) likely due to the loss of mass to solid phase storage as seen previously. Downward leakage ($P_e=3.8, \beta=2883$) in Figure 3-14b results in χ'_{peak} at $\zeta=0.010$ at 25 years and $\zeta=0.031$ at 50 years, compared to χ'_{peak} at $\zeta=0.007$ at 25 years and $\zeta=0.024$ at 50 years for a site without leakage in Figure 3-14a. Conversely, upward leakage ($P_e=-12.5, \beta=7500$) in Figure 3-14c results in χ'_{peak} at $\zeta=0.004$ at 25 years and $\zeta=0.014$ at 50 years. In

comparing the sorption sites to the non-sorption sites, we also see the y-axis is scaled much closer to the surface to capture the profiles, ranging from $\zeta = 0.000 - 0.100$ instead of $\zeta = 0.00 - 0.25$, respectively due to the decreased depth of penetration. Figure 3-15 shows the χ' depth profiles for the three $R = 8.0$ sites at specific times (5, 15, 25, 50 and 75 years) for $P_e = 0$ (solid lines), $P_e = 3.8$ (dotted lines), and $P_e = -12.5$ (dashed lines). The differences were reduced compared to the sites shown in Figure 3-13, due to the effects of sorption. During the time after back diffusion began for these sites ($t > 18$ years), the downward leakage increased the depth of the peak but also the depth of the tailing in χ', while upward leakage decreased penetration and the tailing in χ'. The mass storage and mass flux results of the aquitard diffusion modeling for the sites with leakage and sorption are summarized in Table 3-9. The effects of

Table 3-9. Summary of results for 1D leakage modeling with sorption, $R' = 8.0$.

P_e	$M'(t)$ mg m^{-2}					$J'(t)$ mg m^{-2} d^{-1}				
	5 yrs	25	30	50	75	5 yrs	25	30	50	75
0	24777	28886	27417	21548	16554	-9.89	1.61	1.83	1.54	0.92
3.8	31283	37658	35995	29067	23025	-11.59	2.20	2.43	1.96	1.14
-12.5	16337	17949	16810	12535	9054	-7.43	0.85	1.06	0.98	0.60
			MR					FR		
	5 yrs	25	30	50	75	5 yrs	25	30	50	75
3.8:0	-0.26	-0.30	-0.31	-0.35	-0.39	-	-0.37	-0.33	-0.27	-0.25
-12.5:0	0.34	0.38	0.39	0.42	0.45	-	0.47	0.42	0.36	0.35

Note: aquitard mass storage and mass flux for $\beta = \{3500,\ 2883,\ 7500\}$. $P_e = \{0,\ 3.8,\ -12.5\}$. Negative flux ($J'$) is loading direction, positive flux is back diffusion flux. Fractional mass reduction (MR) and fractional flux reduction (FR) are compared to $P_e = 0$ results. (-) FR indicates back diffusion flux not occurring.

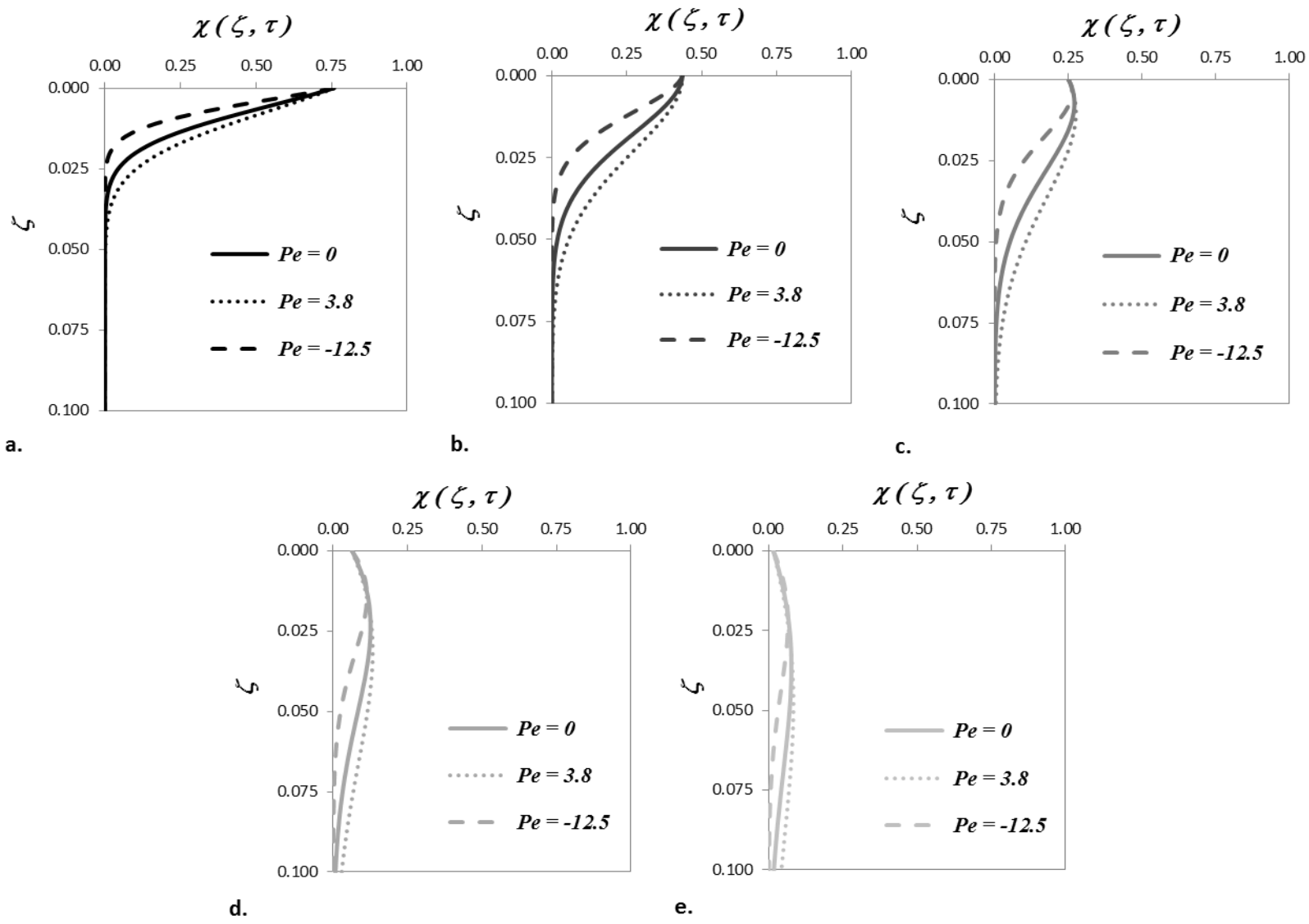

Figure 3-15. χ' depth profiles for diffusion and sorption ($R' = 8.0$) with leakage ; $P_e = \{0,\ 3.8,\ -12.5\}$ for specific times.

Note: χ' depth profiles for $R'=8.0$, $P_e=\{0,\ 3.8,\ -12.5\}$; (a) $t=5$ (b) $t=15$, (c) $t=25$, (d) $t=50$, (e) $t=75$ years.($P_e=-12.5, \beta=7500$) resulted in decreased M' with $MR=\{0.38,\ 0.42\}$ at $t=\{25,\ 50\}$ years compared to the $P_e=0$ site.

downward leakage ($P_e=3.8, \beta=2883$) resulted in increased M' compared to the $P_e=0$ site. The $MR=\{-0.30,\ -0.35\}$ at $t=\{25,\ 50\}$ years. On the other hand, a site represented by upward leakage Mass flux showed the same trend. The loading flux was increased by $P_e=3.8$ and decreased by $P_e=-12.5$. Additionally after back diffusion began, J' increased with downward leakage while it decreased with upward leakage. The $FR=\{-0.37,\ -0.27\}$ at $t=\{25,\ 50\}$ years compared to the $P_e=0, \beta=3500$ site. For the $P_e=-12.5, \beta=7500$ site $FR=\{0.47,\ 0.36\}$ at $t=\{25,\ 50\}$ years

Aquitard Source Functions for Diffusion with Leakage

Aquitard source functions were generated to compare the effect of leakage on mass loading and back diffusion. In Figure 3-16a, these are shown for $R'=1.14$ with $P_e=\{0,\ 4.5,\ -23.9\}$. The relative flux and the relative mass in the aquitard, shown in Figure 3-16a, were both greater for a site with downward leakage (medium gray line) compared to the non-leaky site (black line), and were both reduced for a site with upward leakage (light gray line). The mass storage increase for $P_e=4.5$ and decrease for $P_e=-12.5$ were demonstrated by the location of the maximum relative mass at τ_{BD}. The peak of back diffusion flux increased with $P_e=4.5$, and decreased with $P_e=-12.5$. The most interesting result of the downward leakage modeling was the very slight rightward lean of the $P_e=4.5$ curve in Figure 3-16a. Mass storage increased very slightly after back diffusion began. This is counterintuitive, but knowing that for any site

represented by $\Gamma = 1$, back diffusion will begin at about $\chi(\tau) = 0.35$, and that the downward flow is unchanged throughout the timescale, it is likely that the downward leakage overwhelms the very low back diffusion flux in the early stages of release, such that some loading continues from the plume by advection even though stored mass is being released through back diffusion.

The dimensioned mass per unit area and the dimensioned flux time series are shown in Figure 3-16b for $R = 1.14$ with $P_e = \{0,\ 4.5,\ -23.9\}$. The mass storage per unit area in the aquitard is shown on the right vertical axis for the three sites with the non-leaky site (black dashed line), the downward leakage site (medium gray dashed line), and the upward leakage site (light gray dashed line). Where the M' meets the left vertical axis is $M'_{\max}$, and $M'_{\max} = \{8.95,\ 13.20,\ 3.14\}$ g m^{-2} for $P_e = \{0,\ 4.5,\ -23.9\}$. Similarly, the remaining mass at the end of the simulation (200 years) showed the same pattern with $M'(200) = \{2.51,\ 6.31,\ 0.12\}$ g m^{-2}. The flux (solid lines) peaked at $t_{peak} = \{17.8,\ 16.6,\ 19.8\}$ years for $P_e = \{0,\ 4.5,\ -23.9\}$, at a magnitude of $J'_{peak} = \{0.26,\ 0.39,\ 0.07\}$ g m^{-2} yr^{-1} respectively. After 100 years, the flux was below 0.075 g m^{-2} yr^{-1} and by 200 years it was below 0.025 g m^{-2} yr^{-1} in all cases.

For the sites with aquitard sorption and leakage, the aquitard source functions are shown in Figure 3-16c. The relative mass storage and the relative back diffusion flux displayed similar patterns to those in the no sorption case in Figure 3-16a, but the differences from the $P_e = 0$ site to those with leakage were slightly reduced due to sorption. The magnitude of each axis was greater from additional solid phase mass

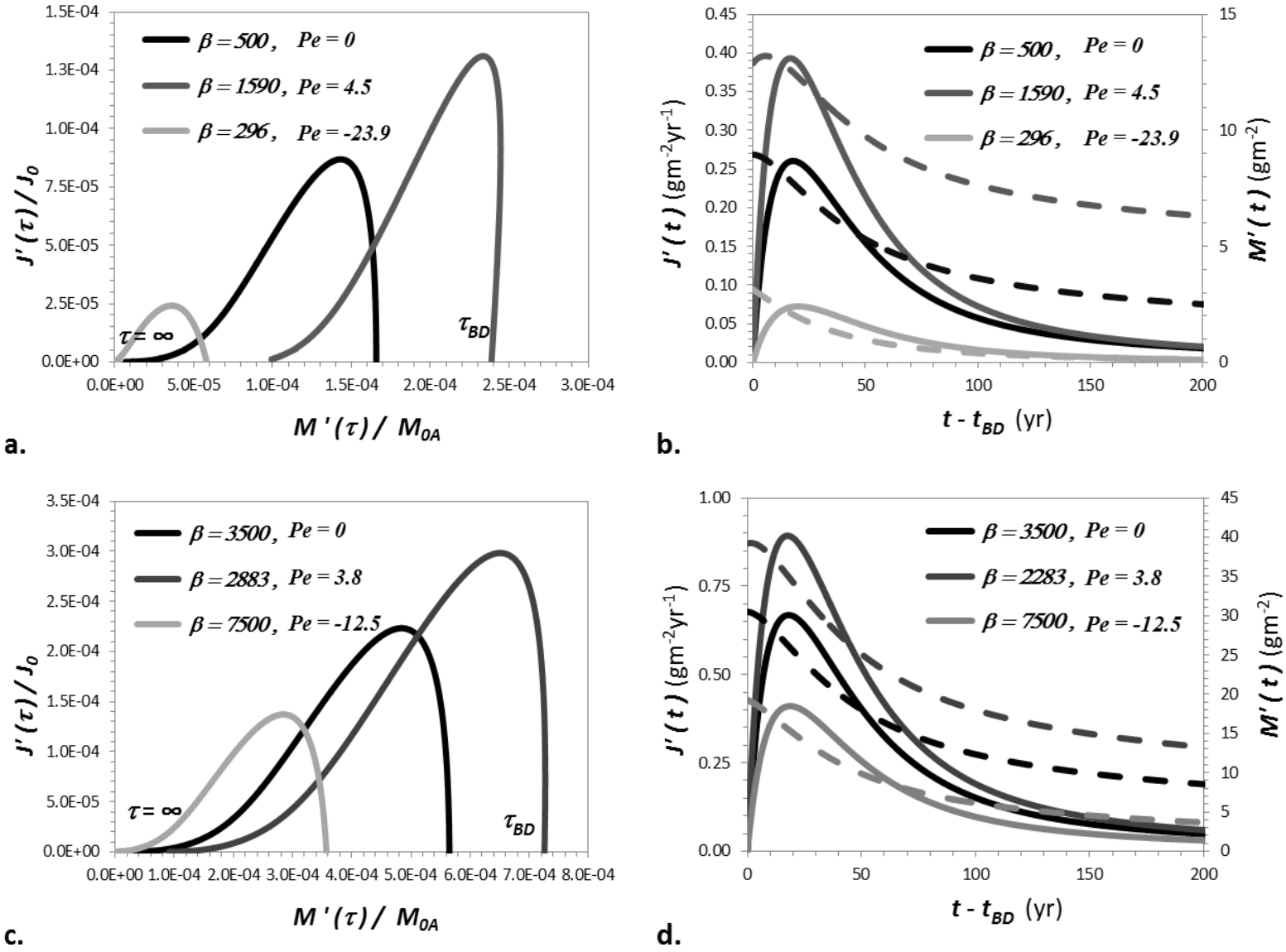

Figure 3-16. Aquitard source functions for diffusion with leakage and $M'(t)$ and $J'(t)$.

Note: (a) Aquitard source functions for $R' = 1.14$, $\beta = \{500,\ 296,\ 1590\}$ and $P_e = \{0,\ 4.5,\ -23.9\}$. Temporal progression is from right to left, from τ_{BD} to $\tau = \infty$. (b) Dimensioned mass storage $M'(t)$ and back diffusion flux $J'(t)$ time series for (a). (c) Aquitard source functions for $R' = 8.0$, $\beta = \{3500,\ 2883,\ 7500\}$ and $P_e = \{0,\ 3.8,\ -12.5\}$. (d) Dimensioned mass storage $M'(t)$ and back diffusion flux $J'(t)$ time series for (c).

stored. The maximum relative mass on the x-axis is at τ_{BD}. It increased for $P_e = 3.8, \beta = 2883$ compared to $P_e = 0, \beta = 3500$ and decreased for $P_e = -12.5, \beta = 7500$. The maximum relative mass was 7.5x10^{-4} for $R' = 8.0$ (x-axis in Figure 3-16c) and it was 2.5x10^{-4} for $R = 1.14$ (x-axis in Figure 3-16a). Flux also increased due to sorption. The maximum relative flux was 3.0x10^{-4} for $R' = 8.0$ (y-axis in Figure 3-16c) and 1.4x10^{-4} for $R = 1.14$ (y-axis in Figure 3-16a).

In Figure 3-16d, the dimensioned mass and flux time series are presented for the sites with leakage and sorption ($R' = 8.0$), with M' (dashed lines) and J' (solid lines). Maximum mass occurs where the mass line intersects the y-axis on the left side of the figure and for these sites $M'_{\max} = \{30.5,\ 39.3,\ 19.3\}$ g m^{-2} for $P_e = \{0,\ 3.8,\ -12.5\}$. At the end of simulation, the mass storage remaining in the aquitard was $M'(200) = \{8.52,\ 13.26,\ 3.68\}$ g m^{-2}. The flux peaked at $t_{peak} = \{18.0,\ 17.6,\ 18.8\}$ years for $P_e = \{0,\ 3.8,\ -12.5\}$, at a magnitude of $J'_{peak} = \{0.67,\ 0.89,\ 0.41\}$ g m^{-2} yr^{-1} respectively. By 100 years the flux was below 0.2 g m^{-2} yr^{-1} and by 200 years it was below 0.1g m^{-2} yr^{-1} in all cases. Similar to the sites without sorption, the simulation of sites with sorption demonstrated the same trends but the differences were reduced.

CHAPTER 4
REMEDIATION RESULTS

Source Removal Effects on Diffusion

Aquitard Concentration Profiles with Source Remediation

The effects of source zone mass removal on aquitard storage and release for diffusion alone are illustrated in Figure 4-1 and Figure 4-2. The remedial SDM (Figure 4-1a) and the χ' profiles were generated using Eq. 2-5c and Eq. 2-13c, and represent a $\Gamma = 1$ site where $R' = 8.0, \beta = 3500$ under three cases: (1) no remediation (Figure 4-1b), (2) 70 % DNAPL mass reduction (i.e., *X* = 0.7) at $\tau_R = 0.0002$ (12.6 yrs) (Figure 4-1c), and (3) 70 % DNAPL mass reduction at $\tau_R = 0.0045$ (28.5 yrs) (Figure 4-1d). Compared to Figure 4-1b, Figures 4-1c and 4-1d show a reduction in concentration in the aquitard due to remediation. In Figure 4-1c, remediation occurs prior to the start of back diffusion but, in Figure 4-1d remediation occurs after the start of back diffusion. Thus, the maximum potential mass storage in the aquitard is attained in Figure 4-1b and Figure 4-1d, but not in Figure 4-1c.

Aquitard Source Functions with Source Remediation

Figure 4-2a shows the impact of partial source remediation on the aquitard source function. The earlier remediation occurs, the greater the reduction in the aquifer concentration, and hence reduced concentration distributions in the aquitard as shown previously (Figure 4-1). While remediation had a lesser impact on the mass that diffused into the aquitard (i.e. the starting point on the x-axis), the relative flux out of the aquitard increased as a result of remediation. In Figure 4-2b, the dimensioned aquitard mass storage and mass flux time series are shown. Abrupt changes in flux and mass due to the remedial events are evident.

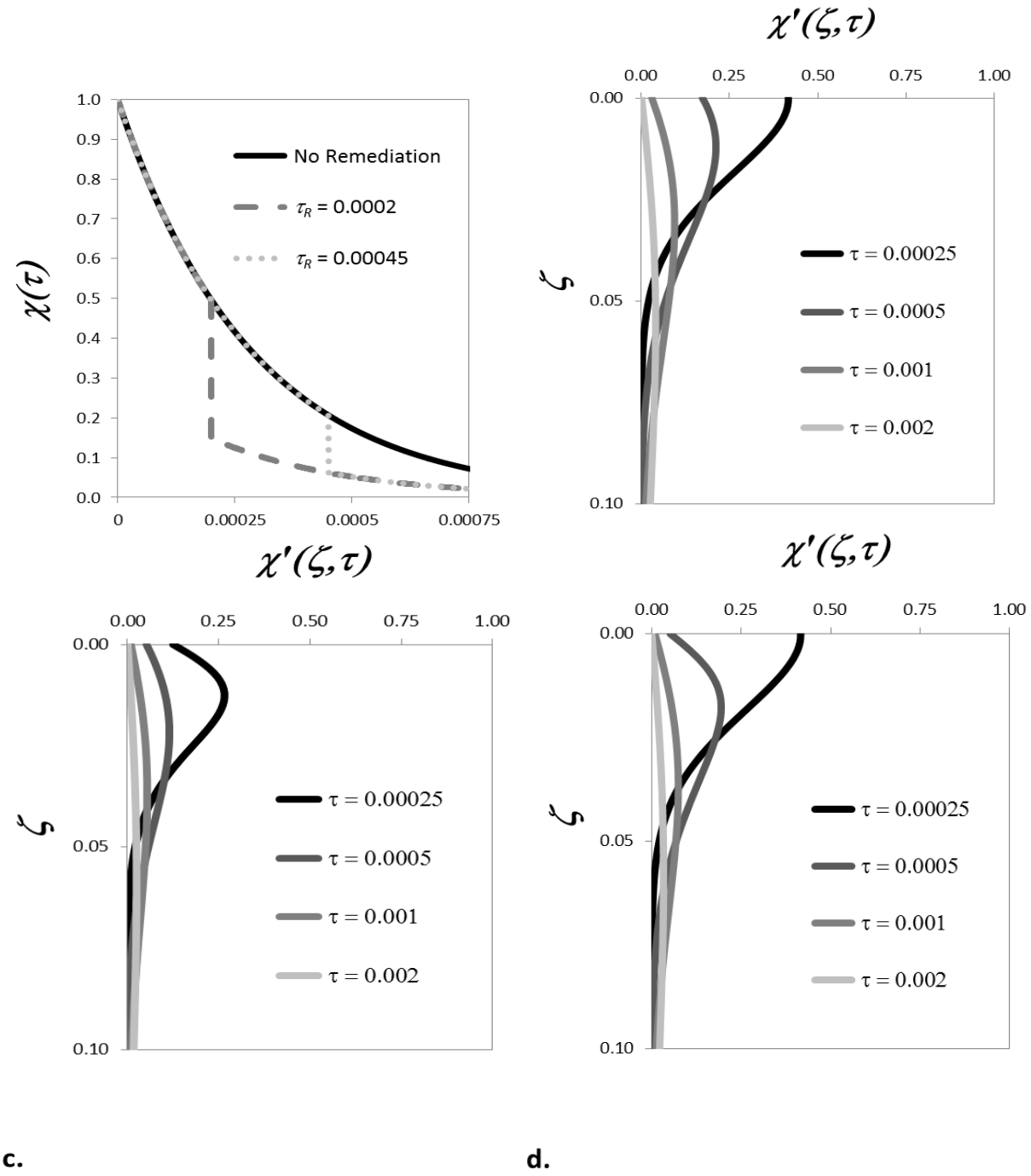

Figure 4-1. Remedial SDM and resultant χ' depth profiles.

Note: (a) Remedial SDM and resultant χ' depth profiles are shown for (b) no remediation, (c) remediation at $\tau = 0.0002$ (12.6 yrs), and (d) remediation at $\tau = 0.00045$ (28.5 yrs); $\beta = 3500$, $\Gamma = 1$, and $X = 0.7$ for all cases

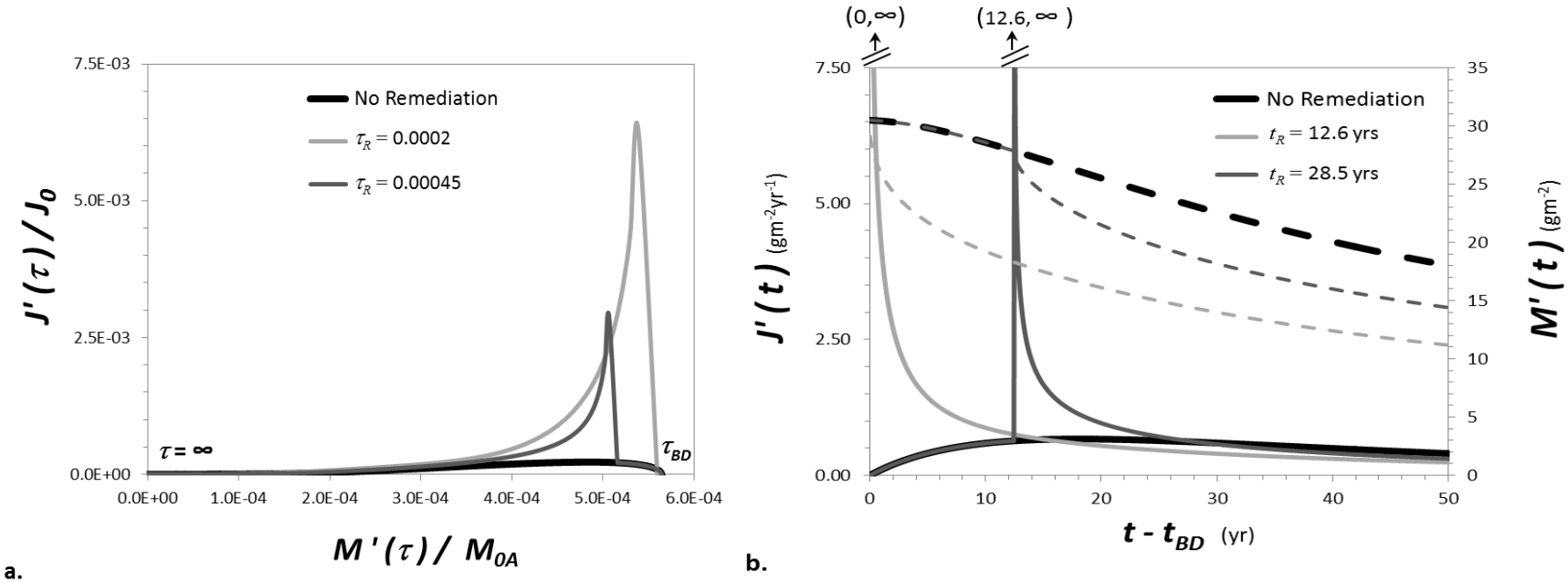

Figure 4-2. Aquitard source functions for diffusion with remediation

Note: (a) Aquitard source functions for remediation at $\tau = 0.00045$ (28.5 yrs) and $\tau = 0.0002$ (12.6 yrs); $\beta = 3500$, $\Gamma = 1$, and $X = 0.7$ for all cases. (b) Dimensioned mass storage and mass flux time series for (a).

While remediation reduces the source strength, it may increase the initial back diffusion flux. However, as illustrated in Figure 4-2b, the rate of decline of both mass and flux out of the aquitard were greater for the remediation cases than the non-remedial case. Therefore, the risk of long-term back diffusion flux was reduced as a result of remediation. While the increased initial mass flux may be an impediment to near-term site closure, longer term reductions in back diffusion can help achieve remedial goals.

Source Removal Effects on Diffusion with Decay

Aquitard Depth Profiles for Diffusion with Decay with Source Remediation

The effects of source zone remediation on sites with decay in the aquitard are shown in Figures 4-3, 4-4, and 4-5. The χ' profiles for a site with $\Gamma = 1$ and $R' = 1.14, \beta = 500$ and $\Lambda = \{0,\ 72,\ 180\}$ are presented in Figure 4-3 for a partial source removal of $X = 0.7$ at 25 years after the contaminant release. Figures 4-3 a-c show the χ' profiles with increasing Λ. As expected, as Λ increased, the peak concentrations decreased. This effect was increased in the post remedial profiles ($\tau > 25$ years) for $\Lambda = \{0,\ 72,\ 180\}$. The concentrations were reduced and the peaks flattened. In Figures 4-3 d-f, the same χ' profiles are shown in the post-remedial years only (solid lines) with the no-remediation profiles for the same Λ. In the earlier post-remedial years (30 and 50 years after spill; i.e. $T_R = 5$ and $T_R = 25$), the reduction in χ' compared to the no-remediation lines was more pronounced than the late time profiles (75 years). The significance of this is that the early post-remedial times capture the higher stored mass and the greater back diffusion flux, so remediation will manifest as a reduction in stored mass and long term back diffusion flux, and therefore a reduction in overall site risk. However, as Figure 4-1 and 4-2 demonstrated, there will be an initial increase in flux due to the sudden change in the diffusion gradient and the increase in flux compared to the no remediation case may last for 15 to 20 years after remediation. Then, the post-remedial flux will be lower than the no remediation case.

Aquitard Source Functions for Diffusion with Decay and Remediation

Aquitard source functions were generated to assess the mass storage and flux response to remediation for sites with aquitard decay (shown in Figure 4-4).

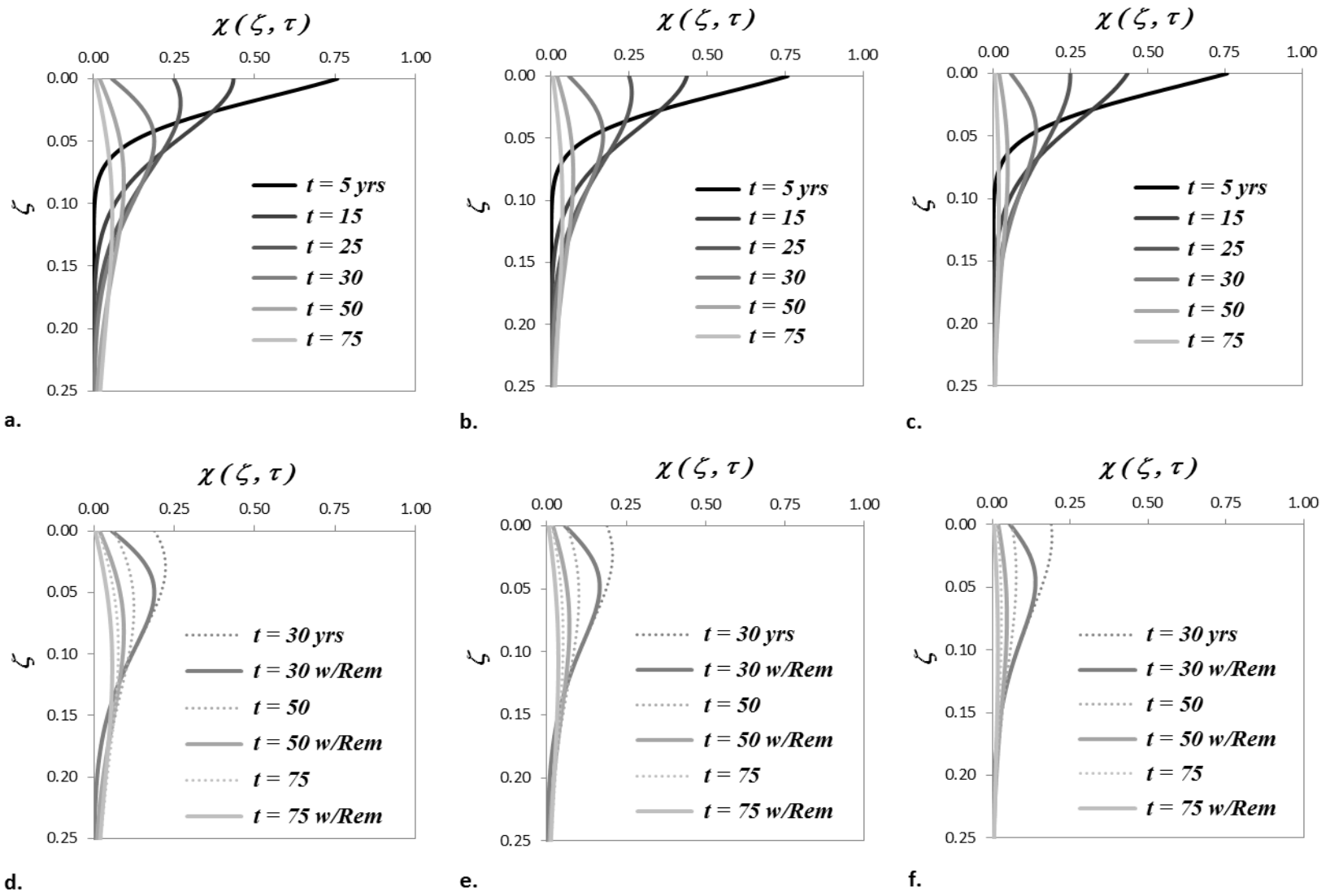

Figure 4-3. χ' depth profiles for diffusion ($R'=1.14$, $\beta=500$) with decay $\Lambda=\{0,\ 72,\ 180\}$ and 70% source remediation at 25 years.

Note: χ' depth profiles with remediation. (a) $\Lambda = 0$, (b) $\Lambda = 72$, (c) $\Lambda = 180$, (d) comparison of post remedial profiles in (a) (solid lines) to no remediation (dashed lines), (e) comparison of (b) to no remediation, and (f) comparison of (c) to no remediation; all cases are $R' = 1.14$, $\beta = 500$, $\Gamma = 1$, $X = 0.7$ at $t = 25$ years.

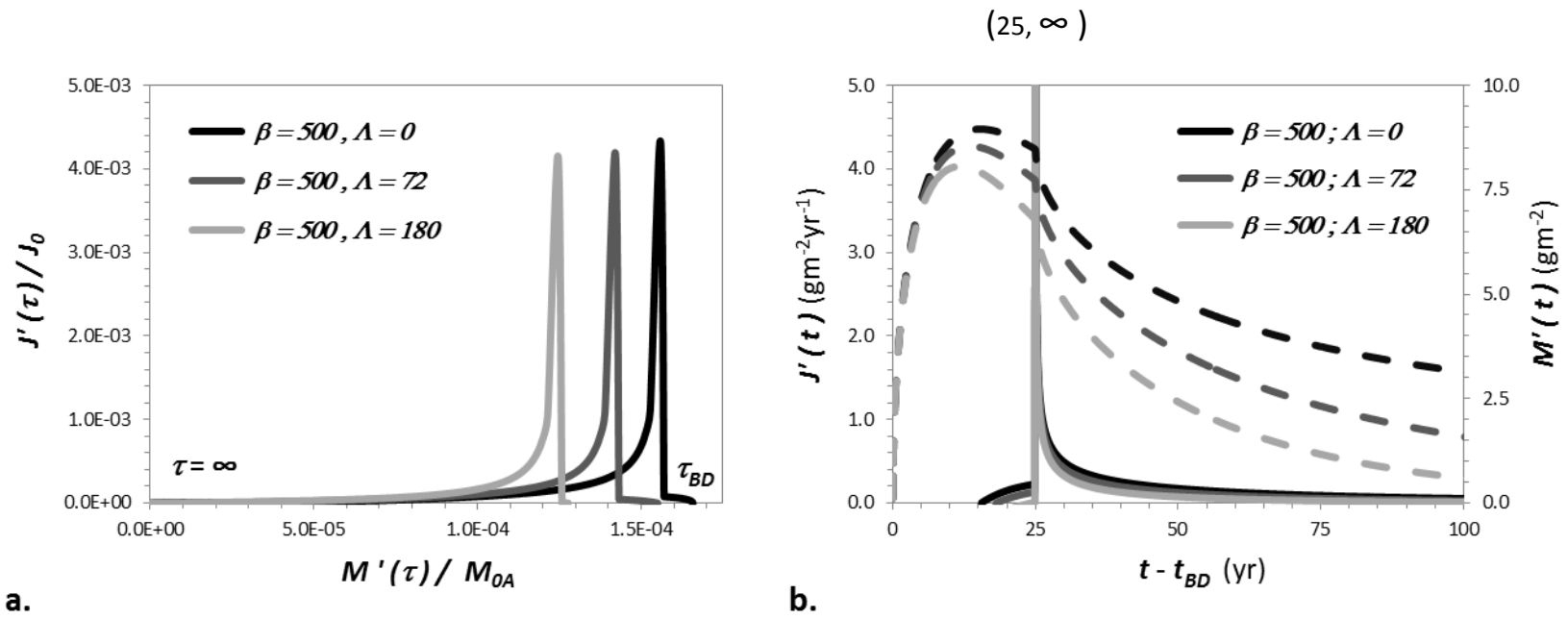

Figure 4-4. Aquitard source functions for diffusion and decay $\Lambda = \{0,\ 72,\ 180\}$ with remediation and without sorption.

Note: (a) Aquitard source functions for remediation at $t = 25$ years; $R' = 1.14$ $\beta = 500$, $\Gamma = 1$, and $X = 0.7$ for all cases. (b) Dimensioned mass storage and mass flux time series for (a).

On the x-axis of Figure 4-4a the maximum relative mass was unchanged compared to the relative mass in Figure 3-11a since the remediation occurred after τ_{BD}. The remedial lines demonstrate a marked increase in relative flux compared to the aquitard source functions for diffusion with decay and without remediation (Figure 3-11). The maximum relative

flux increased almost two orders of magnitude with remediation from 4.5×10^{-3} (Figure 3-11a) to 9.0×10^{-5} (Figure 4-4a). In Figure 4-4b, the dimensioned times series are presented for the curves in Figure 4-4a. Looking at the mass (dashed lines), there is an steep decrease in mass due to the source removal effects (i.e. the large decrease in concentration gradient). The flux (solid lines) goes off-scale instantaneously at the time of source mass removal (25 years) due to the large change in the diffusion gradient. As a result, the flux increase removes mass from the aquitard rapidly, leading to a large reduction in mass. This effect tapers off in the first five years, evident in the reduced slopes of both the mass and flux lines after 30 years ($T_R = 5$).

The dimensioned time series for each Λ in Figure 4-4b were plotted separately in Figure 4-5, adding the non-remedial lines for each Λ for comparison. Due to the flux decrease as Λ increased, the left-hand y-axis for flux (solid lines) is scaled differently for each figure. The right-hand y-axis remained the same scale for mass (dashed lines). The M' reduction was highly visible in the divergence of the remedial and non-remedial lines. Five years after remediation ($T_R = 5$, 30 years), $MR = \{0.16,\ 0.20,\ 0.18\}$. Because flux was increased by the sharp gradient drop from remediation, it took a few years before the benefits of source removal were realized in back diffusion flux. However, from then on the flux will be lower than without remediation. The initial FR due to remediation occurred at $T_R = \{15.6,\ 18.2,\ 24.3\}$ for $\Lambda = \{0,\ 72,\ 180\}$. Five years later at $T_R = \{20.6,\ 23.2,\ 29.3\}$, $FR = \{0.12,\ 0.13,\ 0.13\}$.

A summary of the mass and flux for a site with $\Gamma = 1$ and $R' = 1.14, \beta = 500$ and $\Lambda = \{0,\ 72,\ 180\}$ is shown in Table 4-1for partial source removal ($X = 0.7$ at $t = 25$ years).

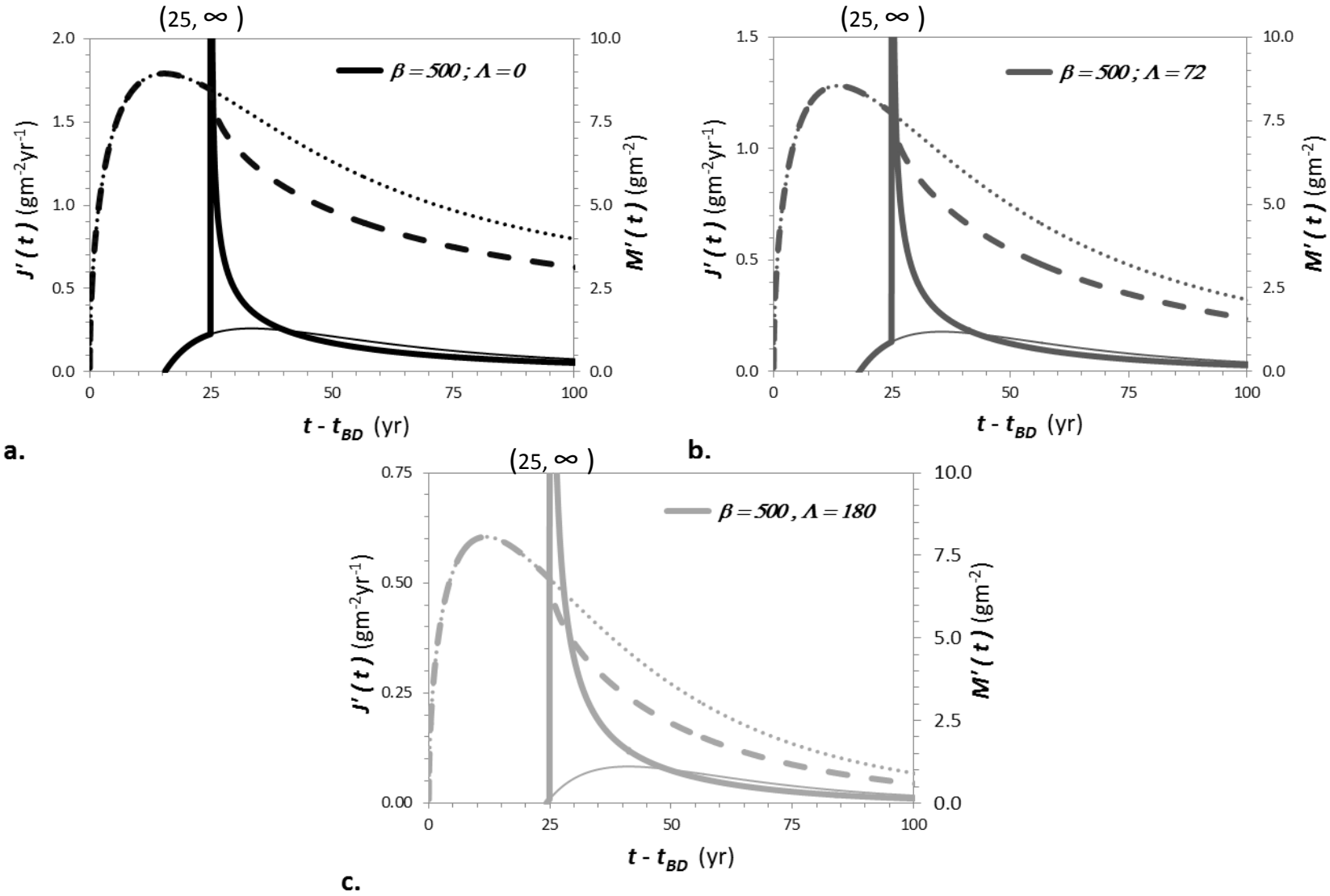

Figure 4-5. Dimensioned aquitard source functions for diffusion and decay with and without remediation, all without sorption, $R' = 1.14, \beta = 500$.

Note: Remediation at $t = 25$ years; $R' = 1.14$ $\beta = 500$, $\Gamma = 1$, and $X = 0.7$ for all cases. (a) Dimensioned mass storage and mass flux time series for (a) $\Lambda = 0$, (b) $\Lambda = 72$, (c) $\Lambda = 180$. Thin solid line is flux without remediation; thin dotted line is aquitard mass storage without remediation.

Table 4-1. Summary of Aquitard Diffusion with Decay and Source Remediation, $R' = 1.14, \beta = 500$.

Λ	$M'(t)$ mg m^{-2}					$J'(t)$ mg m^{-2} d^{-1}				
	30 yrs	40	50	75	200	30 yrs	40	50	75	200
0 R	6760	5564	4835	3746	2119	1.340	0.694	0.476	0.175	0.045
72 R	3773	3107	2601	1745	392	1.141	0.536	0.344	0.150	0.010
180 R	2124	1583	1192	598	30	0.890	0.353	0.203	0.071	0.001
			MR					FR		
	30 yrs	40	50	75	200	30 yrs	40	50	75	200
0 R : 0	0.16	0.22	0.23	0.23	0.19	-0.91	-0.02	0.19	0.30	0.22
72 R :72	0.27	0.28	0.28	0.26	0.23	-1.46	-0.12	0.16	0.32	0.27
180 R :180	0.34	0.35	0.35	0.35	0.32	-4.75	-0.55	0.02	0.34	0.37

Note: aquitard mass storage and mass flux for remediation with $\Lambda = \{0,\ 72,\ 180\}$. Λ with an R designates remediation results. Fractional mass reduction (MR) and fractional flux reduction (FR) are compared to Λ without remediation results. (-) FR indicates an increase in back diffusion flux.

Twenty five years after the remedial effort ($T_R = 25$, 50 years), $MR = \{0.23,\ 0.28,\ 0.35\}$ and $FR = \{0.19,\ 0.16,\ 0.02\}$ compared to the no remediation case for $\Lambda = \{0,\ 72,\ 180\}$, respectively. By $T_R = 50$ (75 years), $MR = \{0.23,\ 0.26,\ 0.35\}$ and $FR = \{0.30,\ 0.32,\ 0.34\}$. At the end of the simulations (200 years), $MR = \{0.19,\ 0.23,\ 0.32\}$ and $FR = \{0.22,\ 0.27,\ 0.37\}$ for $\Lambda = \{0,\ 72,\ 180\}$, and the back diffusion flux is extremely low ($J' < 0.02$ g m^{-2} yr^{-1}) at this time so it is likely indistinguishable from the remaining source zone flux.

Source Removal Effects on Diffusion with Leakage

Aquitard Concentration Profiles for Diffusion with Leakage and Remediation

Source zone remediation affected aquitard diffusion with leakage as well. The χ' profiles for a site with $\Gamma = 1$ and $R' = 8.0$ and $\beta = \{500,\ 1590,\ 296\}$, $P_e = \{0,\ 3.8,\ -12.5\}$ are presented in Figure 4-6 for a partial source removal of $X = 0.7$ at 25 years after the contaminant release. Figures 4-6a-c show the χ' profiles with source remediation. Figures 4-6d-f show both the no remediation cases (dotted lines), and the post remediation cases (solid lines) χ' profiles for comparison. The earliest post remedial lines at $T_R = 5.0$ years (30 years) in Figures 4-6a-c demonstrate the effects of the drop in boundary concentration from source removal. In particular, the upper portion of the profile (near interface) drops considerably in the 30 year solid lines. In Figures 4-6d-f, the post-remedial χ' profiles show a reduction in peak concentration at all times for the remedial lines compared to the no remediation lines.

Aquitard Source Functions for Diffusion with Leakage and Remediation

Presented in Figure 4-7 are the aquitard source functions generated for sites with $\Gamma = 1$ and $R' = 8.0$ and $\beta = \{500,\ 1590,\ 296\}$, $P_e = \{0,\ 3.8,\ -12.5\}$ and remediation ($X = 0.7$ at $t = 25$ years). The relative mass and relative flux are shown in Figure 4-7a and the dimensioned mass storage and back diffusion flux time series are shown in Figure 4-7b for $P_e = 0$, $\beta = 3500$ (black lines), $P_e = 3.8$, $\beta = 2883$ (darker gray lines), and $P_e = -12.5$, $\beta = 7500$ (light gray lines). Looking along the x-axis, there was a large increase in maximum relative mass due to $P_e = 3.8$ (at τ_{BD}) and a decrease for $P_e = -12.5$. Similarly, the flux was increased due to $P_e = 3.8$ but there was not a

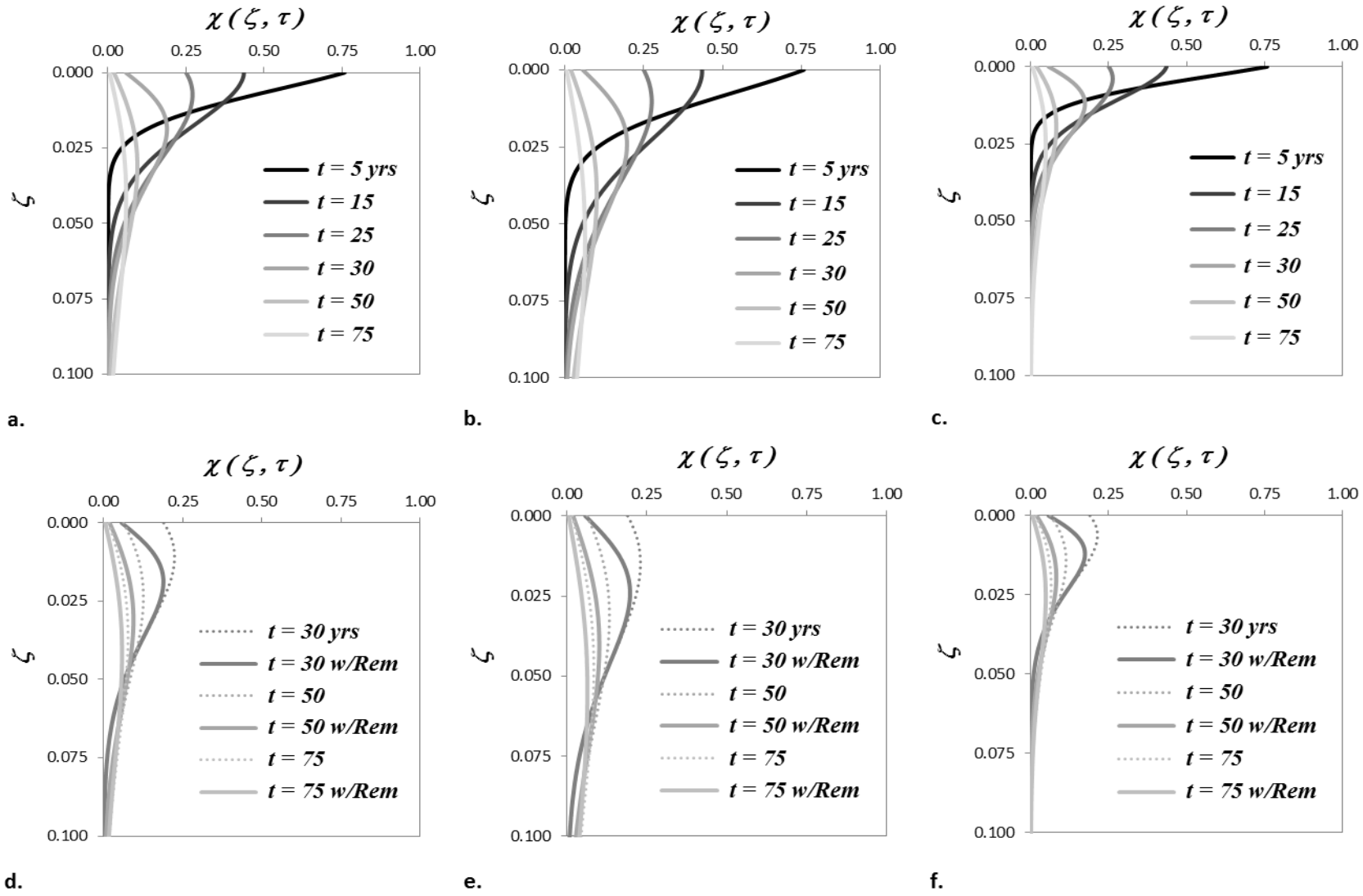

Figure 4-6. χ' depth profiles for diffusion with sorption ($R' = 8.0$) and leakage with 70% source remediation at 25 years.

Note: Note: χ' depth profiles with remediation: (a) $P_e = 0$, $\beta = 3500$;(b) $P_e = 3.8$, $\beta = 2883$ (c) $P_e = -12.5$, $\beta = 7500$ (d) comparison of post remedial profiles in (a) (solid lines) to no remediation (dashed lines), (e) comparison of (b) to no remediation, and (f) comparison of (c) to no remediation; all cases are $R' = 8.0$, $\Gamma = 1$, $X = 0.7$ at $t = 25$ years.

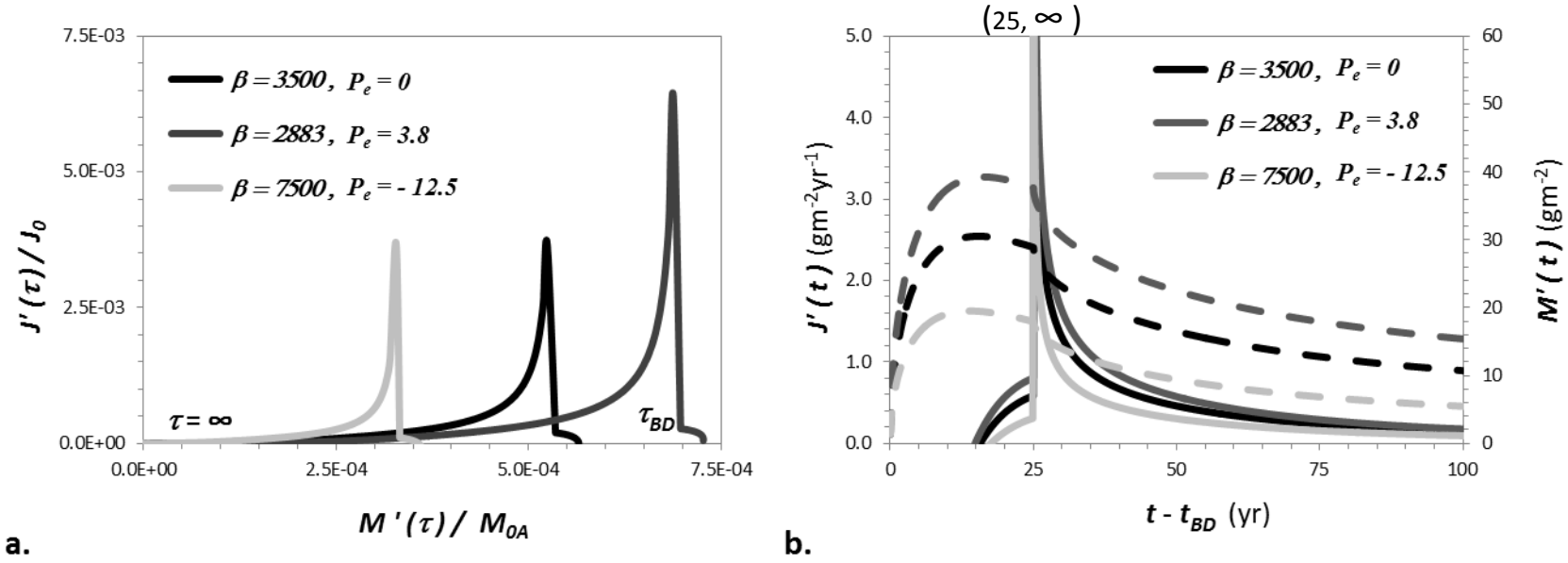

Figure 4-7. Aquitard source functions for diffusion and leakage with remediation.

Note: (a) Aquitard source functions for remediation at $t = 25$ years; $R' = 8.0$, $\Gamma = 1$, and $X = 0.7$ for all cases. (b) Dimensioned mass storage and mass flux time series for (a).

noticeable change in initial post remedial flux for $P_e = -12.5$ compared to the initial post remedial flux for $P_e = 0$. In the dimensioned time series (Figure 4-7b), the changes in mass due to leakage are visible in the dashed lines, and the decreases in mass as result of source remediation are evident by the decrease in slope beginning at $T_R = 0$ (25 years).

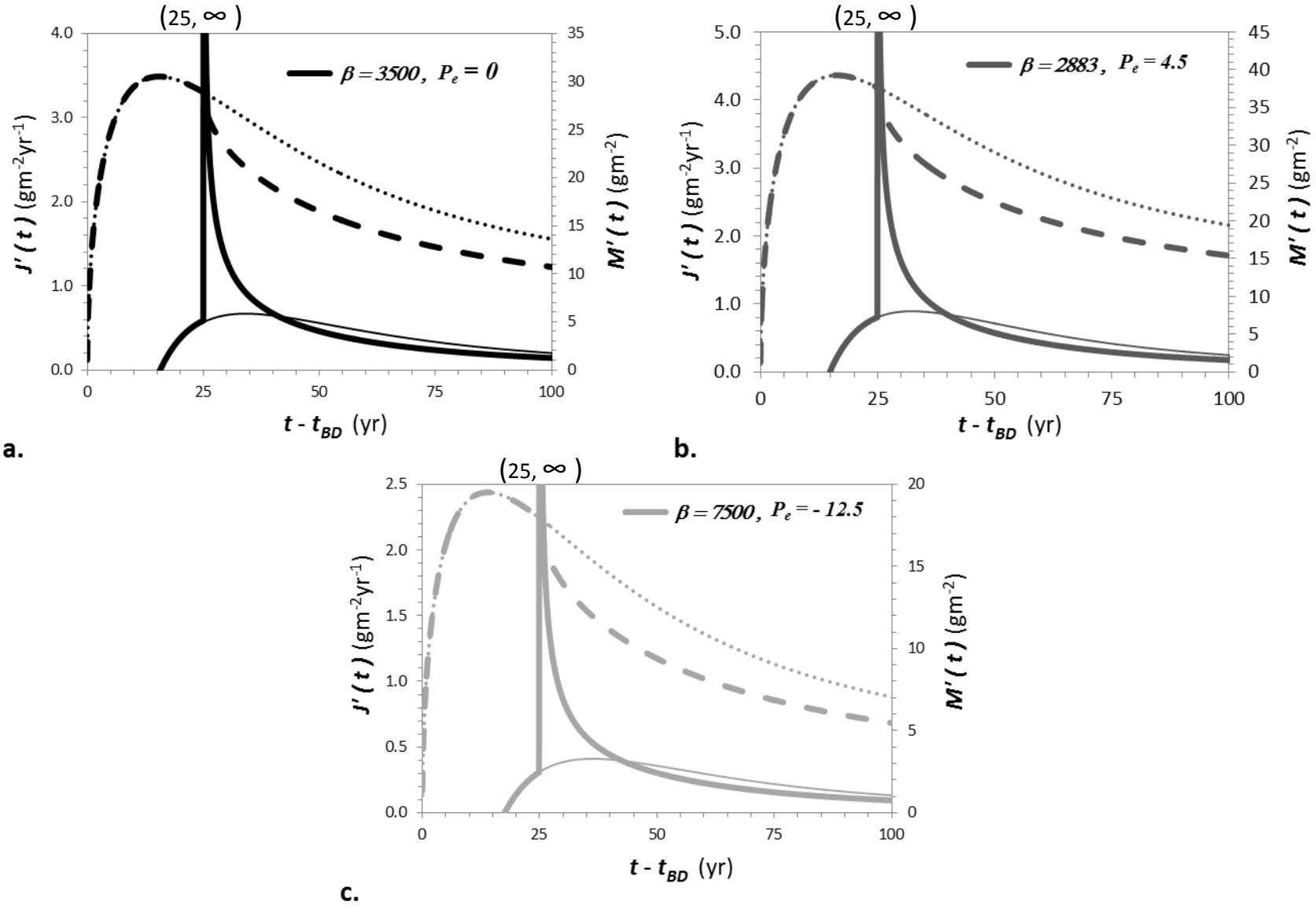

Figure 4-8. Dimensioned aquitard source functions for diffusion and leakage with remediation for specific leakages.

Note: Solid lines are remediation at $t = 25$ years; $R' = 8.0$, $\Gamma = 1$, and $X = 0.7$ for all cases. (a) Dimensioned mass storage and mass flux time series for (a) $P_e = 0$, $\beta = 3500$;(b) $P_e = 3.8$, $\beta = 2883$ (c) $P_e = -12.5$, $\beta = 7500$. Thin solid lines are flux without remediation; thin dotted line is aquitard mass storage without remediation.

Table 4-2. Summary of Aquitard Diffusion with Leakage and Source Remediation, $R' = 8.0$.

P_e	$M'(t)$ mg m^{-2}					$J'(t)$ mg m^{-2} d^{-1}				
	30 yrs	40	50	75	200	30 yrs	40	50	75	200
0 R	23054	18979	16487	12771	7237	3.542	1.835	1.258	0.644	0.119
3.8 R	30513	25524	22402	17912	11145	4.450	2.298	1.561	0.794	0.145
-12.5 R	13940	11108	9390	6853	3171	2.352	1.208	0.831	0.427	0.077
			MR					FR		
	30 yrs	40	50	75	200	30 yrs	40	50	75	200
0 R : 0	0.16	0.22	0.23	0.23	0.19	-0.98	-0.04	0.17	0.29	0.22
3.8 R :3.8	0.15	0.21	0.23	0.22	0.19	-0.83	0.01	0.20	0.30	0.22
-12.5 R :-12.5	0.17	0.23	0.25	0.24	0.19	-1.22	-0.09	0.15	0.29	0.22

Note: aquitard mass storage and mass flux for remediation with $P_e = \{0,\ 3.8,\ -12.5\}$. Λ with and R designates remediation results. Fractional mass reduction (MR) and fractional flux reduction (FR) are compared to Λ without remediation results. (-) FR indicates an increase in back diffusion flux.

The dimensioned time series for each P_e are shown in Figures 4-8a-c. The post-remediation (thick lines) and the corresponding no remediation (thin lines) cases are plotted together for comparison. The dashed lines are M' and the solid lines are J'. In these cases, the maximum mass storage was different for each value of P_e such that the right- hand y-axis is scaled accordingly. Likewise, the left-hand y-axis for flux is also scaled accordingly but the maximum flux (25, ∞) was offscale in each case. Compared to $P_e = 0$, the scale for each y-axis for $P_e = 3.8$ was greater and $P_e = -12.5$ was reduced, as expected. The divergence of the mass lines for the post-remedial and non-

remedial lines was highly visible but the change is flux was less evident. Five years after remediation ($T_R = 5.0$), $MR = \{0.19,\ 0.21,\ 0.07\}$. The initial FR due to remediation occurred at $T_R = \{16.2,\ 14.8,\ 17.6\}$ for $P_e = \{0,\ 3.8,\ -12.5\}$. Five years later at $T_R = \{21.2,\ 22.8,\ 19.6\}$, $FR = \{0.13,\ 0.14,\ 0.13\}$. At the end of the simulations (200 years), $MR = \{0.22,\ 0.09,\ 0.24\}$ and $FR = \{0.25,\ 0.28,\ 0.29\}$ for $P_e = \{0,\ 3.8,\ -12.5\}$, and the back diffusion flux is extremely low ($J' < 0.05$ g m^{-2} t^{-1}) at this time, so it is likely indistinguishable from the remaining source zone flux.

CHAPTER 5
CONCLUSIONS

1D Aquitard Diffusion

A one-dimensional aquitard diffusion model with a semi-infinite domain, which used a source depletion model (SDM) as a boundary condition, was used to investigate the effects of DNAPL source architecture and aquitard properties on the risk of back diffusion. Two key variables used in this assessment were: 1) the power-law exponential term Γ, which reflects the source zone architecture, and 2) the source to aquitard mass transfer coefficient β, which reflects the influence of both the source characteristics (ψ) and the aquitard properties (σ). The amount of contaminant mass in the aquitard, the back diffusion flux magnitude, and their longevity were used as measures of back diffusion risk. The use of a semi-infinite domain presents an inherent limitation to applying the model to finite thickness aquitards, particularly if the aquitard is quite thin. If sorption is high, the model may be applicable to ~1m thick aquitards. It is not appropriate to thin lenses but could be utilized if the lens is several meters thick and superposition is used. The greatest potential for back diffusion occurs when the source strength is constant until source mass is exhausted (i.e., $\Gamma = 0$), as is often assumed in back diffusion assessments. For sites where mass discharge decreases with time as source mass is depleted (i.e., $\Gamma > 0$), less risk is expected. Specifically, the aquitard mass per unit area M', the dimensionless start time for back diffusion τ_{BD}, the depth of penetration, and the magnitude of back diffusion flux J' all decreased as Γ increased, indicating reduced risk due to back diffusion.

Additional source-zone characteristics that were investigated include the initial source mass M_0, the initial source concentration C_0, the groundwater flux q, and the source zone control plane area A_{SZ}. These terms were combined to represent the ratio of initial source-zone mass discharge to initial DNAPL mass (i.e., ψ, the source decay function). In general, site conditions that lead to an increased ψ, and hence β, (i.e., large initial mass discharge and small M_0) result in higher, short-term back diffusion flux due to more rapid source dissolution. However, they also result in a lower long-term risk due to the reduced stored mass and penetration depth in the aquitard. Conversely, sites with a decreased ψ (i.e. small initial mass discharge and large M_0) generate a lower back diffusion flux due to slower source depletion. These sites present a greater long-term risk due to back diffusion from the additional mass stored in the aquitard.

Increasing aquitard sorption, represented by a larger σ, and hence β, had no effect on the loading concentration gradient, but increased both the mass storage M' and the back diffusion flux J'. However, increased sorption also decreased the depth of penetration of contaminants. This suggests that sites with greater sorption of contaminants are at greater risk for back diffusion, particularly in the short term.

If contaminant decay λ' occurs in the aquitard, the mass storage and back diffusion flux decrease proportionally with the magnitude of the decay. The reduction in mass and flux will also decrease site longevity if back diffusion is the constraint on reaching MCL. Sites with sorption demonstrate less decay due to the reduction in available contaminant from solid phase storage. For a site with a greater λ', the loading flux direction continues longer compared to a site without decay or one with low decay. In fact, if the decay rate is great enough, back diffusion never occurs due to the

increase of degradation of contaminant in the aquitard which never allows the concentration gradient to reverse. If the aquitard is leaky, downward vertical flow v_z' increases mass storage, depth of penetration, back diffusion flux, and site longevity, whereas upward leakage reduces mass storage, penetration, back diffusion flux, and longevity. Sorption tended to reduce the effects of leakage compared to sites without sorption.

The modeling effort presented here represents the worst case scenario for back diffusion for a simplified aquitard with a time varying boundary immediately down gradient of the DNAPL source because advection, dispersion, and degradation in the aquifer were neglected. The assumption of a homogenous aquitard also leads to increased diffusion, storage, and mass flux. Degradation in the aquitard was modeled conservatively, up to 3 orders of magnitude less than the literature range for aquifers, and only included aqueous phase decay.

Source Removal

By employing an SDM as the time variable boundary condition, the effects of remediation on aquitard diffusion were simulated. A delay in DNAPL source-zone remediation increases long-term, back diffusion risk, which is similar to the conclusion made by *Falta et al.* [2005b] regarding the impact of delays in source-zone remediation and the resulting increase in plume mass.

Source removal can decrease the amount of mass loaded into the aquitard by reducing the aquifer concentration and hence the diffusion gradient. Even after back diffusion has started, source-zone remediation will provide long-term reductions in back diffusion risk by accelerating the rate at which mass is removed from the aquitard. For

sites with decay in the aquitard, remediation will reduce the mass storage and site longevity, but will increase the back diffusion flux in the early years after remediation. In the long term back diffusion flux will be reduced as well. Similarly, for sites with leakage, partial source removal will decrease mass storage and longevity, but also increase the back diffusion flux after remediation. In the long term, remediation demonstrates benefits by reducing the back diffusion flux and the site longevity.

Future Work

Future modeling could investigate the combined effects on diffusion for a site with aquitard decay and leakage. Decay could be modeled as a time changing decay rate due to remedial enhancements and the effects of solid phase decay could be modeled as well. Daughter product formation was neglected in this effort and for many DNAPL species may be significant, and could be accounted for in further model developments. Leakage was held constant in this work and could be altered through the site lifespan to simulate the effects of pumping through injection of extraction in an underlying aquifer. This could be further explored with 2D models as well. Additionally, the impact of increasing interfacial areas associated with distributed lenses of high or low conductivity media on mass storage and flux should be explored in 2D models.

APPENDIX

Zhu and Sykes [2004] provide a detailed derivation of Eq. 2-5a and Eq. 2-5b. First, Eq. 2-2 can be represented by

$$\frac{C(t)}{C_0} = \left[\int_t^\infty C(t)dt \Big/ \int_0^\infty C(t)dt \right]^\Gamma \quad . \tag{A-1}$$

Then, differentiating both sides with respect to t twice leads to

$$\Gamma C \frac{d^2C}{dt^2} = (2\Gamma - 1)\left(\frac{dC}{dt}\right)^2 \quad , \tag{A-2}$$

which has a general solution of

$$C(t) = [at + b]^{\frac{\Gamma}{(1-\Gamma)}} \quad . \tag{A-3}$$

Similarly, *Zhu and Sykes* [2004] provide the specific case of $\Gamma = 1$, where Eq. 2-2 can represented by

$$\frac{C(t)}{C_0} = \left[\int_t^\infty C(t)dt \Big/ \int_0^\infty C(t)dt \right] \quad . \tag{A-4}$$

Again, differentiating both sides with respect to t leads to

$$C = \frac{d^2C}{dt^2} = \left(\frac{dC}{dt}\right)^2 \quad , \tag{A-5}$$

The solution to Eq. A-5 with an initial condition $C(0) = C_0$ is

$$\frac{C(t)}{C_0} = e^{-\lambda t} \quad . \tag{A-6}$$

This becomes Eq. 2-5c in dimensionless form.

The model verification utilized several existing analytical models for specific Γ and boundary conditions. First, for the simple, infinite constant concentration boundary

case ($\Gamma = 0$) in Eq. 2-5a, for the conceptual model with time invariant boundary conditions of

$$\chi'(\zeta = 0, \tau) = 1.0 \quad , \tag{A-7a}$$

and

$$\chi'(\zeta = \infty, \tau) = 0 \quad , \tag{A-7b}$$

and an initial condition of

$$\chi'(\zeta, \tau = 0) = 0 \quad , \tag{A-7c}$$

an analytical solution [Crank, 1975] to Eq. 2-8 is

$$\chi'(\zeta, \tau) = erfc\left(\frac{\zeta}{2\sqrt{\tau}}\right) \quad . \tag{A-8}$$

The diffusive flux and dimensionless mass storage per unit area are given by *Crank* [1975] and have been transformed to dimensionless forms:

$$\varphi'(\zeta = 0, \tau) = -\sqrt{\frac{1}{\pi\tau}} \quad , \tag{A-9}$$

and

$$\mu'(\tau) = 2\sqrt{\frac{\tau}{\pi}} \quad , \tag{A-10}$$

respectively. For the $\Gamma = 0.5$ case, a new analytical solution was derived and used to verify the general solution for that case. This model incorporates linear decay of the source mass due to dissolution, but is only valid for the time prior to the initiation of back diffusion. .

$$\chi'(\zeta, \tau) = erfc\left[\frac{\zeta}{2\sqrt{\tau}}\right] + \alpha\left\{\left(\tau + \frac{\zeta^2}{2}\right) erfc\left[\frac{\zeta}{2\sqrt{\tau}}\right] - \zeta\left(\sqrt{\frac{\tau}{\pi}}\right)\exp\left(-\zeta^2 / 4\tau\right)\right\}, \tag{A-11}$$

where $\alpha = -0.5\beta$.

For the $\Gamma = 1$ case, *Bear et al.* [1994] developed an analytical solution that models exponential decay of the boundary concentration through the time period of layer diffusive loading,

$$\chi'(\zeta,\tau) = \frac{1}{2} e^{-\beta\tau} \left\{ e^{-\zeta\sqrt{-\beta}} erfc\left[\frac{\zeta}{2\sqrt{\tau}} - \sqrt{-\beta\tau} \right] + e^{\zeta\sqrt{-\beta}} erfc\left[\frac{\zeta}{2\sqrt{\tau}} + \sqrt{-\beta\tau} \right] \right\} \quad \text{(A-12)}$$

The flux for this case is

$$\varphi'(\tau) = e^{-\beta\tau} \left[i\sqrt{\beta} \cdot erf\left(i\sqrt{\beta\tau} \right) + \frac{e^{\beta\tau}}{\sqrt{\pi\tau}} \right] \quad . \quad \text{(A-13)}$$

Finite difference methods were employed to verify the new analytical model. The general analytical solution, equation (9), was verified with the central difference approximation for the second derivative [*Grathwolh,* 1998].

$$\chi'(\zeta,\tau) = \frac{\Delta\tau}{\Delta\zeta^2} \left(\chi'^{k}_{J+1} - 2\chi'^{k}_{J} + \chi'^{k}_{J-1} \right) \quad \textit{for any} \quad \chi'(\zeta = 0, \tau) \quad . \quad \text{(A-14)}$$

The finite difference solution is valid for any imposed boundary changes but is subject to a stability criteria of $\Delta\tau / \Delta\zeta^2 = 0.1$. The flux into and out of the layer was verified with the spatial derivative approximation

$$\varphi'(\tau) = \frac{\partial\chi}{\partial\zeta} \cong \frac{\Delta\chi}{\Delta\zeta} = \frac{(\chi_1 - \chi_0)}{(\zeta_1 - \zeta_0)} \quad , \quad \text{(A-15)}$$

comparing the boundary concentration to that of a very small location below the interface.

Verification of the remediation model was performed for the $\Gamma = 0$ case. Previous investigations have considered the impact of source treatment on aquitard diffusion by considering a step change in concentration at the upper boundary of the aquitard [*Bear*

et al., 1994; *Chapman and Parker,* 2005; *Sale et al*., 2008]. To model complete source depletion, a constant concentration would be applied to the upper boundary of the aquifer for a period of time, and then the boundary condition concentration would be set to zero thereafter. In practice, this corresponds to the time at which the source was exhausted either through natural dissolution or remedial treatment, or isolated by physical or hydraulic barriers. In the dimensionless framework of this work, a boundary condition of $\chi(\tau)=1.0$ (i.e., Eq. 2-5a with $\Gamma=0$) would be applied to the initially clean aquitard (i.e., $\chi'(\zeta,\tau=0)=0$) for a time period $\tau \le \tau^*$. If the $\Gamma=0$ case source exhaustion occurred through natural dissolution, then $\tau^*=\beta^{-1}$ in Eq. 2-12, and the solution for the aquitard concentration is Eq. A-8 for $\tau \le \tau^*$. This represents concentration resulting from the mass loaded into the aquitard. When complete source exhaustion or isolation occurred, the boundary would change to zero $\chi(\tau>\tau^*)=0$. The analytical solution for the concentration distribution in the aquitard for $\tau \ge \tau^*$, was given by *Bear et al.* [1994] and the dimensionless version is

$$\chi'(\zeta,\tau)=erfc\left(\frac{\zeta}{2\sqrt{\tau}}\right)-erfc\left(\frac{\zeta}{2\sqrt{(\tau-\tau^*)}}\right) \quad for \quad \tau \ge \tau^* \quad . \qquad \text{(A-16)}$$

This represents concentration resulting from the contaminant mass in the aquitard after loading is complete. It includes the diffusion of mass back to the aquifer due to the concentration gradient reversal at the interface, and the continued downward migration due to diffusion within the aquitard. The diffusive flux after source exhaustion was given by *Bear et al.* [1994] and has been modified to the dimensionless form:

$$\varphi'(\zeta=0,\tau)=-\sqrt{\frac{1}{\pi}}\left(\frac{1}{\sqrt{\tau}}-\frac{1}{\sqrt{\tau-\tau^*}}\right) \quad . \qquad \text{(A-17)}$$

This solution was also utilized for remediation $\Gamma = 0$ cases where 100% of the source mass is removed at τ^*. However, rarely does perfect remediation or complete source exhaustion occur. Thus, the effects of partial source removal were investigated with our new model.

LIST OF REFERENCES

Abramowitz, M., and I. A. Stegun (1970), *Handbook of Mathematical Functions,* Dover Publications, Inc., New York.

Alexander, M., (1999), *Biodegradation and Bioremediation,* 2nd Ed., Academic Press, San Diego, CA.

Annable, M. D. , L. H. Motz, and W. D. Beddow, (1996), Investigation of lake and surficial aquifer interaction in the upper Etonia Creek Basin: Interim Report, St. Johns River Water Management District, SJ96-SP14.

Ball, W. P., C. Liu, G. Xia, and D. F. Young (1997), A diffusion-based interpretation of tetrachloroethene and trichloroethene concentration profiles in a groundwater aquitard, *Water Resour. Res., 33,* 2741-2757, doi:10.1029/97WR02135.

Basu, N. B., Rao, P. S. C., R. W. Falta, Jr., M. D. Annable, J. W. Jawitz and K. Hatfield (2008a), Temporal evolution of DNAPL source and contaminant flux distribution: Impacts of source mass depletion, *J. Contam. Hydrol., 95,* 93–108, doi:10.1016/j.jconhyd.2007.08.001.

Basu, N. B., A. D. Fure, and J. W. Jawitz (2008b), Simplified contaminant source depletion models as analogs of multiphase simulators, *J. Contam. Hydrol.*, *97*, 87-99, doi:10.1016/j.jconhyd.2008.01.001.

Basu, N. B., P. S. C. Rao, I. C. Poyer, S. Nandy, M. Mallavarapu, R. Naidu, G. B. Davis, B. M. Patterson, M. D. Annable, and K. Hatfield (2009), Integration of traditional and innovative characterization techniques for flux-based assessment of Dense Non-aqueous Phase Liquid (DNAPL) sites, *J. Contam. Hydrol., 105,* 161–172, doi:10.1016/j.jconhyd.2008.12.005.

Bear, J., E. Nichols, J. Ziagos, and A. Kulshrestha (1994), Effect of diffusion into and out of low-permeability zones, Environmental Protection Department, Environmental Restoration Division, Lawrence Livermore National Laboratory, University of California, UCRL-ID-115626.

Booker, J. R. and R. K. Rowe (1987), One-dimensional advective–dispersive transport into a deep layer having a variable surface concentration, *Int. J. for Num. & Anal. Meth. in Geomech.,11,* 131-141, doi:10.1002/nag.1610110203.

Brooks, M. C. B., A. L. Wood, M. D. Annable, K. Hatfield, C. Holbert, P. S. C. Rao, C. G. Enfield, L. Lynch, and R. E. Smith, (2008), Changes in contaminant mass discharge from DNAPL source mass depletion: Evaluation at two field sites, *J. Contam. Hydrol.*, *102*, 140-153, doi: 10.1016/j.jconhyd.2008.05.008.

Brown, G. H., M. C. Brooks, M. D. Annable, A. L. Wood, and J. Huang (2012), Aquitard contaminant storage and flux resulting from dense nonaqueous phase liquid source zone dissolution and remediation, *Water Resour. Res., 48*: W06531, doi:10.1029/ 2011WR011141.

Brusseau, M. L., E. L. DiFilippo, J. C. Marble, and M. Oostrom (2008), Mass-removal and mass-flux-reduction behavior for idealized source zones with hydraulically poorly-accessible immiscible liquid, *Chemosphere*, *71*, 1511-1521, doi:10.1016/j.chemosphere.2007.11.064.

Chapman, S. W., and B. L. Parker (2005), Plume persistence due to aquitard back diffusion following dense nonaqueous phase liquid source removal or isolation, *Water Resour. Res.*, *41*, doi:10.1029/2005WR004224.

Chapman, S. W., B. L. Parker, T. C. Sale, and L. A. Doner (2012), Testing high resolution numerical models for analysis of contaminant storage and release from low permeability zones, , *J. Contam. Hydrol*. *136-137*, 106-116.

Chen, Y., X. Haijian, K. Han and R. Chen (2009), An analytical solution for one-dimensional contaminant diffusion through multi-layered system and its applications, *Environ. Geol.,58*, 1083-1094, doi:10.1007/s00254.008.1587.3.

Chen, X., and J. W. Jawitz (2009) Convergence of DNAPL source strength functions with site age, *Environ. Sci. & Techn.*, 43, 9374-9379, doi:10.1021/es902108z.

Christ, J. A., C. A. Ramsburg, K. D. Pannell and L. M. Abriola (2006), Estimating mass discharge from dense nonaqueous phase liquid source zones using upscaled mass transfer coefficients: An evaluation using multiphase numerical simulations, *Water Resour. Res.*, *42*, doi:10.1029/2006WR004886.

Crank, J. (1976), *The mathematics of diffusion*, 2nd Ed., pp. 1-38, Oxford University Press, New York.

DiFilippo, E. L., and M. L. Brusseau (2008), Relationship between mass-flux reduction and source-zone mass removal: Analysis of field data, *J. Contam. Hydrol*. *98*, 22-35, doi:10.1016/j.jconhyd.2008.02.004.

DiFilippo, E. L., and M. L. Brusseau (2011), Assessment of a simple function to evaluate the relationship between mass flux reduction and mass removal for organic-liquid contaminated source zones, *J. Contam. Hydrol*. *123*, 104-113, doi:10.1016/j.jconhyd.2010.12.011.

Falta, R. W., P. S. C. Rao, N. Basu (2005a), Assessing the impacts of partial mass depletion in DNAPL source zones—I. Analytical modeling of source strength functions and plume response, *J. Contam. Hydrol, 78,* 259–280, doi:10.1016/j.jconhyd.2005.05.010.

Falta, R. W., N. Basu, and P. S. C. Rao (2005b), Assessing impacts of partial mass depletion in DNAPL source zones: II. Coupling source strength functions to plume evolution, *J. Contam. Hydrol.*, *79*, 45–66, doi:10.1016/j.jconhyd.2005.05.012.

Falta, R. W., M. B. Stacy, N. A. Ahsanuzzaman, M. Wang, and R. C. Earle (2007), REMChlor: Remediation Evaluation Model for Chlorinated Solvents, User's Manual Version 1.0, Center for Subsurface Modeling Support, US EPA, RSKERC/GWERD, Ada, OK.

Falta, R. W., (2008), Methodology for comparing source and plume remediation alternatives, Ground Water, 46, 2, 272-285, doi:10.1111/j.1745-6584.2007.00416x.

Foose, G. J., C. H. Benson and T. B. Edil (2001), Predicting leakage through composite landfill liners, *J. Geotech. Geoenviron. Eng.,127,* 510–520, doi:10.1061/(ASCE)1090-024(2002)128:5(391).

Fure, A. D., J. W. Jawitz, and M. D. Annable (2006), DNAPL source depletion: linking architecture and flux response, *J. Contam. Hydrol*, *85,* 118–140, doi:10.1016/j.jconhyd.2006.01.002.

Gardner, W. P., G. A. Harrington, and B. D. Smerdon (2012), Using excess ^{4}He to quantify variability in aquitard leakage, *J. Hydrol*, *468-469,* 63–79.

Grathwohl, P. (1998), Modeling Diffusion Processes, in *Diffusion in natural porous media: Contaminant Transport, Sorption/Desorption and Dissolution Kinetics*, Kluwer Academic Publishers, Boston, MA.

Harrison, B., E. A. Sudicky, and J. A. Cherry (1992), Numerical-analysis of solute migration through fractured clayey deposits into underlying aquifers, *Water Resour. Res., 28*: 515-526.

Johnson, R. L., J. A. Cherry, and J. F. Pankow (1989), Diffusive contaminant transport in natural clay: A field example and implications for clay-lined waste disposal sites, *Environ. Sci. Technol*, *23*, 340-349.

Kaye, A. J., J. Cho, N. B. Basu, X. Chen, M. D. Annable, and J. W. Jawitz (2008), Laboratory investigation of flux reduction from dense non-aqueous phase liquid (DNAPL) partial source zone remediation by enhanced dissolution, *J. Contam. Hydrol.*, *102,* 17–28, doi:10.1016/j.jconhyd.2008.01.006.

Jawitz, J. W., A. D. Fure, G. G. Demmy, S. Berglund, and P. S. C. Rao (2005), Groundwater contaminant flux reduction resulting from nonaqueous phase liquid mass reduction, *Water Resour. Res., 41*, doi:10.1029/2004WR003825.

Liu, C., and W. P. Ball (1998), Analytical modeling of diffusion-limited contamination and decontamination in a two-layer porous medium, *Adv. in Wat. Res., 21,* 297-313, doi:10.1016/S0309-1708(96)00062-0.

Liu, C., and W. P. Ball (1999), Application of inverse methods to contaminant source identification from aquitard diffusion profiles at Dover AFB, Delaware, *Water Resour. Res., 35*, 1975-1985, doi:10.1029/1999WR900092.

Liu, C., and W. P. Ball (2002), Back diffusion of chlorinated solvent contaminants from a natural aquitard to a remediated aquifer under well-controlled field conditions: predictions and measurements, *Ground Water, 40,* 175-184, doi: 10.1111/j.1745-6584.2002.tb02502.x.

McGuire, T. M., J. M. McDade and C. J. Newell (2006), Performance of DNAPL source depletion technologies at 59 chlorinated solvent-impacted sites, *Ground Wat. Monit. & Rem*., *26*, 73-84, doi: 10.1111/j.1745-6592.2006.00054.x

Motz, L. H. (1998), Vertical leakage and vertically averaged vertical conductance for Karst Lakes in Florida, *Water Resour. Res., 34*, 159-167, doi: 10.1029/97WR03134.

National Research Council (NRC) (2004), *Contaminants in the Subsurface: Source Zone Assessment and Remediation*, National Academies Press, Washington, D.C.

Newell, C. J., H. S. Rifai, J. T. Wilson, J. A. Connor, J. A. Aziz, and M. P. Suarez (2002), *Calculation and Use of First-Order Rate Constants for Monitored Natural Attenuation Studies*, Groundwater Issue EPA/540/S-02/500, US EPA, NRMRL, Cincinnati, OH.

Page, J. W. E., K. Soga, and T. Illangasakare (2007), The significance of heterogeneity on mass flux from DNAPL source zones: An experimental investigation, *J. Contam. Hydrol., 94,* 215– 234, doi:10.1016/j.jconhyd.2007.06.004.

Parker, B. L., J. A. Cherry, and S. W. Chapman (2005), Field study of TCE diffusion profiles below DNAPL to assess aquitard integrity, *J. Contam. Hydrol., 74,* 197– 230, doi:10.1016/j.jconhyd.2004.02.011.

Parker, B. L., S. W. Chapman, and M. A. Guilbeault (2008), Plume persistence caused by back diffusion from thin clay layers in a sand aquifer following TCE source-zone hydraulic isolation, *J. Contam. Hydrol., 102,* 86-104, doi:10.1016/j.jconhyd.2008.07.003.

Parker, J. C. and E. Park (2004), Modeling field-scale dense non-aqueous phase liquid dissolution kinetics in heterogeneous aquifers, *Water Resour. Res., 40*, doi:10.1029/2003WR002807.

Rao, P. S. C., J. W. Jawitz, C. G. Enfield, R. W. Falta, Jr., M. D. Annable, and A. L. Wood (2002), Technology integration for contaminated site remediation: clean-up goals and performance criteria, *Groundwater Quality: Natural and Enhanced Restoration of Groundwater Pollution*, Proceedings of the Groundwater Quality 2001 Conference, Sheffield, UK, June 2001, IAHS Publication # *275*, 25-31.

Rao, P. S. C. and J. W. Jawitz (2003), Comment on "Steady state mass transfer from single-component dense nonaqueous phase liquids in uniform flow fields" by T.C. Sale and D.B. McWhorter, *Water Resour. Res., 39,* 1068, doi:10.1029/2001WR000599.

Rubin, H. and A. J. Rabideau (2000), Approximate evaluation of contaminant transport through vertical barriers, *J. Contam. Hydrol., 40,* 311-333, doi:10.1016/S0169-7722(99)00060-1.

Sale, T. C., J. A. Zimbron, D. S. Dandy (2008), Effects of reduced contaminant loading on downgradient water quality in an idealized two layer granular porous media, *J. Contam. Hydrol., 102,* 72-85, doi:10.1016/j.jconhyd.2008.08.002.

Seyedabbasi, M. A., C. J. Newell, D. T. Adamson, and T. C. Sale (2012), Relative contribution of DNAPL dissolution and matrix diffusion to the long-term persistence of chlorinated solvent source zones, *J. Contam. Hydrol., 134-135,* 69-81.

Suchomel, E. J., and K. Pennell (2006), Reductions in contaminant mass discharge following partial mass removal from DNAPL source zones, *Environ. Sci. & Techn.*, 40, 6110-6116, doi: 10.1021/es060298e.

Takeuchi, M., Y. Kawabe, E. Watanabe, T. Oiwa, M. Takahashi, K. Nanba, Y. Kamagata, S. Hanada, Y. Ohko, and T. Komai (2011), Comparative study of microbial dechlorination of chlorinated ethenes in an aquifer and a clayey aquitard, *J. Contam. Hydrol., 124,* 14-24.

Wood, A. L., M. D. Annable, J. W. Jawitz, R. W. Falta, M. C. Brooks, C. G. Enfield, P. S. C. Rao, and M. N. Goltz (2009), DNAPL source zone parameters, in *Impacts of DNAPL Source Treatment: Experimental and Modeling Assessment of the Benefits of Partial DNAPL Source Removal*, pp 9-34, Office of Research and Development National Risk Management Research Laboratory, US Environmental Protection Agency, Ada, Oklahoma.

Zhang, C., H. Yoon, C. J. Werth, A. J. Valocchi, N. B. Basu, and J. W. Jawitz (2008), Evaluation of simplified mass transfer models to simulate the impacts of source zone architecture on nonaqueous phase liquid dissolution in heterogeneous porous media, *J. Contam. Hydrol., 102,* 49-60, doi:10.1016/j.jconhyd.2008.05.007.

Zhu, J. and J. F. Sykes (2004), Simple screening models of NAPL dissolution in the subsurface, *J. Contam. Hydrol., 72,* 245– 258.

BIOGRAPHICAL SKETCH

Gordon Hitchings Brown was born on June 19, 1969, in Rochester, NY. He was raised by two scientists and grew up in and around the Helmer Nature Center that his mother directed. After moving to Northern California in 1985, he graduated from Palo Alto Senior High School, Palo Alto, California, in 1987.

He enrolled at the State University of New York College at Brockport in 1996 and received a Bachelor of Science degree in chemistry and earth science in 2003. He graduated as a departmental scholar in earth sciences, and received both analytical chemistry and sigma xi awards for excellence in undergraduate research at Brockport.

He continued his education at the University of Florida in the Department of Environmental Engineering Sciences and received a Master of Science degree in 2006. Gordon was a National Science Foundation Science Partners In Collaborative Inquiry-based Education (SPICE) fellow from August 2005 through August 2008. He has served as an officer of the University of Florida's student chapter of the American Water Resources Association (AWRA) from 2003 to 2009, and served on the AWRA Florida Section Board of Directors from 2006-2009.

He pursued this research at the US EPA's National Risk Management Research Laboratory, Ground Water and Ecosystem Restoration Division center in Oklahoma from 2009-2011 as a student services contractor. He has been working in health, safety, and environmental compliance in the oil and gas industry in Oklahoma since. He desires to return to Florida to work in environmental consulting and eventually to teach at the university level.